ACTIVATED IRON MEDIA FOR WASTEWATER TREATMENT: MECHANISMS FOR ANIONIC CONTAMINANTS IMMOBILIZATION AND TRANSFORMATION

A Dissertation

by

XIAO WANG

Submitted to the Graduate and Professional School of
Texas A&M University
in partial fulfillment of the requirements for the degree of

DOCTOR OF PHILOSOPHY

Chair of Committee,	Yongheng Huang
Committee Members,	Youjun Deng
	Ronald E. Lacey
	Xingmao "Samuel" Ma
Head of Department,	Patricia Smith

December 2022

Major Subject: Biological and Agricultural Engineering

ABSTRACT

Activated iron media has been proven effective for treating a variety of environmental contaminants with more strengths and less drawbacks comparing to conventional zero-valent iron (ZVI) technology. Despite its success, some of the detailed mechanistic understandings of the activated iron media are still in mystery. This study embarks on laboratory experiments and analyses mainly focusing on the roles of green rusts as part of the effective ingredients of the activated iron media for immobilization and transformation of anionic contaminants from water. The investigation centers on the anionic exchanging capacity of the green rust enabled by the unique intercalation layer of the green rust structure.

In the Chapter II and III, green rusts are found to exist as a precursor/intermedia towards the formation of the activated iron media. A model is proposed where green rust as a coating on iron is oxidized by nitrate but also regenerated on the ZVI particle surface under certain conditions. Externally-added ferrous ion participates in nitrate reduction directly as an electron donor; in excess, ferrous ion could further facilitate the transformation of the final products to green rust instead of magnetite. Roles of green rust coating are postulated as a combination of two models, semiconductor and coordinating surface: on one hand, green rust concatenates zero-valent iron with the outer surface and delivers electrons to where nitrate is reduced; on the other hand, green rust as a reactive layered double hydroxide provides substantial redox-active sites through its anion exchanging capacity.

Chapter IV of the study focused on the potential mechanism of selenocyanate transformation and immobilization by an activated iron media system. A series of screening tests were conducted, and the results accentuate the importance of dissolved oxygen on selenocyanate removal by ZVI. Radicals that generated from oxidation of ZVI by dissolved oxygen might play an important role in $SeCN^-$ removal. A stoichiometry relationship between ferrous ion and selenocyanate has been established, and the fates of selenium and cyanide group are discussed.

This study generates new knowledge that might be useful for developing a novel reactive media with enhanced ion exchanging capacity for removing selected contaminants, and a more robust AIM treatment system that is not only capable of reductive treatment of target contaminants, but also advanced oxidative degradation of certain contaminants.

ACKNOWLEDGEMENTS

I would like to thank my committee chair, Dr. Yongheng Huang, and my committee members, Dr. Deng, Dr. Lacey, and Dr. Ma, for their guidance and support throughout the course of this research.

Thanks also go to my friends and colleagues and the department faculty and staff for making my time at Texas A&M University a great experience.

Last but not the least, thanks to my mother and father for their encouragement and to my wife for her patience and love.

CONTRIBUTORS AND FUNDING SOURCES

Contributors

This work was supervised by a dissertation committee consisting of Professor Yongheng Huang and Professor Ronald E. Lacey of the Department of Biological and Agricultural Engineering, Dr. Youjun Deng of the Department of Soil and Crop Sciences, and Dr. Xingmao "Samuel" Ma of the Department of Civil & Environmental Engineering.

The XRD for Chapter III was provided by Professor Youjun Deng and the XRD analyses depicted was provided by Chia-wei Lin of the Department of Soil and Crop Sciences.

All other work conducted for the dissertation was completed by the student independently.

Funding Sources

This study was supported by research project “Fundamental and Applied Research and Development of the Activated Iron Media Technology”, which was funded by Evoqua Water Technologies Inc.

NOMENCLATURE

AIM	Activated Iron Media
Br^-	Bromide Ion
Cl^-	Chloride Ion
cm	Centimeter
CO_3^{2-}	Carbonate Ion
CSTR	Continuous Stirred-Tank Reactor
d	Day(s)
DDI	Deoxygenated Deionized
DI	Deionized
DO	Dissolved oxygen
EX_{CAP}	Exchange Capacity
EX_Cl	Exchanged Chloride Ion from Media
F^-	Fluoride Ion
Fe^0	Elemental Iron
Fe^{2+}	Ferrous Ion
Fe^{3+}	Ferric Ion
Fe_3O_4	Magnetite
$FeCl_2$	Ferrous Chloride
$FeCl_2 \cdot 4H_2O$	Ferrous Chloride Tetrahydrate
FeO_x	Iron Oxides

GR(s)	Green Rust(s)
GR_{Cl}	Chloride Green Rust
GR_{SeO4}	Selenate Green Rust
h	Hour(s)
H^+	Hydrogen Ion
H_2O	Water
HCl	Hydrochloric Acid
HRT	Hydraulic Retention Time
IC	Ion Chromatography
KSeCN	Potassium Selenocyanate
L	Liter
LDH	Layered Double Hydroxides
M	Molarity
mg/L	Milligram Per Liter
mM	millimolar
N_2	Nitrogen Gas
N_xO	Nitrogen Oxide
Na_2SeO_4	Sodium Selenate
Na_2SO_4	Sodium Sulfate
NaBr	Sodium Bromide
NaCl	Sodium Chloride
NaF	Sodium Fluoride

$NaNO_3$	Sodium Nitrate
NH_4^+	Ammonium
NO_3^-	Nitrate Ion
nZVI	Nano Zero-Valent Iron
O_2	Oxygen Gas
OH^-	Hydroxyl Ion
ORP	Oxidation-Reduction Potential
rpm	Revolutions Per Minute
Se	Selenium
Se^{2-}	Selenide
$SeCN^-$	Selenocyanate Ion
SeO_3^{2-}	Selenite Ion
SeO_4^{2-}	Selenate Ion
SO_4^{2-}	Sulfate Ion
SSW	Stripped sour waters
USEPA	U.S. Environmental Protection Agency
XPS	X-Ray Photoelectron Spectroscopy
XRD	X-Ray Diffraction
ZVI	Zero-Valent Iron
α-Fe_2O_3	Hematite
α-FeOOH	Goethite
γ-Fe_2O_3	Maghemite

γ-FeOOH	Lepidocrocite
μm	microMeter
μS	microSiemens

TABLE OF CONTENTS

Page

LIST OF FIGURES

Page

LIST OF TABLES

Page

CHAPTER I INTRODUCTION

Iron and Its Impacts on the Environment

Iron (Fe), a metal with atomic number 26, is the fourth most abundant element in the earth's crust after oxygen, silicon and aluminum [1]. As a transitional metal with an electron configuration of [Ar] 3d6 4s2, iron can form compounds with oxidation states ranging from -2 to +7. In the natural environment on Earth, however, iron exists mostly in two valence states: ferrous iron Fe^{II} and ferric iron Fe^{III}. In a very rare case, elemental iron (Fe^0) may be found in meteorites and their deposits. Most of iron in the earth crust is combined with other elements to form various minerals or iron ores. Iron and iron-bearing compounds possess many unique physical, chemical and biogeochemical properties. Iron compounds may exist either in crystalline forms of various particle sizes or in amorphous forms. Some iron minerals exhibit various degrees of magnetic properties. For example, metallic iron (Fe^0) is ferromagnetic while magnetite (Fe_3O_4) is a well-known ferrimagnetic material. While Fe^0 is a relatively reactive metal that can be easily oxidized in contact with O_2 and/or H_2O to form iron oxides or (oxy)hydroxides (commonly referred as iron rusts), iron in most iron-bearing minerals (e.g., goethite, hematite) is relatively stable, but can be dissolved or redox transformed under some conditions. For example, pyrite (FeS_2), commonly present in ores and coals, could be rapidly oxidized by O_2 upon exposure to air, resulting in the oxidation of Fe^{II} to Fe^{III} and the formation of ferric oxides, accompanied by production of acid that is responsible for acidic mining drainage problems [2]. Similarly, under reducing environments, Fe^{III} may be reduced to Fe^{II}, resulting the presence of dissolved Fe^{2+} in some groundwater. Moreover, many species of

microorganisms were found capable of oxidizing Fe^{II} to Fe^{III} or reducing Fe^{III} back to Fe^{II} [3]. The highly reactive Fe^{II}/Fe^{III} redox couple and its interactions with or involvements in many biogeochemical processes play an important role in defining the fate and transport of many pollutants in the environment. The solubilities of Fe^{II} and Fe^{III} in water are highly dependent on the pH and compositional matrix of the water. Fe^{II} may remain relatively stable in forms of Fe^{2+}, $Fe(OH)^{+}$, or $Fe(OH)_2$ in acidic and near-neutral pH, whereas Fe^{3+} in general remains soluble only under a strong acidic environment, but starts to form precipitate $Fe(OH)_3$ once pH rises above 3.0 [4].

In the environment, many iron-bearing minerals have a beneficial effect on contaminant sorption and degradation. Amorphous iron oxyhydroxide-based substrate could work as effective adsorbents for removing various types of contaminants: heavy metals, metalloids, and even organic matters [5-10], thanks to their high specific surface area and the ability to provide electrons (e.g., from the oxidation of Fe^{II} to Fe^{III}). Iron-based layered double hydroxides (LDH), also known as green rusts (GRs), features an intercalation layer of anions in the structure, which are weakly bonded to the main ≡Fe-OH layers and thus provide an anion exchange capacity that may be used to immobilize inorganic and organic anionic contaminants [11].

With such diverse and flexible physical/chemical properties, iron materials and chemistries have provided numerous potentials. Iron-based technologies have been widely used in environmental engineering, e.g., in water treatment and groundwater remediation. Iron materials, generally non-toxic and environmentally friendly, are widely available at low or moderate costs. Among the most important applications, for example, iron salts

such as ferric sulfates are widely used as coagulant in drinking water treatment. Iron ores are often used as sorbent media to adsorb and filter out arsenic from contaminated groundwater [6]. Ferric salts are also used to precipitate phosphate as a polishing posttreatment of municipal wastewater treatment to mitigate nutrient pollution problem [12]. Iron compounds can be used to activate H_2O_2 to facilitate Fenton reactions for the oxidative destruction of persistent organic compounds [13]. Among the newer applications, the use of zero-valent iron (ZVI or Fe^0) as a reactive media for treating environmental contaminants have attracted great interests, resulting numerous research publications and reports of successful industrial application stories, which will be discussed below.

Zero-Valent Iron and its Applications in Environmental Technologies

Zero-valent iron (ZVI, or Fe^0) rarely exists in natural environment because elemental iron, as a reductant, can readily react with O_2 and H_2O, donating electrons and subsequently being oxidized to Fe^{II} or Fe^{III} to form iron rusts (iron oxides). The standard redox potential E^0 of Fe^{2+}/Fe^0 is -0.44 V and E^0 of Fe^{3+}/Fe^{2+} is +0.77 V. As a relatively strong reductant, ZVI can react with many contaminants by directly or indirectly providing electrons and facilitating reductive transformations of contaminants. Such redox reactions could result in destruction of the contaminants or transformation of the contaminants to become less toxic or less soluble thus more readily to be immobilized from the environments. In addition, corrosion of ZVI will produce iron rusts (various iron oxides, hydroxides or oxyhydroxides), which could provide reactive sites for adsorption of contaminants onto the surface, contributing to additional removal of the contaminants

from the environment. In addition, the corrosion products of ZVI may provide a versatile and flexible structure that can incorporate various contaminants, e.g., heavy metals, into its structure and thus safely lock the contaminants inside the iron oxide structures, which can then be securely disposed of.

Thanks to extensive research since 1990s, researchers around the world have developed a rich body of knowledge in ZVI and its uses for environmental applications and a full understanding of the complexity of the underlying chemistries as well as the limitations and challenges of applying ZVI technologies in the real-world implementations [14]. In general, ZVI as a reactive media has been proven effective for treating a variety of environmental contaminants including heavy metals, nutrients, munition wastes, and halogenated organic pollutants in impaired water, soils, and waste streams [6, 15-17].

The great potential of ZVI, however, has yet to be fully fulfilled for environmental applications, mostly due to the ZVI passivation problem --- the loss of ZVI reactivity in aquatic environments due to the formation of a passive iron rust coating on the ZVI surface. Upon the application of ZVI media, the surface of ZVI grains is exposed to not only the target contaminants, but also various constituents in the treated water/soil. ZVI with virgin metallic surface might react with reactive contaminant compounds of target (such as SeO_4^{2-} and Cu^{2+}), but a more significant fraction of ZVI may be consumed by reacting with dissolved oxygen (DO), acidity, or even water:

$$Fe^0 + 3O_2 + H_2O \rightarrow 4\gamma - FeOOH$$

$$Fe^0 + 2H^+ \rightarrow Fe^{2+} + H_2$$

$$Fe^0 + 2H_2O \rightarrow Fe^{2+} + 2OH^- + H_2$$

The initial iron corrosion products such as Fe^{2+}, $Fe(OH)_2$, or $Fe(OH)_3$ could further interact with other constituents in water such as carbonate, silicate, and sulfate and evolve to become more complicated iron corrosion products. These iron corrosion products generated from both the desired or the unintended reactions would gradually wrap around the ZVI surface or fill up the pores within the ZVI media bed, thus isolating the ZVI particles from its surrounding environment. For most aqueous chemical conditions, these iron oxides (in this study, for simplicity, including iron hydroxides and oxyhydroxides) formed are chemically passive. Even if the iron oxides formed during the early stages of the reaction might be porous, adsorptive and partially activated, the continued buildup of corrosion products and the aging process from dehydration, cementation and (re)crystallization of iron oxides will further lower the surface and structural porosity and eventually prevent direct ZVI-contaminant interactions. The surface iron rust layers become an insurmountable barrier for electron transfer and ion migration, which is imperative for any reactions between ZVI and target contaminants. Surface passivation is a natural process that will restrain and eventually stop the ZVI core from interacting with contaminants, which leads to loss of its reactivity [18].

In the past decades, many trials and efforts have been attempted to overcome this passivation tendency of ZVI media to fulfill its potential for environmental application. Guan, Sun [14] had summarized the mechanism and drawbacks of most important developments in ZVI technology based on the commonalities and characteristics of these countermeasures. Taking one of the popular topics as an example, nano-sized ZVI (nZVI) has many advantages comparing to regular iron powder (measured in micron in particle

size) employed in common ZVI techniques. As particle size decreases, its specific surface area increases dramatically, giving it a highly reactive feature to adsorb and interact with other atoms, molecules and complexes [19]. Such high reactivity, however, will lead to poor longevity. Much of the nZVI media may be wasted by reacting with O_2 and H_2O, thus reaching the reactive exhaustion in a very short timescale. Even then, nZVI may still face the passivation problem in the groundwater remediation [14]. NZVI is much more expensive due to the relatively complex manufacturing process, which would reduce the competitiveness of nZVI against other in situ treatments [20, 21].

Among many modified techniques to overcome the limitations of conventional ZVI technology, the activated iron media (AIM) technology, also known as hybrid ZVI technology developed by Huang's group stands out with great strengths and less drawbacks [22, 23]. The activated iron media technology overcomes the passivation problem, does not require extra amounts of energy input, and has a relatively long service lifetime. The schematic diagram is shown in Figure 1. According to Guan, Sun [14], the only drawback is the generation of extra sludge and introduction of some unexpected anions (e.g., SO_4^{2-}) in the treated solution.

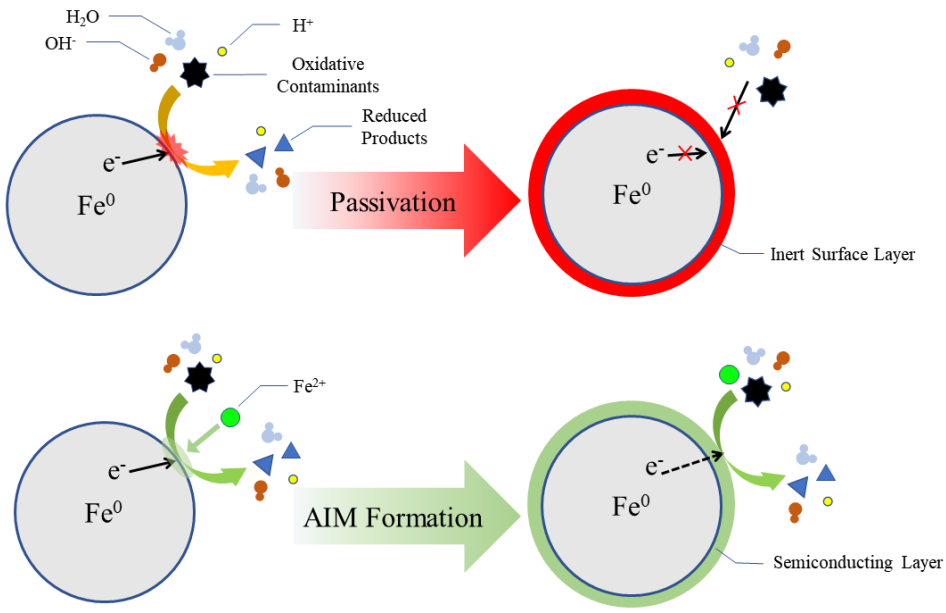

Figure 1 Schematics of ZVI passivation and the mechanism of AIM to overcome surface passivation problem and maintain high reactivity of the media system.

Activated Iron Media

The fundamental approach by Huang and his group to overcome the ZVI passivation problem is to regulate the aqueous chemical environment to manipulate iron corrosion chemistry towards formation of an iron oxide coating(s) that is conducive to electron transfer and ion migration. With high electron and ion conductivities, an iron oxide coating can still effectively media redox reactions even if the ZVI is not in direct contact with the contaminants. Huang identified a magnetite-like iron oxide with an inverse spinel structure and non-stoichiometric Fe^{II}/Fe^{III} ratio as the preferred iron corrosion products to sustain ZVI reactivity. The engineered FeO_x features a flexible structure with adequate lattice holes and vacancies, which enable fast electron transfer and

rapid oxygen and iron ion migrations to support redox reactions. The effort results in the development of the activated iron media technology.

One method to prepare the activated iron media could be achieved by introducing ferrous ion (Fe^{2+}) into a ZVI-NO_3^- system to enable rapid reduction of nitrate by Fe^0 and form magnetite as the corrosion product instead of other forms of iron oxides [17]. The stoichiometry of the overall reaction is described as Eq. (1).

$$NO_3^- + 2.82Fe^0 + 0.75Fe^{2+} + 2.25H_2O \rightarrow NH_4^+ + 1.19Fe_3O_4 + 0.50OH^- \quad (1)$$

Huang [24] proposed a two-layer semiconducting model to explain the iron corrosion mechanism involved in the rapid nitrate reduction by Fe^0 enabled by externally added Fe^{2+}. The theory lay the groundwork that helped develop an engineered mixed ZVI and FeO_x reactive media that is now called the activated iron media technology. The model features a layered iron oxide coating to explain the reactivity of ZVI and the role of Fe^{2+}. The inner layer is mainly magnetite (Fe_3O_4), which is a very good semiconductor. Magnetite, a mixed Fe^{II} and Fe^{III} oxide with an inverse spinel structure, features a narrow band gap (~0.1 V) between the valence band and conduction band, which allow e^- to move almost freely within the structure. As such magnetite can serve as an electron bridge between ZVI core and the outer layer. The outer layer of iron corrosion coating, however, is often exposed directly to contaminants (e.g., nitrate), DO (O_2) and other strong oxidants, and thus tends to be fully oxidized to become ferric oxides. Huang theorized that the outer layer could be maghemite (γ-Fe_2O_3) or lepidocrocite (γ-FeOOH), which are poorly conductive and thus inhibitive for electron migration. To maintain the high Fe^0 reactivity,

external Fe^{2+} was provided to facilitate transformation of passive ferric oxide coating to a reactive magnetite layer.

The new engineered media solve the surface passivation problem of traditional ZVI technology [17, 23, 25], which was then applied to develop a hybrid ZVI/Fe_3O_4 treatment system for remediating various contaminants in impaired water [26, 27]. Since only regular ZVI powder (not nZVI) and limited supplementary chemicals are consumed and more importantly, since all ZVI could now be utilized without the passivation problem, the overall consumption of ZVI and solid waste production has been greatly decreased [22]. In both laboratory and field tests as well as full-scale industrial implementation, the AIM technology has been proved cost-effective in treating various dissolved heavy metals from industrial wastewater such as mining drainage, refinery stripped sour water and flue-gas desulfurization wastewater from coal-fired power plants.

Huang, Zhang [17] also noticed that in the process of forming a Fe_3O_4 coating on ZVI grains (using the ZVI / NO_3^- / Fe^{2+} recipe), a thin, unstable intermediate coating was formed initially on the surface, which would subsequently transform into magnetite as reaction continued. This transient precursor of magnetite was not positively characterized at the time, but it was postulated to be a green-rust type iron compound. Recent studies on the mechanism of SeO_4^{2-} transformation and immobilization by the AIM [28] shown a phase of rapid SeO_4^{2-} decrease at the very beginning of the reaction (though not highlighted by the author). Similar phenomena of a fast-initial removal of SeO_4^{2-} were also observed in most of our recent AIM batch tests. Simple surface adsorption of selenate on FeO_x could not account for such a large-scale removal of selenate since selenate barely

adsorb on iron oxide surface. Based on our experimental observation, such rapid selenate removal could be achieved by an ion exchange process. All anecdotal evidence suggested that the unidentified intermediate or precursor iron oxides may be responsible for the initial rapid removal of selenate via an anion exchanging process and that a green rust may be the source of such ion-exchangeability, which will be the center subject of this study.

Statement of Problems and Knowledge Gaps

The chemistries and processes in a ZVI-based treatment system can be extremely complicated, entangling a variety of physical and chemical parameters and processes. The complexities are multi-faceted. First, for applications in industrial wastewater, groundwater or soil remediations, the water or soil media, composed of different constituents, is often a complex system with constantly changing conditions. Second, iron chemistry by itself could be extremely complicated. Besides the reactivities of the target contaminants, the chemistry of ZVI and the system performance may be affected by many factors such as pH, ORP, alkalinity/acidity, ionic strength, ionic charges, constituents in water, initial conditions of ZVI surface, compositions/impurities of ZVI. Aquatic chemistries such as Fe^{2+} interactions with H_2O and O_2, interfacial chemistries such as the interactions between contaminants and the surface reactive sites on the iron corrosion coatings on ZVI surface, the crystallography and solid-state chemistry responsible for the development, growth and evolution of the iron corrosion coating are all an extremely complicate chemical process. In addition, mass transfer, a physical process, could be another key factor. Adding to the complexity, these different factors and processes are

intertwined with each other, and the system often proceeds in a dynamic way that changes and evolves over time.

Despite of the great effort and advancement made by ZVI researchers over the past decades, our current knowledge of the ZVI technology is still far from adequate to reliably predict the behavior of many ZVI treatment system and solve many known or unexpected challenges. Regardless of the success of AIM in water and wastewater treatment and the general understanding of the underlying mechanisms, there are still many key questions unanswered and many phenomena unexplained. The intricacy of the chemistry/mechanisms will require much more in-depth investigations to elucidate. Specifically, this study aims to address three fundamental questions remained unanswered so far in the practice of the AIM for wastewater treatment.

Preferential reactivity of the AIM for contaminants

We repeatedly observed preferential removal of certain anions over other anions by the AIM. In the tests, AIM was found to remove certain anion contaminants prior to others. For example, when using AIM to treat a simulated wastewater with the copresence of nitrate and selenate, the reduction of NO_3^- appeared to be significantly inhibited by SeO_4^{2-}: nitrate reduction would start only after SeO_4^{2-} was completely removed from the water. Similarly, in an earlier study, it was found that in the co-presence of nitrate and nitrite, nitrite reduction proceeded prior to nitrate reduction [29]. In contrast, in the co-presence of nitrate and DO, both nitrate and O_2 could be removed by ZVI/Fe^{2+} simultaneously [25]. These phenomena of preferential removal hierarchy for reactive anions in a Fe^0/Fe^{2+} system could not be convincingly explained by our understanding of

the two-layer semiconductor model or from the literature reports of our peer researchers. For the selenate and nitrate scenario, it is particularly intriguing that for a biological metal removal system such as ABMet® (GE), microbes were found to remove nitrate first and only when nitrate was completely removed, microbes would start to target selenate. A better understanding of the mechanism involved may help predict the performance of AIM when dealing with unfamiliar wastewater. We might even manipulate the AIM system to treat target contaminants instead of wasting the media's reactivity on other reactants.

Initial removal capacity of the AIM

During our recent studies, we found that freshly prepared activated iron media possess an unusually high capacity that can rapidly (virtually instantly upon contact) remove a large amount of selenate, followed subsequently by a steadier removal of selenate over extended period of reaction time. For example, it was found in some batch tests that a concentration of 50 g/L AIM could remove over 30 mg/L of selenate (as Se) in as short as 5 min contact time. Upon the exhaust of the initial capacity, the same media would take more than 6 hours to reduce additional 30 mg/L selenate. The nature of the high initial removal capacity and its relationship with the subsequent steady reduction capability of the AIM is still mysterious to us. The intuition as well as anecdotal evidence suggest that the initial capacity might be related to adsorption or ion exchanging process and certain intermediate products of FeO_x in the fresh AIM may be responsible for the phenomena. Investigation into this initial capacity of fresh AIM might not only help understand the nature of this capacity, but also produce new clues regarding the mechanism behind the preferential removal of selenate over nitrate as well as shedding

new light on the role of dissolved Fe^{2+}. For the real-world application, understanding of the origin of this initial capacity might help us create a "super-charged" media that could significantly reduce the required reaction time and improve the cost-effectiveness of the AIM system for treating some recalcitrant contaminant such as selenate.

Better method to produce the AIM of higher quality

Using NO_3^- to react with ZVI under controlled conditions (via Eqn.1) to form magnetite as a method of preparing the AIM would result in production of a significant amount of NH_4^+. Unfortunately, ammonia is a regulated pollutant, not an environment friendly product. For the full-scale production and application of the AIM technology, this nitrate-based method may not be a good approach. Developing an alternative method using none or less nitrate to prepare the activated iron media is necessary. Since NO_3^- here serves primarily as an electron acceptor, substitution of nitrate with other oxidants (e.g., oxygen) might be doable, which can reduce the undesirable NH_4^+ production.

Rationales of Proposed Research

Hypotheses

To investigate the mechanism of AIM removing anionic contaminants, this research delves into a phenomenon observed repeatedly in many of trial tests. As mentioned above, a rapid and significant removal of SeO_4^{2-} was observed upon contact with freshly synthesized AIM, which happened only if the AIM was freshly formulated. Such initial removal capacity would quickly diminish once the AIM media was exposed to air, aged, or dried. The initial rapid removal of SeO_4^{2-} by the AIM was accompanied

with a significant release of Cl^- ion from the media into the aqueous phase and a noticeable increase of pH. These results suggested that an anion exchanging process might be responsible for the instant removal of selenate. Fresh AIM media carry exchangeable anions, but once aged or dried, such capacity disappears. Green rust is known to carry exchangeable anions. Green rust, an unstable compound, is also known to readily transform (mostly be oxidized) into more stable forms of iron oxides such as magnetite or lepidocrocite (γ-FeOOH), which does not carry any significant anion exchanging and/or surface adsorption capacity for selenate ions. Based on these observations as well as general understandings from previous works of this group, we formulate a few core hypotheses for this study:

- The observed initial capacity of freshly prepared AIM in wet form is due to the presence of green rusts as an intermediate or precursor product that forms part of the iron corrosion products under controlled conditions. As a layered double hydroxide, green rusts possess a significant anion exchangeable capacity. As a transient phase of the iron corrosion product, green rusts could evolve into more stable iron oxide products.

a) Iron corrosion coating on ZVI surface is not a homogeneous layered structure, but a porous, heterogeneous structure with localized compositions and properties that serve as hot spots for different reactivities: i.e., e- transfer might occur at one site, while OH^- and O^{2-} ions may diffuse from other sites. The green rust structure might be more likely formed at the bottom of pores that is closer to Fe^0.

b) The oxidation of Fe^{II} to Fe^{III} plays an important role in triggering the formation of green rusts. Thus, the presence of an oxidant like nitrate, selenate or O_2 may play an essential role in facilitating green rust formation on ZVI surface.

- For reactive anionic contaminants, incorporation of the anion into the green rust structure (the intercalated layer of layered double hydroxides) is an important pathway towards its final reduction. The anion exchanging coefficient for different anions is responsible for the observed preferential removal of certain anions over other anions.

a) The oxidizing anions such as nitrate and selenate, once entering the intercalating layer, could obtain electrons from the main FeO_x layer and shed O to the FeO_x structure and be reduced. In the process, some Fe^{II} is oxidized to Fe^{III}, triggering further growth of GR structure. For selenate, Se^{VI} could be reduced to become Se^0 and then Se^{-II} to form a bond of -Fe-Se^{-II} in place of -Fe-O^{-II}.

b) Anions in reduced oxidation state such as $SeCN^-$ can also be incorporated into the intercalating layer of the green rust structure. Transformation of the $SeCN^-$ would depends on the oxidative breakdown of the $SeCN^-$. Under an oxic environment, O_2 may be activated by the AIM to become higher reactive O species (such as singlet O_2 or hydroxyl radicals) that can oxidize $SeCN^-$, break up Se-CN bond, and subsequently AIM incorporate Se in reduced =Fe-Se^{-II} form into the structure.

c) Non-reactive anions such as Br^- and Cl^-, if incorporated in the green rust structure, will remain steady. If green rusts are oxidized to become magnetite (or others depending on conditions), most of these anions could be ejected out of the FeO_x structure.

- The externally added Fe^{2+} might play a role in triggering the formation of new green rust in conjunction with anionic contaminant as an oxidative reactant.

Research Objectives

- Elucidate the nature of the initial treatment capacity—the intercalating exchangeable anions of green rusts formed as precursor or intermediate products of ZVI-nitrate-Fe^{2+} reaction system.
- Establish a competitive hierarchy of the green rusts-encompassed AIM for different anions and develop a model to describe the interactions of anions mechanistically and quantitatively with the activated iron media.
- Explore the potential of synthesizing large quantity of green rusts with a small amount of ZVI to produce a media that primarily consists of green rust.
- Using our understanding on the role of anion exchanging capacity to explain the mechanism of $SeCN^-$ removal by an AIM system.

CHAPTER II

ANION EXCHANGE CAPACITY OF ACTIVATED IRON MEDIA: PRELIMINARY MECHANISM ANALYSIS

Introduction

Zero-valent iron, the elemental form of iron, had already been proved to be a relatively low-cost reducing agent. ZVI shows a great potential in removing various environmental contaminants from soils, groundwater, and many other waste streams [15, 16, 23]. However, this desired ability of Fe^0 could not be implemented easily in many practical situations, mostly due to ZVI surface passivation. Fresh Fe^0 tends to react with oxygen in humid environment, and once Fe^0 contacts oxidizing contaminants, layers of iron oxides would start generating on Fe^0 surface due to iron corrosion, wrapping around and isolating the Fe^0 particles from its surrounding environment. For most aqueous conditions, this iron oxide layer is chemically passive and could gradually stop the internal Fe^0 from reacting with pollutants, which leads media to loss its activity [18].

The invention of the Activated Iron Media technique by Yongheng Huang greatly improve the application value of ZVI by introducing ferrous ion (Fe^{2+}) into the system, stimulating the formation of magnetite instead of other forms of iron oxides, generating this new composition of media which successfully conquered the passivation problem caused by corrosion [17, 23, 25]. In both laboratory and field tests, this technology has been proved effective in treating various dissolved heavy metal and NO_3^- from industrial wastewater such as mining drainage, refinery stripped sour water and flue-gas desulfurization wastewater from coal-fired power plants.

Selenate (SeO_4^{2-}) is selenium's fully oxidized Se^{VI} form, which has a tetrahedral oxyanion structure. In solution Se^{VI} exists as $HSeO_4^-$ or SeO_4^{2-} with an acid dissociation constant pK_a =1.7. Due to its structural similarity with SO_4^{2-}, it has been observed by researchers that both oxyanions form similar surface complexes [30]. It has been proved that activated iron media (AIM) has highly effective performance for removing heavy metals and NO_3^- from flue-gas-desulfurization wastewater [26, 27], in which the major selenium source was SeO_4^{2-}. Recently, some studies have been researched concerning the mechanism of SeO_4^{2-} transformation and immobilization by AIM [28]. It was shown in the article that there was a rapid SeO_4^{2-} decrease at the very beginning, and similar phenomenon of a fast-initial removal of SeO_4^{2-} was also observed in most of our AIM batch tests. Based on literatures and experimental facts, it is assumed that ion exchange might be responsible for this rapid SeO_4^{2-} removal.

Ion exchange is widely used in many areas as a water treatment process of purification, separation, and decontamination which targets unwanted ions in aqueous and other ion-containing solutions. Usually the most useful ion-exchange reactions are reversible since the media can be regenerated by an excess pre-saturated ion solution and be reused many times before exhaustion [31]. However, our study subject, the AIM-based ion exchanger, was considered long-term effective by growing new exchanging surface instead of exhaustion/regeneration cycling. Huang et al. [17] reported that in the process of AIM formation (using ZVI & NO_3^- & Fe^{2+} recipe) there was a thin, unstable intermediate layer coating on the surface, which would readily transform into magnetite.

This transient precursor of magnetite, while not positively characterized at the time, was postulated to be a green-rust type iron compound.

Materials and Methods

Materials and Chemicals

All involving chemicals used in the experiments were of analytical reagent grade, including $FeCl_2 \cdot 4H_2O$ (>99%, J.T. Baker, NJ), HCl (6N, BDH, PA), $NaNO_3$ (>98% Alfa Aesar, MA), NaCl (>99% BDH, PA), Na_2SO_4 (>99% BDH, PA), and Na_2SeO_4 (>99.8% Alfa Aesar, MA). All tests were carried out using -325 mesh ZVI (>95% Ferox Target ZVI Reactive Iron Powder, Hepure Technologies Inc., NJ). All reagent solutions were prepared with deionized deoxygenated (DDI) water with resistivity around 18.2 MΩ-cm (E-Pure™, Barnstead, USA) and stored in anaerobic chamber (Coy Laboratory, MI) which was filled with approximate 95% N_2 and 5% H_2 and equipped with a palladium catalytic O_2 removal system and an O_2 sensor to ensure an anoxic environment. Stock solution of 50 mM Fe^{2+}, 140 mM NO_3^-, 1000 mM Cl^-, 31.25 mM SO_4^{2-}, 12.66 mM SeO_4^{2-} were prepared in advance. Serum vials (10 ml, Kimble Chase) were employed with rubber stoppers as reactors. Multiple reactors were prepared under the equivalent condition. The general procedures for batch tests were as followed: (1) DI water was purged with ultra-high purity nitrogen gas for at least 1 hour, then stored in the anaerobic chamber for at least 12 h to make it deoxygenated before use. (2) In anaerobic chamber, stock solutions were prepared by dissolving pre-weighted chemicals (e.g., $FeCl_2 \cdot 4H_2O$) in deoxygenated DI (DDI) water. (3) Reactors with pre-weighted ZVI powder at 50 g/L were transferred in

anaerobic chamber, and 10 ml total of solution consisting of predetermined concentration of chemicals was transferred into each reactor. (4) The reactors were placed in a rotating opaque box at 30 rpm for mixing. (5) At predetermined times, reactors were taken out and the supernatant was extracted and filtrated through 0.45 μm membrane filters (VWR) for later analysis.

Experimental methods

Preparation of the Activated Iron Media

To study the anion exchanging capacity of the AIM for SeO_4^{2-} removal, it is necessary to convert ZVI into the AIM in advance. Following a previous used method [17], the AIM system could be prepared by introducing NO_3^- and Fe^{2+} into a ZVI system, in which NO_3^- could be rapidly reduced by ZVI with magnetite (Fe_3O_4) as the main corrosion product (Eq. (1)).

$$NO_3^- + 2.82Fe^0 + 0.75Fe^{2+} + 2.25H_2O \rightarrow NH_4^+ + 1.19Fe_3O_4 + 0.50OH^- \quad (1)$$

For this study, the AIM was prepared freshly in 10 mL serum vials for each test. For a typical rapid SeO_4^{2-} removal procedure as shown in Figure 2, 0.5 g ZVI and 0.75 mL of 50 mM Fe^{2+}, 0.36 mL of 140 mM NO_3^- and 8.89 mL DDI water (add up to 10 mL liquid) were added into reactors anaerobically, corresponding to the AIM recipe of 50 g/L ZVI + 3.75 mM Fe^{2+} + 5.0 mM NO_3^-. After mixing for 20 h, about 90% of nitrate would be reduced by ZVI, consuming about 8 mg ZVI and forming about 14 mg iron oxide in forms of either a black coating on ZVI surface or as discrete black precipitate in the reactor. The reactors with the freshly prepared media were transferred back to the

anaerobic chamber and rinsed three times before conducting tests. Rinse process aimed to remove any residual reactants such as NO_3^- and Cl^- in solution as possible interfering factors.

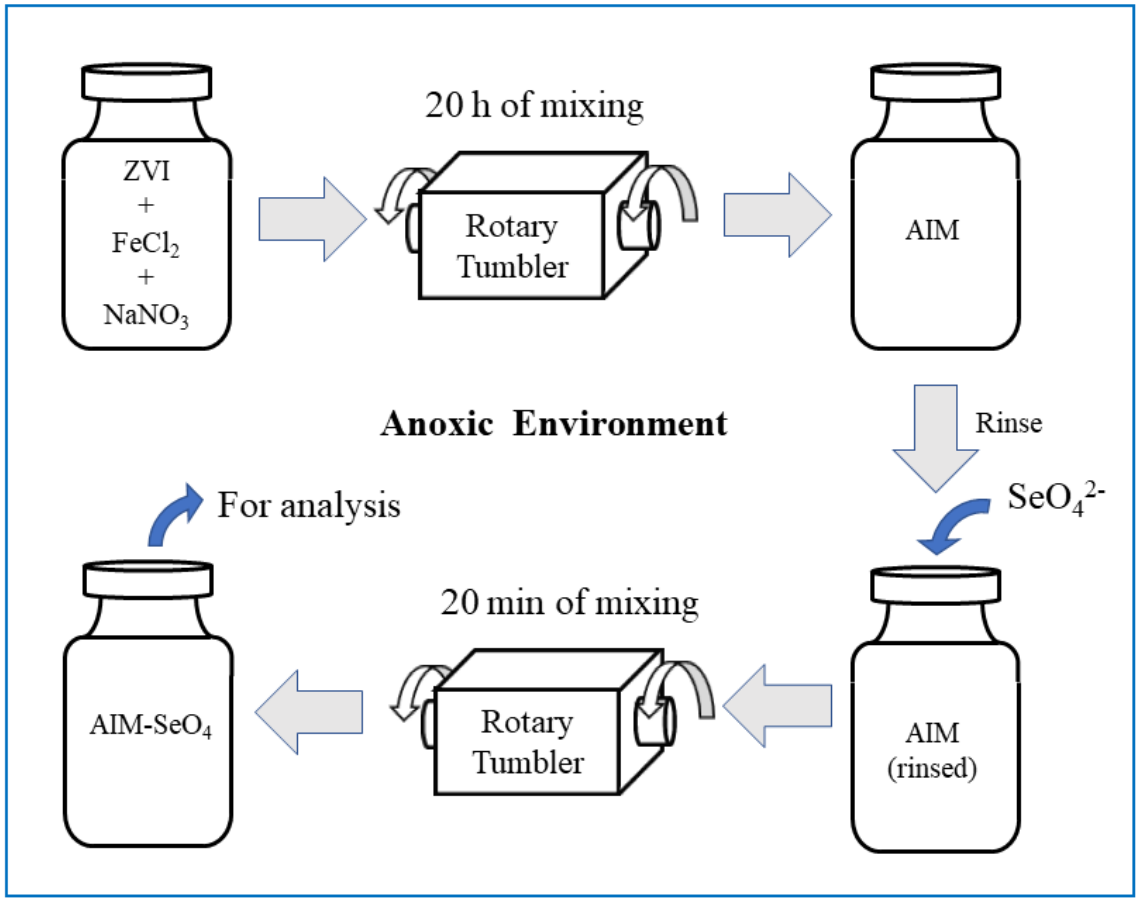

Figure 2 Schematic diagram of a typical rapid SeO_4^{2-} removal procedure.

The rinsing procedures went as followed (shown in Figure 3): (1) put a strong magnet at the bottom of the vial to attract and fix nearly all media to the bottom; (2) removed the capped rubber stopper and dumped the supernatant as much as possible; (3) removed the magnet and filled the vial with about 10 mL DDI water; (4) capped the vial with rubber stopper and then shaked for 10 seconds; (5) let it stand and deposit for 30

seconds, then repeated step 1. After rinsed for 3 times, the media was considered in a steady state in DDI water.

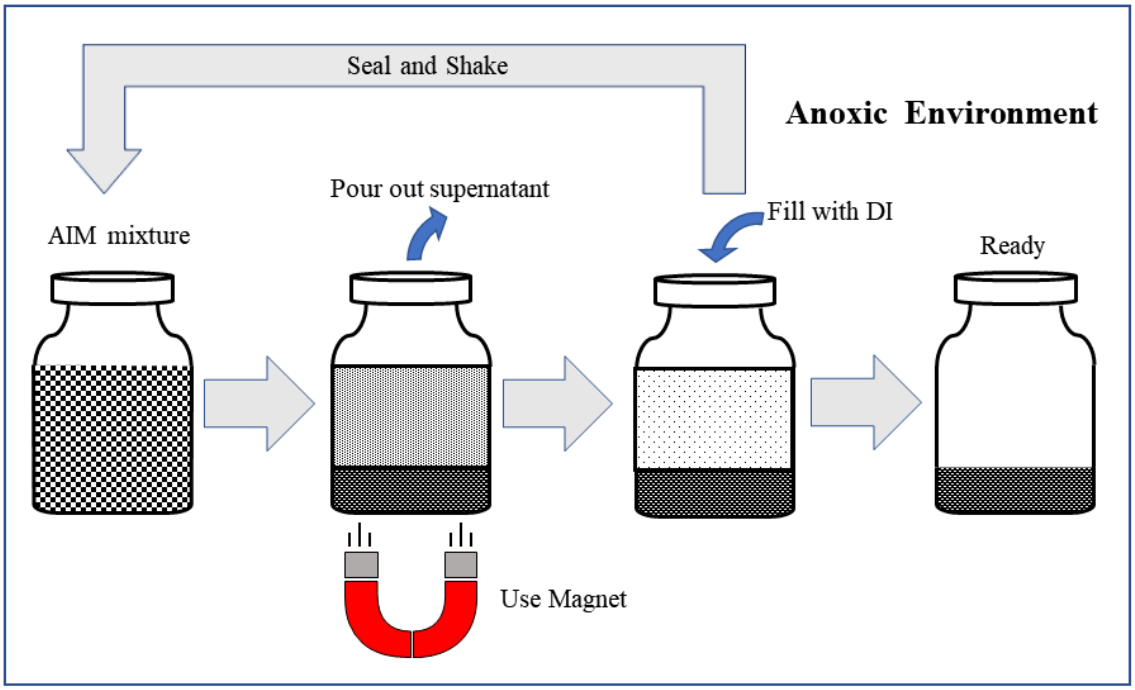

Figure 3 Schematic diagram of the rinsing process.

Anion Exchanging Batch Tests

All batch tests in this study were prepared in the anaerobic chamber to limit O_2 exposure from air. For anion exchanging tests, designed combinations and amounts of reagent solutions (SeO_4^{2-}, SO_4^{2-}, NO_3^- or Cl^-) and DDI water were added into a batch of reactors with freshly prepared AIM under the same recipe and mixing time. The reactors were sealed and transferred into the same rotary tumbler (30 rpm) to provide complete mixing at room temperature while avoiding light. At predetermined intervals (mostly 20 min or specified otherwise), one reactor would be withdrawn and opened for sampling and

analyses. The reactant solution was forced through a 0.45 μm membrane (VWR) and the filtrate was collected for pH and various compositional analyses.

SeO_4^{2-} Re-dissolution Test

Selenate re-dissolution tests were conducted to evaluate the stability and fate of selenate removed upon contact with the AIM. Following the anion exchanging test with SeO_4^{2-}, the resulting SeO_4^{2-}-containing media (noted as AIM-SeO_4^{2-}) was rinsed with DDI for 3 times to remove any residual aqueous SeO_4^{2-} from the system. The reactors were then filled with DDI and placed in the tumbler for additional post-exchanging reaction (0 as the control, 0.5, 1.5, 4, 8, or 24 h). Once reactor was withdrawn, the media was rinsed with 30 mM Cl^- solution for 4 times. All rinsing solution was collected and analyzed for SeO_4^{2-} that was extracted by Cl^-.

Impact of O_2 on AIM Properties

This test was to assess how O_2 would affect the AIM with respect to its anion exchanging capacity. In the reactor with freshly prepared AIM, 1 mL of gas was extracted from the headspace and 1 mL of pure O_2 gas was injected using a syringe. The reactors were mixing in the tumbler for additional 0 (as control), 10, 30 and 60 min, which allowed O_2 to interact with the AIM. The O_2-treated media was sonicated for 2 min; the stripped-off FeO_x fine crystalline were collected and dissolved in 6 N HCl to determined Fe^{II}/Fe^{III} ratio change by O_2 exposure. The O_2-treated media were then used to conduct anion exchanging tests with 2 mM of SeO_4^{2-} to assess impact of O_2 on AIM capacity.

Sample Preparation and Analytical Methods

The filtrate was collected for IC (ion chromatography) analysis. A Dionex ICS-1100 system (Dionex Co., Synnyvale, CA) was used to analyze SeO_4^{2-}, SO_4^{2-}, NO_3^- and Cl^-. Separation was achieved using a Dionex IonPac AS22 column with an AG22 guard column. The minimum detection limit were 0.1 mg/L. Dissolved Fe^{2+} was measured colorimetrically with the 1,10-phenanthroline method at the wavelength of 510 nm [32] on a UV-Vis spectrophotometer (M&A Instruments Inc., CA). pH of filtrate was measured by Orion 2-Star Benchtop pH Meters (Thermo Fisher Scientific Inc., MA).

X-ray powder diffraction (XRD) and X-ray photoelectron spectroscopy (XPS) were used for characterizing iron oxide properties as well as the status of Se in the media. To prevent ZVI from altering iron oxides or interfering with analyses, the iron oxide coating was separated from ZVI. For such purpose, the media of interest was first rinsed with DDI for 3 times and then the reactor were sonicated for 10 min to strip off the iron oxide coating from ZVI surface. The iron oxide crystalline, which was submicron in size, remained suspended while ZVI grains in size of microns quickly settled to the bottom within seconds. Upon transferring into the anaerobic chamber, the reactors were fully shaken and then settled for about 10 s to allow heavier ZVI particle to settle at the bottom. The top half of the liquid with fine suspended FeO_x particles were withdrew and forced through 0.45 μm filter papers (Pall Laboratory, USA), which formed a paste on paper that was used for XRD or XPS analyses.

X-ray powder diffraction (XRD) patterns were recorded by Bruker-AXS D8 Advanced Bragg-Brentano X-ray Powder Diffractometer with Cu Kα radiation at a

wavelength of 1.5406 Å. Because the collected media may be sensitive to oxygen, the filter papers with sample paste will be treated with a few drops of glycerol in the anaerobic chamber and stored in anaerobically sealed containers before testing to prevent oxidation or dehydration [33]. Once prepared, XRD analyses were conducted within 1 hr.

The oxidation state of Se was determined by X-ray photoelectron spectroscopy (Omicron XPS/UPS system with Argus detector) using Mg Kα X-ray radiation at 1253.6 eV. Samples after preparation were dried anaerobically in a vacuum desiccator for two days. Constant Analyzer Energy (CAE) of 20 eV, a step size of 0.05 eV and dwell time of 0.5 s were used to obtain the high-resolution spectra. The binding energy of adventitious carbon (C (1s)) was set at 284.8 eV as the calibration reference peak to compensate the charging effect. The assignment of different Se speciation was based on NIST X-ray photoelectron spectroscopy database.

Results and Discussion

Anion Exchanging Capacity

To study the anion exchanging capacity (EX_{CAP}) of newly synthesized AIM on SeO_4^{2-} removal, it is necessary to set a reacting time interval since AIM could also slowly remove SeO_4^{2-} within a relatively longer period [28]. AIM was prepared with a recipe of 50 g/L ZVI + 3.75 mM Fe^{2+} + 5 mM NO_3^-. Time of synthesis process was controlled at 20 h. Aqueous Fe^{2+} was undetectable after 20 h and NO_3^- remained about 0.45 mM in the reactor. After rinsed with DDI, 2 mM SeO_4^{2-} was added in the reactor. Changes of remaining SeO_4^{2-} and pH was monitored and shown in Figure 4. At 20 min, SeO_4^{2-} had

already reached over 95% removal percentage of which at 2 h. Therefore, the mixing time of EX_{CAP} for SeO_4^{2-} in this study was set at 20 min for any other tests.

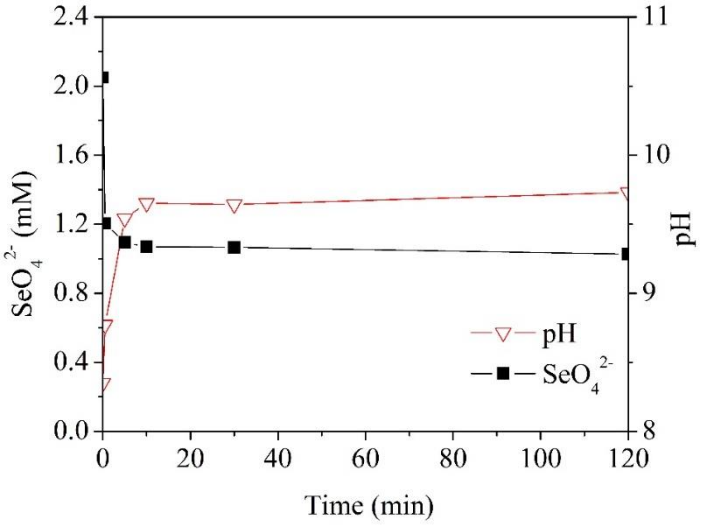

Figure 4 Changes of remaining SeO_4^{2-} and pH after reacting with newly synthesized AIM as a function of time.

In the following sessions, several potential impact factors of EX_{CAP} were evaluated from 3 different aspects: the anion exchanging process, the synthetic process, and the influence of oxygen on EX_{CAP}. Anion affinity order on the newly synthesized AIM was first studied. The influences of synthetic time and the amount of additional Cl^- within the AIM synthetic process were also investigated. After the formation of fresh AIM, whether oxygen could compromise EX_{CAP} was also confirmed. Analyzing these factors would provide much helpful information about the EX_{CAP} mechanism.

Anion Affinity Order

Anion affinity was investigated by introducing different combinations of anions (SeO_4^{2-}, SO_4^{2-}, NO_3^- or Cl^-) into freshly synthesized AIM system. The synthetic time was

set at 20 h. Each combination started with 2 mM of involved anions, and any concentration change after 20 min was marked as "Δcomponent" in Figure 5. Positive/negative values in Figure 5 indicated increase/decrease changes of concentration of that component. It is assumed that any anion concentration variation was hypothetically considered as anion exchange.

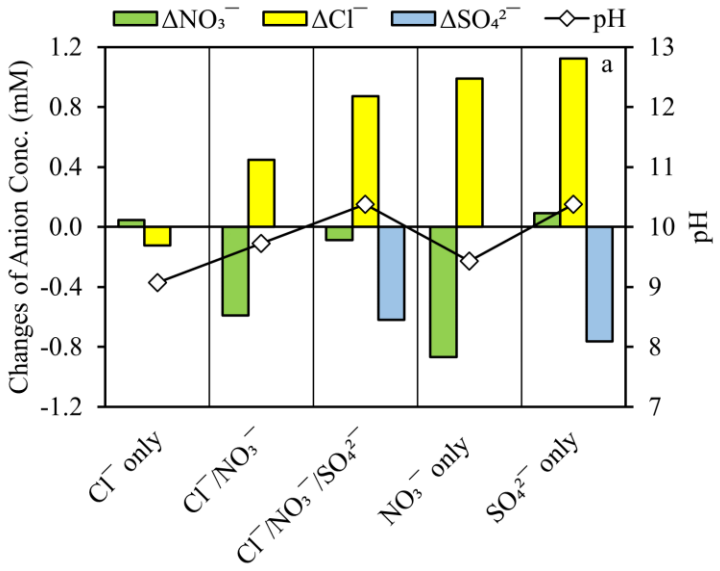

Figure 5 Anion concentration changes and pH after mixing fresh AIM (20 h) with a solution of different combinations of 2.0 mM Cl^-, SO_4^{2-}, NO_3^- or SeO_4^{2-} for 20 min. (a) Combinations without SeO_4^{2-}; (b) Combinations with SeO_4^{2-}.

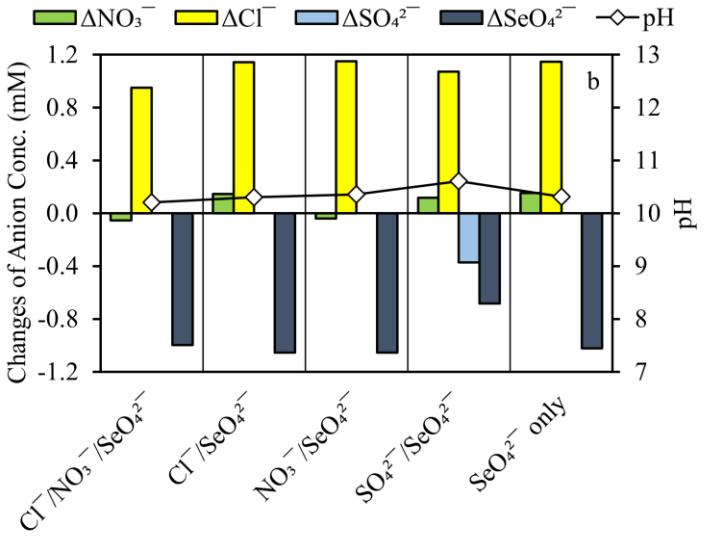

Figure 5 Continued

Comparing the [Cl^-/NO_3^-] set with the [Cl^- only] set, it demonstrated that AIM showed higher ion affinity towards NO_3^- than Cl^- on newly synthesized AIM. Similarly, Cl^- was considered to possess the least affinity comparing to other anions because it was mostly released back to solution in most combinations. The highest exchanged Cl^- amount was ~1.15 mM, which was essentially the amount of Cl^- that disappeared from the recipe after AIM preparation (Figure 6a). Therefore Cl^- would not be incorporated into structures during AIM formation stage, and it will be replaced by other anions easily.

Comparing [$Cl^-/NO_3^-/SeO_4^{2-}$], [Cl^-/SeO_4^{2-}], [NO_3^-/SeO_4^{2-}] and [SeO_4^{2-} only] sets, the reduced amount of SeO_4^{2-} in the four combination sets were all around 1 mM. NO_3^- could only be adsorbed by a very small amount only if it had been in the combination at the beginning. These data strongly suggested that SeO_4^{2-} could be more easily absorbed to the surface of newly synthesized AIM than Cl^- and NO_3^-. Since the amount of

SeO_4^{2-} adsorption was roughly the same for these four sets, it meant that within a similar concentration level, Cl^- and NO_3^- had nearly no impact on SeO_4^{2-} removal. In contrast, the existence of SeO_4^{2-} greatly reduced the ability of AIM to adsorb NO_3^- and Cl^-.

SO_4^{2-} is structurally analogous to SeO_4^{2-}, so it was reasonable to assume that SO_4^{2-} had a similar behavior to SeO_4^{2-}. Hence, the two anions were expected to show competitive evidence to each other on AIM surface adsorption. To test this hypothesis, the data of [SeO_4^{2-} only], [SO_4^{2-}/SeO_4^{2-}] and [SO_4^{2-} only] sets were compared, and the results were consistent with the expectation. SeO_4^{2-} was slightly more attractable than SO_4^{2-} since its individual reduced amount was higher than SO_4^{2-}, and it was less affected when mixed. Both NO_3^- and Cl^- were released from AIM in these combinations.

pH of the final solution was also monitored to help reveal the behavior of H^+ and OH^- during the ion exchanging process. Since AIM was fully rinsed before each test, its ability to change pH within a short time was considered negligible. Most of the stock solutions, including DDI water, were neutral or slightly alkaline (pH = 7~8). The only reagent that might affected the solution's starting pH the most was the SeO_4^{2-} solution, of which the pH at 2 mM was ~8.35. The results showed that pH for all tests increased after mixing, which means that OH^- was one of the anions that had been released from this rapid ion exchange reaction. This pH increase was especially significant (pH > 10) for the combinations with SO_4^{2-} and SeO_4^{2-}, which showed a ~0.2 mM increase in OH^- concentration.

Ion affinity of targeting anions on newly prepared AIM was investigated and it was clearly shown that the SeO_4^{2-} was most attracted to AIM among all mentioned anions,

followed by SO_4^{2-}, NO_3^-, and finally Cl^-. OH^- was also involved in the ion exchange process, but its affinity was not specifically discussed in this experiment.

AIM Synthetic Time

A serial of tests was conducted to investigate the influence of AIM synthetic time on SeO_4^{2-} EX_{CAP} shown in Figure 6. Most steps were exactly as mentioned in preliminary test, and the only difference was the synthetic time of AIM prior to the EX_{CAP} test.

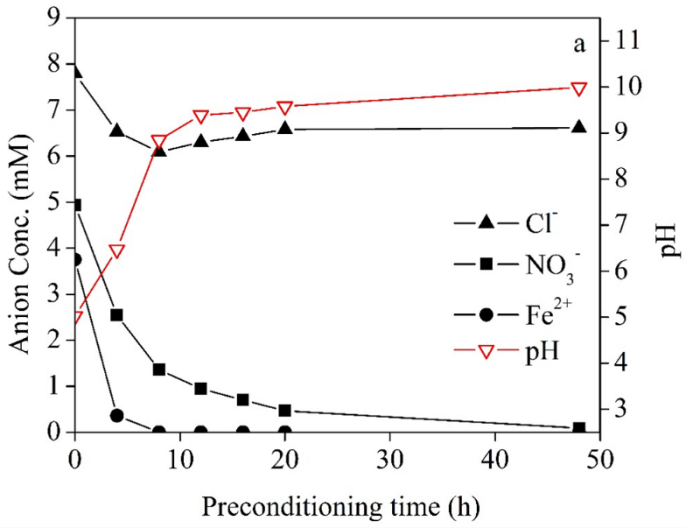

Figure 6 (a) Changes of Cl^- and NO_3^- as a function of synthetic time; (b) Anion concentration changes and pH after mixing newly prepared AIM at different synthetic time with 2.0 mM SeO_4^{2-} for 20 min.

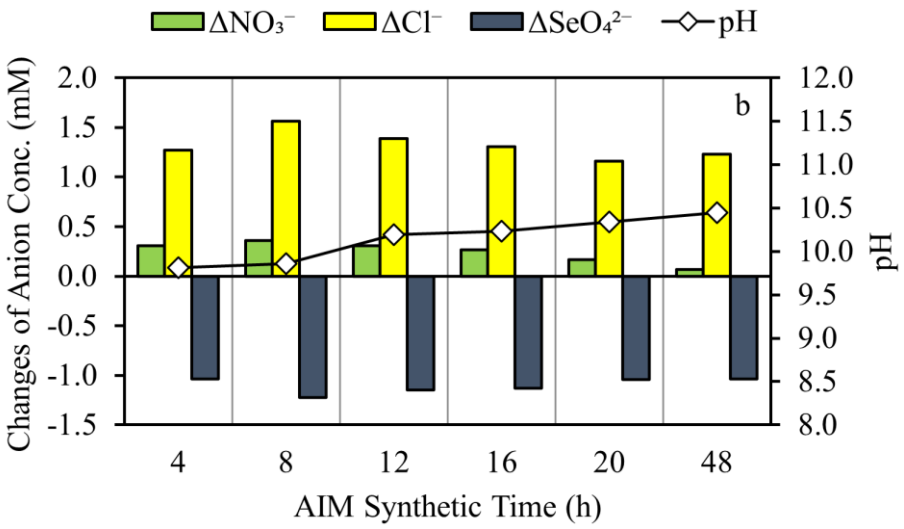

Figure 6 Continued.

According to the NO_3^- consumption and Eq. (1), more magnetite would be produced at a longer synthetic time. The SeO_4^{2-} EX_{CAP} in showed a different trend over synthetic time. Hence the results suggested that the amount of magnetite produced had no direct connection with the EX_{CAP} buildup. The Cl^- concentration trend rebounded at 8 h and remained almost the same after 20 h (Figure 5a), indicating that certain amount of Cl^- was first captured by solid structure and then partially released back to solution. This trend was also in accordance with the displacement of Cl^- from SeO_4^{2-} EX_{CAP} process over synthetic time. Moreover, the sum of residual Cl^- after AIM formation and the Cl^- released after treated with SeO_4^{2-} represented over 98% of initially introduced Cl^- from $FeCl_2$. It was observed that EX_{CAP} was increasing when aqueous Fe^{2+} was not fully consumed and decreased when the system exhausted aqueous Fe^{2+}. Therefore, it was reasonable to assume that EX_{CAP} was tightly related to aqueous Fe^{2+}, and the highest EX_{CAP} was

considered between 4 h to 8 h of synthetic time. This phenomenon could be explained from the GR formation and depletion perspective. With the help of aqueous Fe^{2+}, NO_3^- served as the oxidizing agent and created an environment favorable for GR formation on the surface of ZVI. Under such condition, GR would steadily accumulate, while NO_3^- in solution would continuously consume GR. Before aqueous Fe^{2+} depleted, the generation rate of GR surpassed the reaction rate of GR reacting with NO_3^-, and once system ran out of aqueous Fe^{2+}, GR stopped accumulating and gradually got consumed by the remaining NO_3^-. While reacting with NO_3^-, GR turned into magnetite [34] and released Cl^- back to solution, which was evidenced by the Cl^- trend over synthetic time.

AIM Synthesis in Presence of Elevated Cl^-

Anions are essential for the formation of GR and halogenides as interlayer ions are easily exchangeable anions comparing to higher-valent anions [34]. In this session, the regular AIM synthetic recipe contained 7.5 mM Cl^-, which was from the 3.57 mM $FeCl_2$ solution. In this session, additional Cl^- was introduced in the AIM synthesis process to study its impact on EX_{CAP}. The synthetic time remained at 20 h.

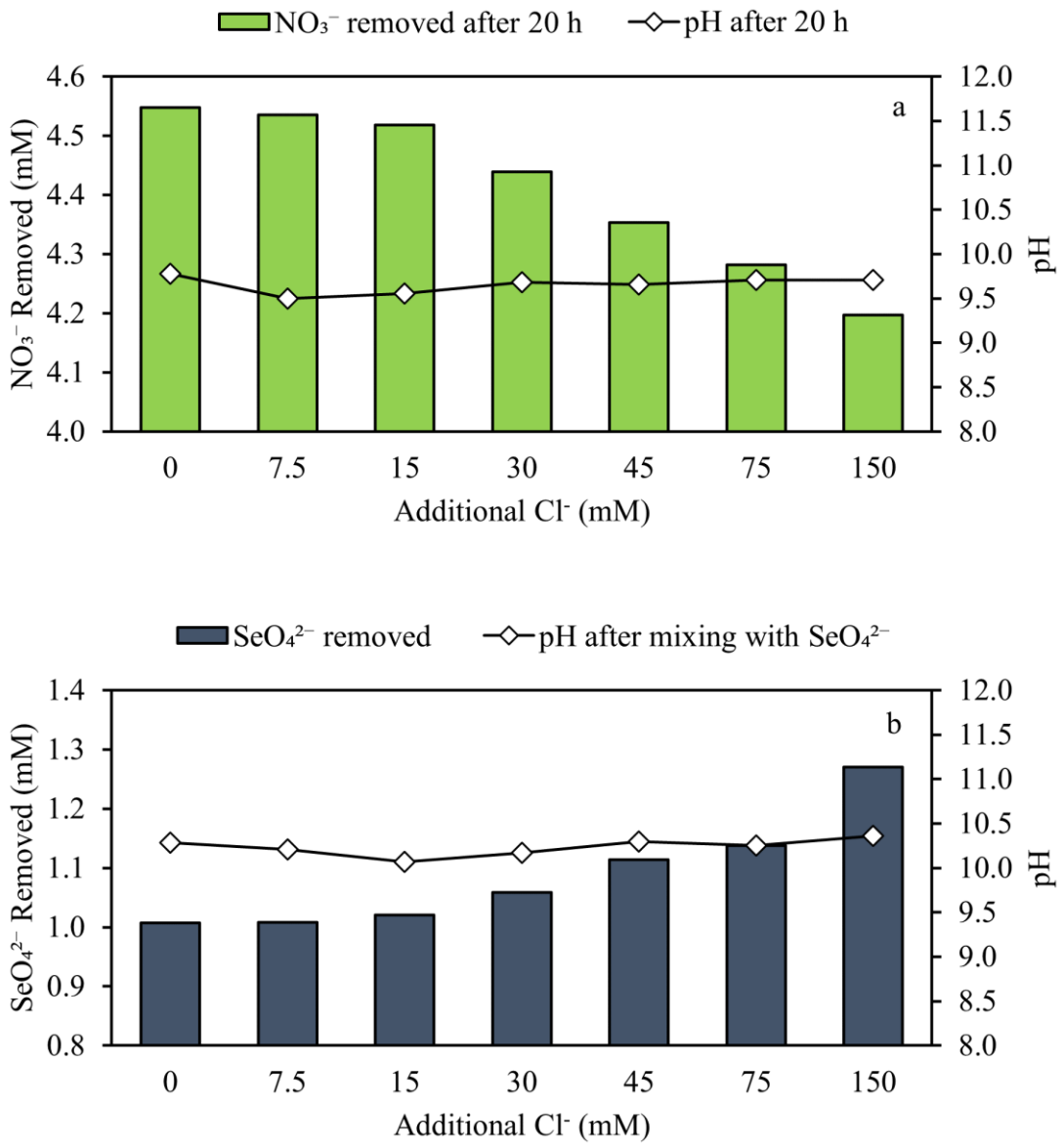

Figure 7 Prepared under different initial Cl^- concentration. (a) Removed NO_3^- and pH after AIM synthesis; (b) SeO_4^{2-} EX_{CAP} and its final pH.

Figure 7a showed that the additional Cl^- affected the AIM synthesis process by slowing down NO_3^- removal rate. However, this hindering effect was not significant since 20 times of the original amount of Cl^- (150 mM) only decreased the removal rate by ~8%.

EX_{CAP}, on the other hand, increased when AIM was prepared under high Cl^- containing conditions (Figure 6b). The highest amount of SeO_4^{2-} EX_{CAP} in this test was ~26% more than the one prepared under the regular recipe. According to the findings from anions affinity order and AIM synthetic time tests, it could be inferred that excessive Cl^- would compete with NO_3^- on entering GR interlays, which as a result hindered the GR consumption by NO_3^-.

Impact of Oxygen on EX_{CAP}

Based on Eq. (1), the product of the AIM synthesis process would be mostly magnetite, which could also be confirmed by XRD (Figure 9). Regarding the Fe^{2+}/Fe^{3+} ratio, since it was very hard to control the exact amount of the solid stripped off by sonication, magnetite would inevitably be part of the suspended solid. Therefore, instead of showing the actual iron composition of the intermedia, the ratio obtained from dissolving such solid would be influenced by magnetite, whose Fe^{2+}/Fe^{3+} ratio was considered as 0.5. However, when assuming the proportion of each composition in the suspended solid was constant, the Fe^{2+}/Fe^{3+} ratio could still indirectly reflect the structural changes of the intermedia.

It was shown in Figure 8 that the Fe^{2+}/Fe^{3+} ratio and EX_{CAP} both decreased with the increase of contact time between fresh AIM and O_2, which indicated that the intermedia formed on AIM surface was highly sensitive to oxygen. This results also signified the importance of a high Fe^{2+}/Fe^{3+} ratio for maintaining the intermedia structure to function as an anion exchange media.

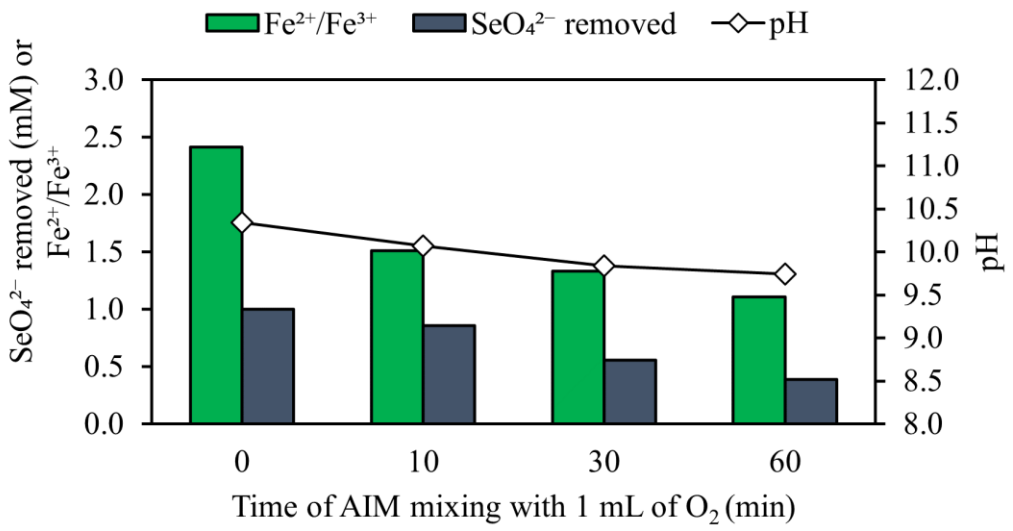

Figure 8 Effect of O_2 exposure time on AIM surface Fe^{2+}/Fe^{3+} ratio and EX_{CAP}.

XRD Analysis

GR is well known for its instability with oxygen. Depending on the oxidation rate, it could be oxidized to lepidocrocite or magnetite [35]. Therefore, it is essential to apply a glycerol overlay on for the XRD samples to protect them from air oxidation. The diffractograms of the intermedia of interest under different phases were attained, and the diffraction lines of magnetite can be clearly seen in all diffractograms (Figure 9). It was discussed in the AIM synthetic time session that the highest EX_{CAP} was speculated to be between 4 h to 8 h. Therefore, a synthetic time of 6 h was used for a better XRD observation. The diffraction pattern of such newly synthesized AIM clearly indicated a typical type I chloride-GR pattern (Figure 9a). These GR_{Cl} peaks diminished greatly after mixing with SeO_4^{2-}, while three other new peaks appeared (Figure 9b), which corresponded with a typical sulfate-GR pattern (type II) [36], indicating an iron(II)-

iron(III) hydroxy-selenate as a GR type II structure [37, 38]. These findings agreed with our suspicions that the GR-like structure was responsible for such rapid selenate removal. One distinct peak was also found at spacing 3.34 Å, which might be from quartz from the impurity of the raw ZVI powder, because similar peaks were observed on the raw ZVI patterns.

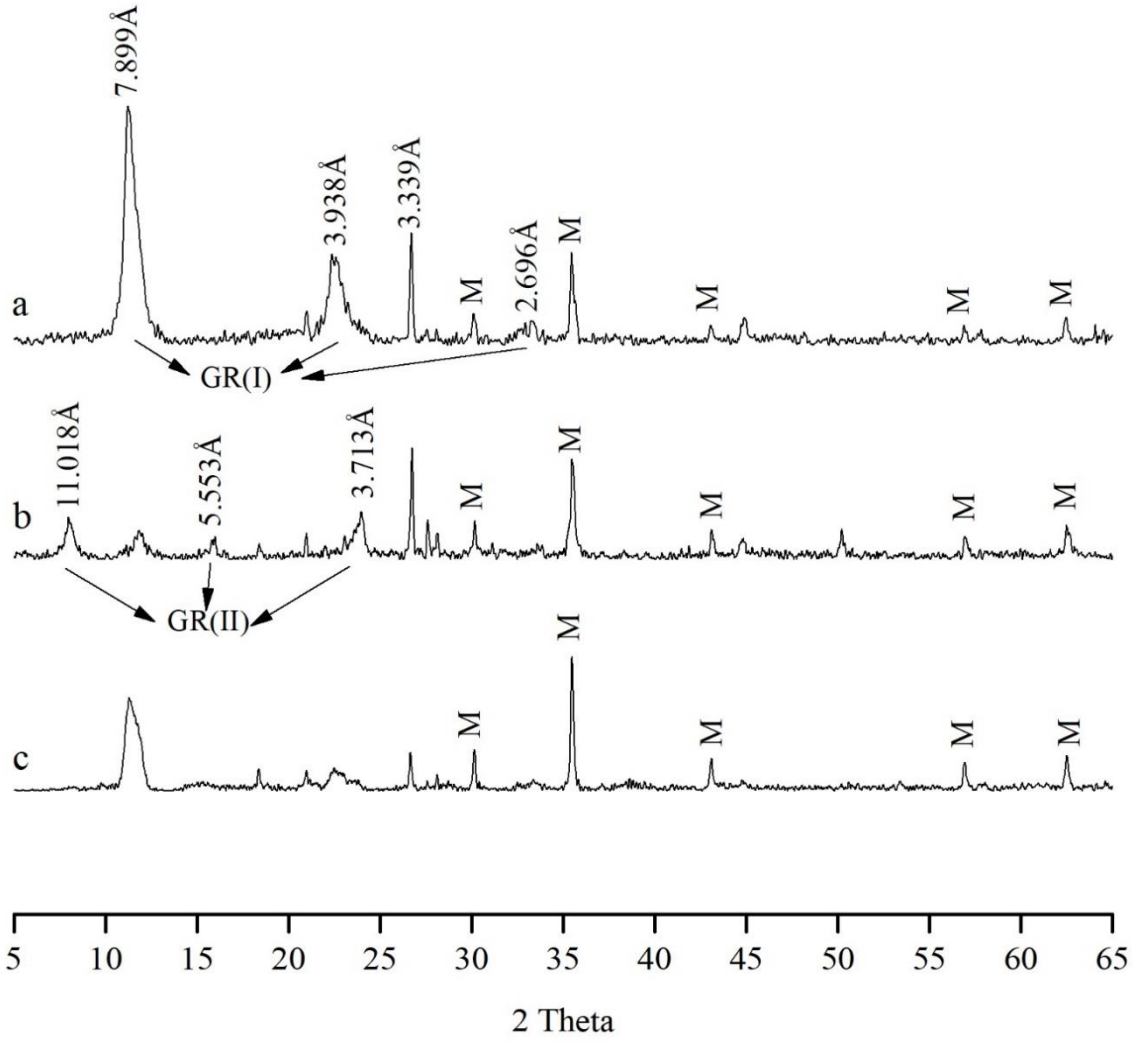

Figure 9 X-ray diffraction (XRD) pattern of the intermedia coating separated from AIM: (a) prepared with a synthetic time of 6 h; (b) prepared with a synthetic time of 6 h and tested for EX_{CAP}; (c) prepared with a synthetic time of 20 h; M: magnetite.

It was also noticeable that GR peaks only showed on the diffraction pattern of newly synthesized AIM. Samples exposed to air or dried anaerobically did not show any GR peaks. Experimental results also indicated that dried AIM had no SeO_4^{2-} removal ability. Comparing samples at synthetic times of 6 h and 20 h (Figure 9a & c), GR_{Cl} peak intensity drastically decreased, indicating the consumption of GR along with the NO_3^- removal (Figure 6a).

Selenium Re-dissolution and XPS Analysis

The results of all the extractions were summarized and presented in Figure 10. Immediately after the EX_{CAP} was completed, DI rinsing was performed three times and it could only extract 1.3% of the pre-removed SeO_4^{2-} out of AIM-SeO_4^{2-}. At 0 h of contact time, 4 times of 30 mM Cl^- solution rinses totally extracted 47.6% out of pre-removed SeO_4^{2-}. These ratios decreased as the pre-contact time increased. At 24 h of pre-contacting, no SeO_4^{2-} could be rinsed out of AIM-SeO_4^{2-} any more by 30 mM Cl^- solution. The results of SeO_4^{2-} re-dissolution test indicated that SeO_4^{2-} would gradually be incorporated and fixed into the AIM structure. No SeO_3^{2-} was detected in any rinsing solution, however, it has been proved that Se^{VI} reduces to Se^{IV} and Se^0 in the presence of GR [39, 40].

High resolution XPS analysis was performed on the sonicated AIM-SeO_4^{2-} samples at contact time of 0, 24 and 96 h to study the fate of Se. Because of the substantial overlap between the binding energy ranges of Se 3d and Fe 3p, the spectrum of Se 3p was collected. A control test on sonicated AIM only was also performed to reduce the influence of sulfur (S) from ZVI powder (~0.1% w/w). Speciation distribution of Se in the AIM-SeO_4^{2-} system over time is illustrated in Figure 11. The doublet separations of

Se 3p and S 2p were set as 5.75 eV and 1.18 eV, respectively, according to NIST X-ray Photoelectron spectroscopy database. Photoelectron lines of $3p_{3/2}$ and $2p_{3/2}$ were drawn with solid lines, and the $3p_{1/2}$ and $2p_{1/2}$ were drawn with dashed lines. The area ratios of Se $3p_{3/2}$ to $3p_{1/2}$ peaks and S $2p_{3/2}$ to $2p_{1/2}$ peaks was both constrained at 2:1. Any binding energies mentioned in the following session for Se species identification were designated to Se $3p_{3/2}$ spectral line.

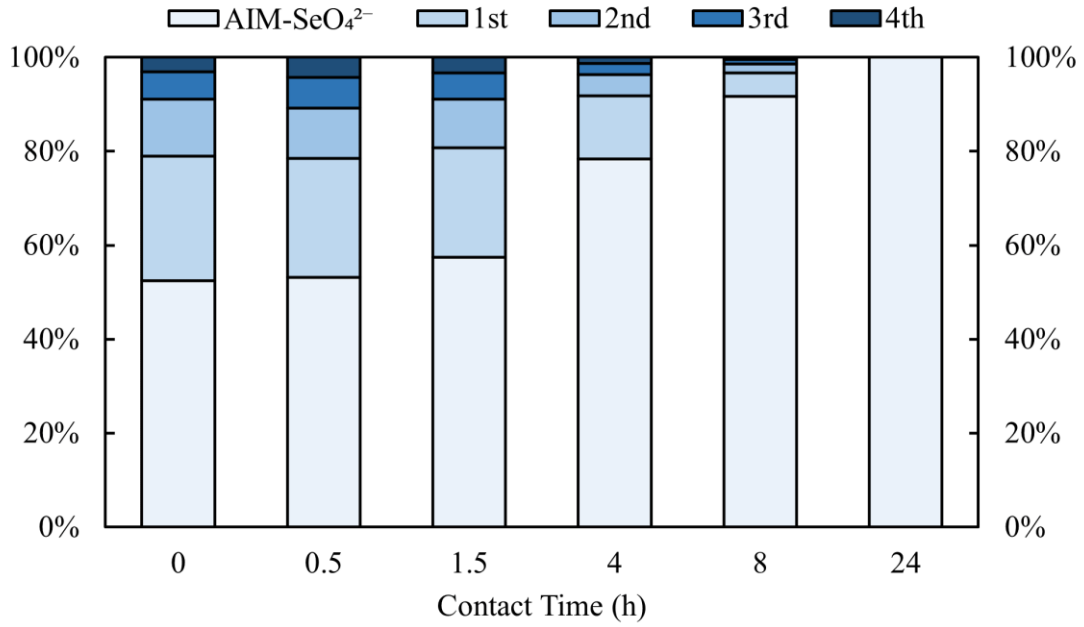

Figure 10 Differences among SeO_4^{2-} extraction percentage by 4 times of 30 mM Cl^- solution rinsing at different contact times.

Sulfur in AIM was presented as S^{VI} in the control sample, and it was assumed the same condition in other Se-containing samples. At 0 h of contact time, Se in AIM-SeO_4^{2-} had not reacted with ZVI core directly or indirectly (through magnetite) yet. Calculated by their peak area at 161.6 eV, about 78.9% of the removed SeO_4^{2-}-Se^{VI} was

transformed to Se^{0}. The binding energy for the rest of Se was deconvoluted to 165.3 eV, which could be Se^{IV} or Se^{VI} since Se^{VI} and Se^{IV} have overlapping binding energy ranges at photoelectron line of 3p. At the contact time of 24 h, the percentage of Se^{0} increased to ~80.5%, and the spectral line for the rest of Se shifted to 164.8 eV (assumed as Se^{IV}). At 96 h, spectral line of Se^{-II} appeared at 160.11 eV with a percentage of 12.6%, and Se^{0} decreased to ~68.1%. The spectral line of Se^{IV} continued shifting to the lower binding energy while its proportion maintained ~20% of the total Se.

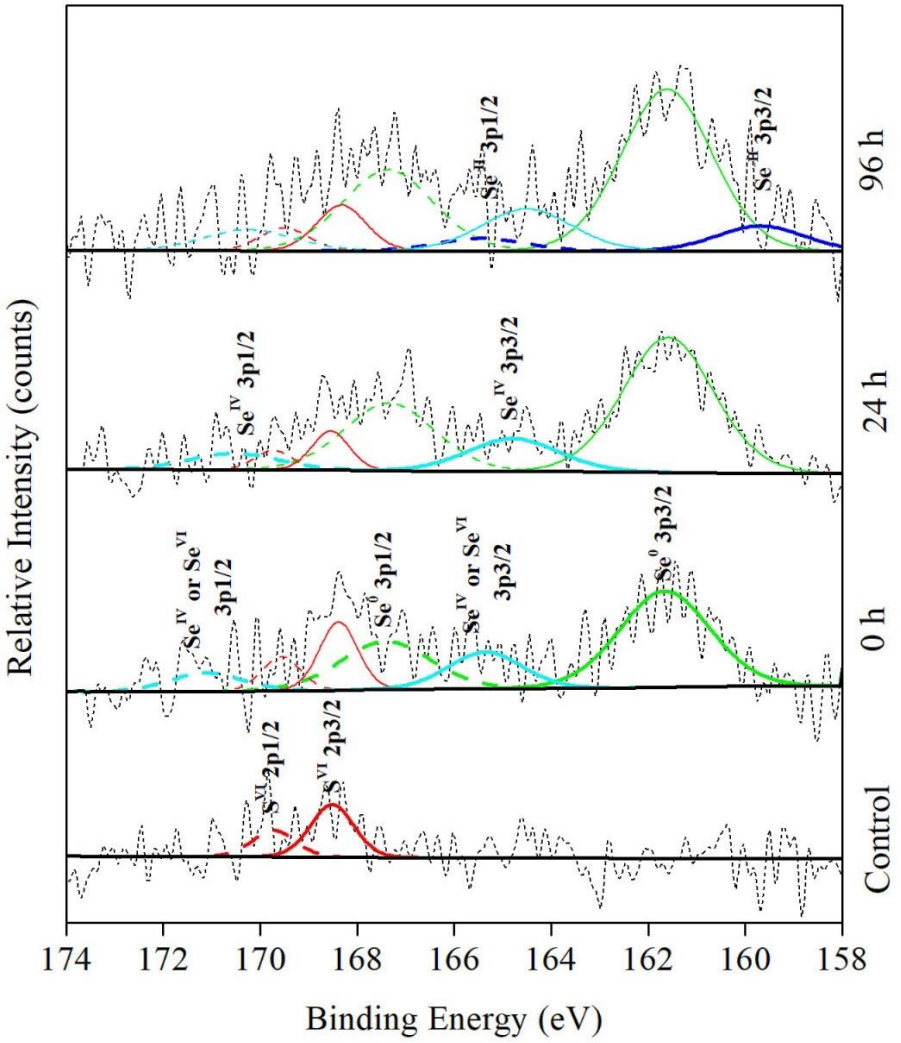

Figure 11 X-ray photoelectron spectroscopy (XPS) high resolution spectra study on control and AIM-SeO_4^{2-} at contact times of 0, 24 and 96 h.

Conclusion

In this chapter, a rapid initial removal of certain anions (mainly SeO_4^{2-}) by newly synthesized AIM was discovered and studied. Green rust as an intermediate was proven to be responsible for such EX_{CAP} and any changes that may affect the formation process of green rust or its structure condition afterwards would also have an impact on the EX_{CAP}

performance. EX_{CAP} affinity order of tested anions was $SeO_4^{2-} > SO_4^{2-} > NO_3^- > Cl^-$. This phenomenon seems appeared on the freshly prepared AIM with the basis of fine ZVI powder (5 μm ZVI performed similarly). There is a great chance to further utilize this feature on large-scale if optimum production of GR and strictly anaerobic environment could be achieved.

CHAPTER III

GREEN RUST FORMATION DURING NITRATE REDUCTION BY ZERO VALENT IRON MEDIA

Introduction

Green rust (GR) is a group of iron minerals featuring layered double hydroxide (LDH) structures containing both Fe^{II} and Fe^{III}. Green rust does not possess a definite composition, whose stoichiometric formula are represented for convenience by many researchers as $[Fe^{II}_{(1-x)}Fe^{III}_{x}(OH)_2]^{x+}[(x/n)A^{n-}\cdot(m/n)H_2O]^{x-}$, where x is the ratio of Fe^{3+}/Fe_{total} that usually ranged from 0.25-0.33, A^{n-} represents the intercalated anion, and (m/n) denotes the intercalated water molecules. The stacking of brucite-like layers (the OH-Fe^{II}/Fe^{III} layer) carries positive charges, which is balanced by negative charges of the intercalating layers constituted of anions and water molecules. It is originally classified by Bernal, Dasgupta [36] into two forms: the chloride form and the sulfate form, which are referred as GR I and GR II. Type I GR has planer or spherical intercalated anions (e.g., CO_3^{2-}, Br^- and Cl^-), resulting in a rhombohedral unit cell, while type II with three-dimensional structure anions (e.g., SO_4^{2-} and SeO_4^{2-}) has a hexagonal unit cell [38].

Green rusts were often identified among the corrosion products on iron and steel surface under anoxic conditions but was also found in nature as mineral fougerite [41, 42]. GRs compounds can be synthesized in various processes. Two main procedures were mostly used: air oxidation method and stoichiometric coprecipitation method. The first one is aimed at oxidizing $Fe(OH)_2$ to GRs, by adjusting pH and the air flow rate to create an environment that alter the Fe^{II}/Fe^{III} ratio to where the GR formation benefits [35]. The

second method adopts a more direct approach: solutions of both Fe^{2+} and Fe^{3+} are first mixed under the stoichiometric ratio of the desired GR, then NaOH solution is added to induce the coprecipitation and GR formation [43]. No oxidation is required for the coprecipitation method. For both methods, an appropriate number of associated anions that will intercalate to GRs must be present in solution during the processes.

GRs are known as an intermediate product from iron corrosion process. As a typical LDHs, GRs have anions located in the interlayer regions that could be easily exchanged [34]. Besides the anion intercalation potential, GR has its own features comparing to common LDHs due to its unique iron-based composition. It has been proved that GR has the potential to react with various anions, which are mostly reduced with concurrent oxidation of Fe^{2+} to Fe^{3+} [44]. Many studies reported that nitrate will be reduced to ammonia by GRs, but nitrite will be reduced to NO or N_2O depending on the pH of the solution [34, 45]. Many metal and metalloid anions removal by GRs usually start with anion exchange/adsorption and followed by reduction at the cost of Fe^{II} oxidation and GR structure transformation. The possible oxidation products of GRs are magnetite (Fe_3O_4), lepidocrocite (γ-FeOOH), maghemite (γ-Fe_2O_3) or goethite (α-Fe_2O_3), depending on the oxidation rate and dehydration of GR. Myneni, Tokunaga [40] and Refait, Simon [37] reported that Se^{VI}-coprecipitated GR_{SeO4} was highly unstable and Se^{VI} could be rapidly reduced to Se^{IV}. Hayashi, Kanie [39] and Myneni, Tokunaga [40] also reported that Se^{VI} could be directly reduced to Se^0 without detectable accumulation of Se^{IV} when reacting with previously precipitated GR_{SO4} surface. Both approaches happened at the cost of GR turning into magnetite or lepidocrocite. Additionally, Myneni, Tokunaga

[40] found a trace quantity of Se^{-II} in the solid while Hayashi, Kanie [39] failed to do so. The work of O'Loughlin, Kelly [46] indicated that nanocrystals of UO_2 can be formed via the abiotic reduction of U^{VI} by GR_{SO4}. Williams and Scherer [44] also observed the rapid Cr^{VI} reduction in the presence of GR_{CO3}.

Materials and Methods

Materials and Chemicals

Unless otherwise indicated, reagents used in this study were all at analytical reagent grade. Ferrous and nitrate solutions were prepared from $FeCl_2 \cdot 4H_2O$ (>99%, J.T. Baker, NJ) and NaNO3 (>98%, Alfa Aesar, MA). Sulfate solution for EX_Cl tests was prepared from Na_2SeO_4 (>99.8% Alfa Aesar, MA), respectively. The industrial -325 mesh iron powder (>95% Ferox Target ZVI Reactive Iron Powder, Hepure Technologies Inc., NJ) was used as the ZVI powder. Glycerol (>99.5%, OnlineScienceMall, USA) was used for sample overlap for XRD tests. Deionized deoxygenated (DI) water was supplied by E-pure (Barnstead, USA) with resistivity around 18.2 M-cm. All batch tests in this study were prepared in the anaerobic chamber (Coy Laboratory, MI), which was filled with approximate 95% N_2 and 5% H_2 and equipped with a palladium catalytic O_2 removal system and an O_2 sensor to ensure an anoxic environment.

Experimental Methods

Batch tests

Serum vials (10 ml, Kimble Chase) were employed with rubber stoppers as reactors. Multiple reactors were prepared under the equivalent condition. The general procedures were as followed: (1) DI water was purged with ultra-high purity nitrogen gas for at least 1 hour, then stored in the anaerobic chamber for at least 12 h to make it deoxygenated before use. (2) In anaerobic chamber, stock solutions were prepared by dissolving pre-weighted chemicals (e.g., $FeCl_2 \cdot 4H_2O$ and $NaNO_3$) in deoxygenated DI (DDI) water. (3) Reactors with pre-weighted ZVI powder at 50 g/L were transferred in anaerobic chamber, and 10 ml total of solution consisting of predetermined concentration of chemicals was transferred into each reactor. (4) The reactors were placed in a rotating opaque tumbler box at 30 rpm for mixing. (5) At predetermined times, reactors were taken out and the supernatant was extracted and filtrated using 0.45 μm membrane filters (VWR) for later analysis. In this chapter, any results reported with standard deviation bars are the average of triplicate tests.

Continuous Stirred Tank Reactor Tests

A series of continuous stirred tank reactor (CSTR) tests were designed to study the accumulation effect of the GR coating on ZVI and its longevity under Fe^{2+} enrich environment. A two-liter reactor (L*W*H = 10cm * 10cm * 20cm) with a overhead mixer was set up as the CSTR reactor as shown in Figure 12. The mixer was set at a 1600 rpm to make sure the media in the reactor was in a fluidized state, indicating a completely

mixed condition. Two pieces of foam floating at the top of the water were designed to reduce air contact with liquid surface, hence, to minimize the oxygen impact on green rust formation. There was a settling zone connected to the mixing zone that stopped media from flowing away with the effluent.

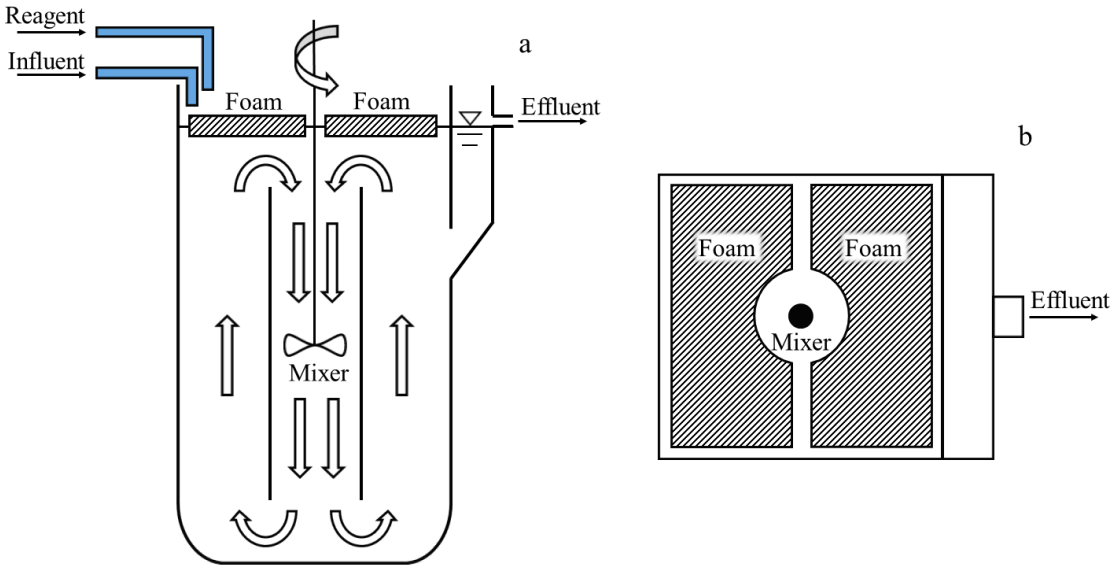

Figure 12 Schematic view of the CSTR reactor (a) Side sectional view; (b) Top view.

All influents and reagents were prepared using DI water. At start of each CSTR test, 2L DI water and 200 g -325 mesh ZVI powder (100 g/L) were added in the reactor. The HRT was set at 6 h, which made the flow rate at 5.56 ml/min, including reagent and influent. The influent was prepared as 1 mM NO_3^- solution and the reagent were 0.75, 1.5, 2.25, 3, or 4.5 mM Fe^{2+} solution for each test. 5 ml mixture of media and solution were taken into a 10 ml serum vial at the same spot of the reactor (approximately half height of the reactor) at the same time each day after start of each test. The vial would be transferred

in anaerobic chamber and the media would be rinsed 3 times (as described in Chapter II). After rinsing, 50 mM SO_4^{2-} solution was filled in the vial up to 10 ml and the vial was capped and put in the mixing tumbler for 20 min. The supernatant was then extracted and filtrated using 0.45 µm membrane filters and collected for later analysis.

In addition, after feeding influent and reagent for 10 days, the GR stability test was performed on media with 4.5 mM Fe^{2+}. The influent and reagent were switched off, and the mixer was turned slow, leaving the reactor idle, but the media was lightly agitated at the bottom to avoid agglomeration. The mixer was restarted to re-fluidize the media after 10 and 40 days of inactivity, a 5 ml sample was obtained for EX_Cl testing.

Sample Preparation and Analytical Methods

The filtrate was collected for IC (ion chromatography) analysis. A Dionex ICS-1100 system (Dionex Co., Synnyvale, CA) was used to analyze NO_3^- and Cl^-. Separation was achieved using a Dionex IonPac AS22 column with an AG22 guard column. The minimum detection limit of NO_3^- and Cl^- were both 0.1 mg/L. Dissolved Fe^{2+} was measured colorimetrically with the 1,10-phenanthroline method at the wavelength of 510 nm [32] on a UV-Vis spectrophotometer (M&A Instruments Inc, CA). In some experiments NH_4^+ was also determined. Filtrate solution with NH_4^+ was processed and tested on UV-Vis spectrophotometer at 640 nm following phenate methods [47]. pH of filtrate was measured by Orion 2-Star Benchtop pH Meters (Thermo Fisher Scientific Inc., MA).

When necessary, certain experiments were repeated, and the reactors were transferred in the anaerobic chamber to prepare samples for X-ray powder diffraction

(XRD) analysis. XRD was used to characterize the corrosion products on ZVI surface. The media in reactors was sonicated for 5 min before transferred in anaerobic chamber. Most suspended solid was withdrawn from the reactor using a syringe, and then forced through a 0.45 μm filter paper (Pall Laboratory, USA). Because the collected media may be sensitive to oxygen, the filter papers with sample paste will be treated with a few drops of glycerol in the anaerobic chamber and stored in anaerobically sealed containers before testing to prevent oxidation or dehydration [33]. Once the XRD samples were prepared, XRD analyses would be conducted within 1 hr. XRD patterns were recorded by Bruker-AXS D8 Advanced Bragg-Brentano X-ray Powder Diffractometer with Cu Kα radiation at a wavelength of 1.5406 Å.

Results and Discussion

Reduction of NO_3^- at a Fixed Fe^{2+}/NO_3^- Ratio

According to Huang [17], nitrate would be rapidly removed by ZVI with the help of external Fe^{2+} (aq) following an proposed reaction:

$$NO_3^- + 2.82Fe^0 + 0.75Fe^{2+} + 2.25H_2O \rightarrow NH_4^+ + 1.19Fe_3O_4 + 0.5OH^- \quad (1)$$

Eq. (1) indicates that converting 1 mol of NO_3^--N to NH_4^+-N requires 0.75 mol of Fe^{2+}. Therefore, the ratio between NO_3^- and Fe^{2+} was controlled at 1 to 0.75 in this test. As illustrated in Figure 13, a series of batch tests were conducted to reproduce the missing Cl^- phenomenon during AIM preparation.

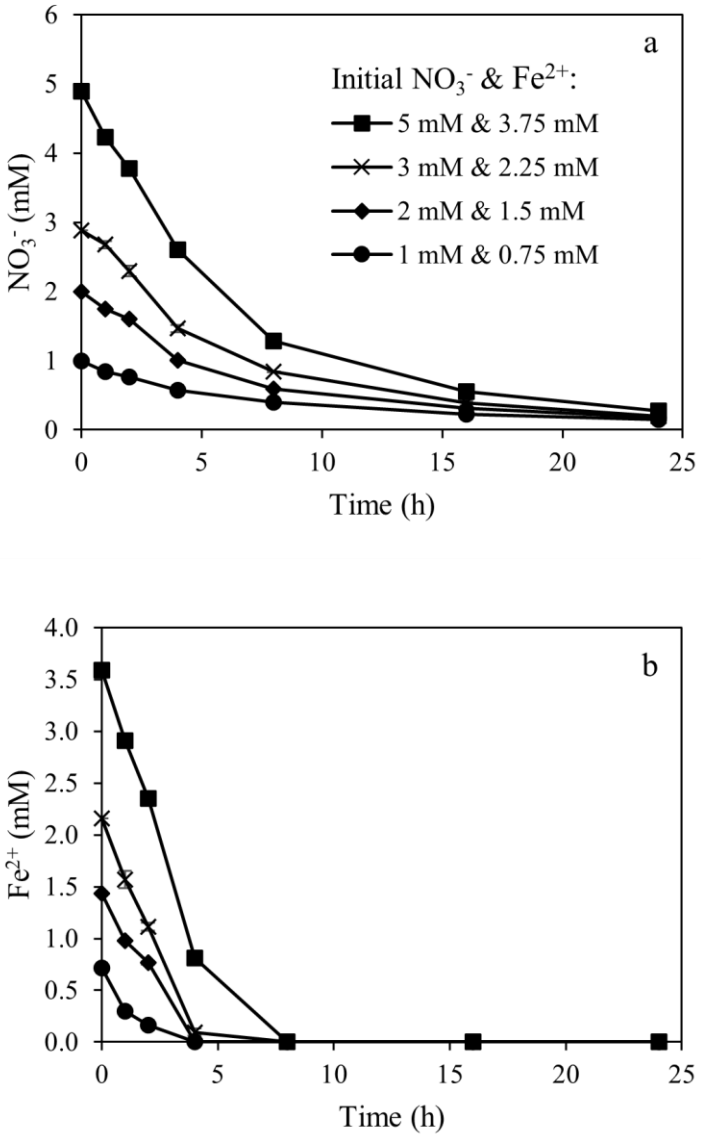

Figure 13 Time courses of (a) NO_3^-; (b) Fe^{2+} and (c) Cl^- from nitrate removal by Fe^0 under various initial NO_3^- and Fe^{2+} concentrations. The initial conditions of batch tests: 50 g/L Fe^0 + varying NO_3^- and Fe^{2+} concentrations at a fixed ratio of $NO3^-/Fe^{2+}$ = 1/0.75.

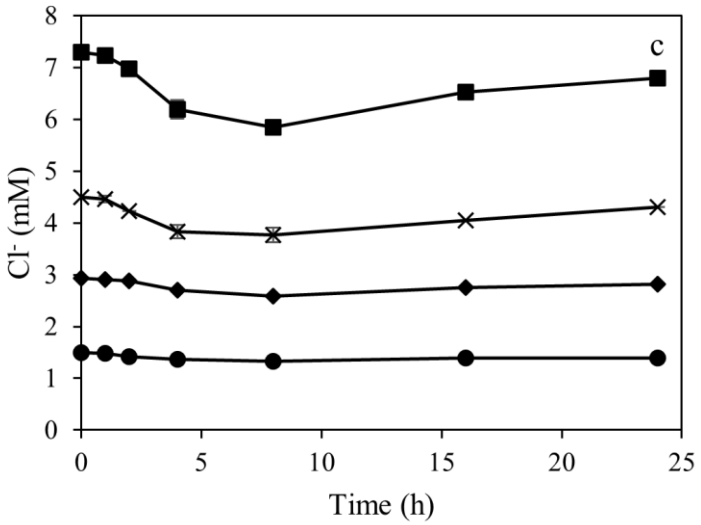

Figure 13 Continued.

When $Fe^0/NO_3^-/Fe^{2+}$ system started at a NO_3^-/Fe^{2+} ratio of 1/0.75, the entire nitrate reduction process could be separated into three stages for all sets of tests. In Stage 1 (the first 0.5 to 1 h), nitrate concentrations rapidly decreased (~10% removed within 1 h) along with a sharp decrease of Fe^{2+} in solution. Cl^- concentrations remained stable at this stage. Stage 2 was marked from when Cl^- concentrations started to decrease to the depletion of aqueous Fe^{2+}. During this stage, both NO_3^- and Fe^{2+} reduction maintained at a rapid rate. Cl^- started to disappear from water. The changes of Cl^- at this stage was not obvious when initial NO_3^- and Fe^{2+} was low, but once both concentrations increased, the Cl^- missing effect became progressively noticeable (Figure 13c). When NO_3^- and Fe^{2+} started at 5 mM and 3.75 mM, the largest dip of about 1.44 mM Cl^- loss was observed at 8 h, at which Fe^{2+} was completely consumed (Figure 13b) but there was still 1.28 mM of NO_3^- remaining in solution (Figure 13a). The depletion of the aqueous Fe^{2+} in solution denoted the beginning

of Stage 3, which was characterized by the reduced NO_3^- removal rate and the reappearance of the missing Cl^-. Upon completion of the reaction, the remaining NO_3^- (approximately 50%) was removed at the end of Stage 3, and the Cl^- in solution reached about 93-95% recovery of the initial Cl^- (Figure 13c).

Comparing these results with Huang's finding [17], the most significant difference is the disappearance and reappearance of Cl^- in solution in Stage 2 and 3. The iron particles used by Huang were approximately 0.5 mm in diameter, which is greatly larger than -325 mesh (smaller than 44 μm). Therefore, it is speculated that an intermediate was formed during AIM preparation and Cl^- was involved in the intermedia formation. The reason why such Cl^- fluctuation was not observed in the past was presumably because powdery particles (like -325 mesh) provided a substantial amount of surface area, which is favorable for intermediate accumulation per unit of time. In Stage 2, accumulation of intermediate initiated, which can be represented by the reduction of Cl^- in water. Since NO_3^-, Fe^{2+} and Cl^- are unlikely to react with each other directly under similar conditions, the essential components for intermediate formation are speculated to be NO_3^-, Fe^0, Fe^{2+}, and Cl^-. Based on these presumptions, there are reasons to believe that the intermediate was the chloride form of GR, which was also confirmed by XRD later in this research. Assuming GR existed as the typical chloride form ($Fe^{II}_3Fe^{III}(OH)_8Cl$) at a Fe^{2+} to Fe^{3+} ratio of 3: 1, 1 mol of GR generated would require 1 mol of Cl^- as the intercalated anion, therefore the accumulated GR can be represented by the decrease of Cl^- from solution at any given time.

ZVI powder has a thin layer of iron oxides due to air oxidation, and this passive coating needs to be hydrolyzed and activated before inner iron core could participate in further reaction [48-50]. According to literatures [17, 48, 51], this passive layer could be consumed by adsorbing aqueous Fe^{2+} to form surface-bound Fe^{II}, which evolved into a mixture of amorphous iron oxides and readily transformed to magnetite. In Stage 1, under the help of aqueous Fe^{2+}, the activation of the passivating layer allowed the lasting rapid nitrate removal. No obvious reduction on Cl^- indicating no significant amount of GR-like compound was generated in Stage 1. Stage 2 started with the beginning of the fast Cl^- decline. Aqueous Cl^- incorporated into the structure of GR, which as an intermediate started to accumulate in system. When Fe^{2+} was exhausted in Stage 3, NO_3^- removal only slowed down instead of immediately ceased. Since GR could convert to magnetite by reduction of NO_3^- to NH_4^+ following Eq. (2) [34, 52], it is speculated that the main mechanism for NO_3^- removal in Stage 3 was by GR reduction.

$$4.8Fe_3^{II}Fe^{III}(OH)_8Cl + NO_3^- \rightarrow 6.4Fe_3O_4 + NH_4^+ + 4.8Cl^- + 2.8H^+ + 15.8H_2O \quad (2)$$

Given the above discussions, it is reasonable to assume a $Fe^0/NO_3^-/Fe^{2+}$ system under a NO_3^-/Fe^{2+} ratio of 1/0.75, will draw Cl^- from solution and form GR while aqueous Fe^{2+} presents in system, and the generated GR will also react with NO_3^- and turn into magnetite, which releases Cl^- back in solution.

Reduction of NO_3^- under Various Initial Fe^{2+} Concentrations

In the previous test results, it has been noticed that increasing the concentration of both NO_3^- and Fe^{2+} seemed to contribute to Cl^- decline in Stage 2. Therefore, effect of increasing only Fe^{2+} on NO_3^- removal by Fe^0 was investigated in a test with initial

conditions as 3 mM of NO_3^- and 50 g/L ZVI, and the ratios of NO_3^- to Fe^{2+} ranged from 1/0.75 to 1/6. Time courses of NO_3^-, Fe^{2+}, and Cl^- are shown in Figure 14.

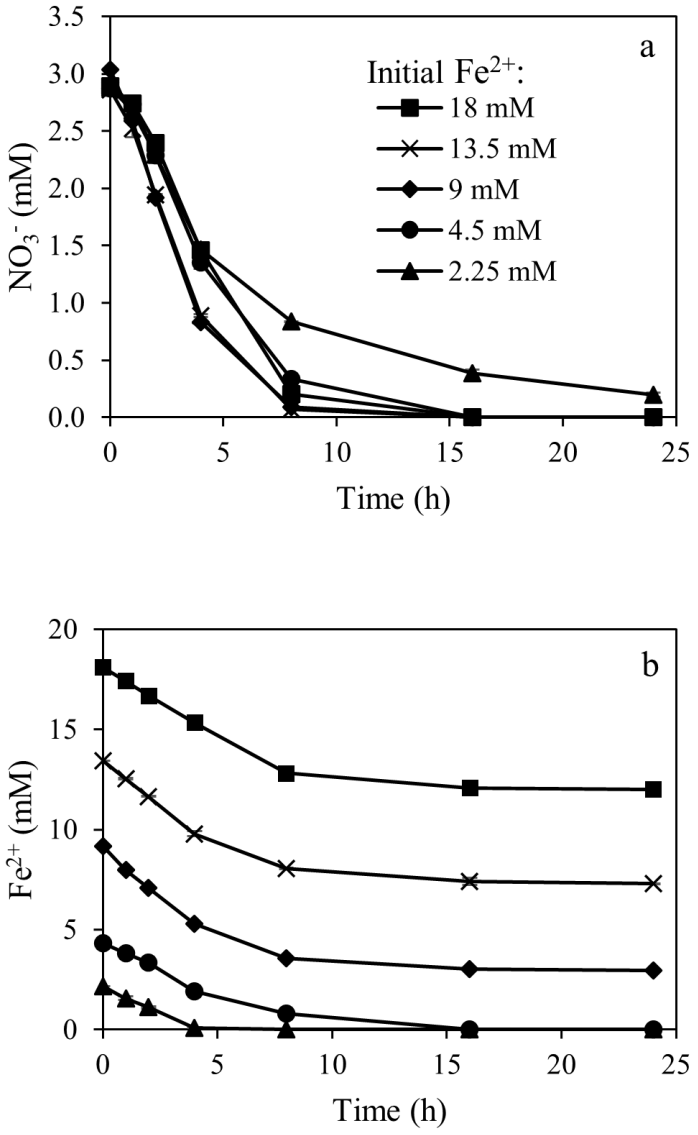

Figure 14 Time courses of (a) NO_3^-; (b) Fe^{2+} and (c) Cl^- from nitrate removal by Fe^0 under various initial Fe^{2+} concentrations. (d) Maximum nitrate removal rate as a function of initial Fe^{2+} concentrations. The initial conditions of batch tests: 50 g/L Fe^0 + 3 mM NO_3^-+ varying Fe^{2+} concentrations.

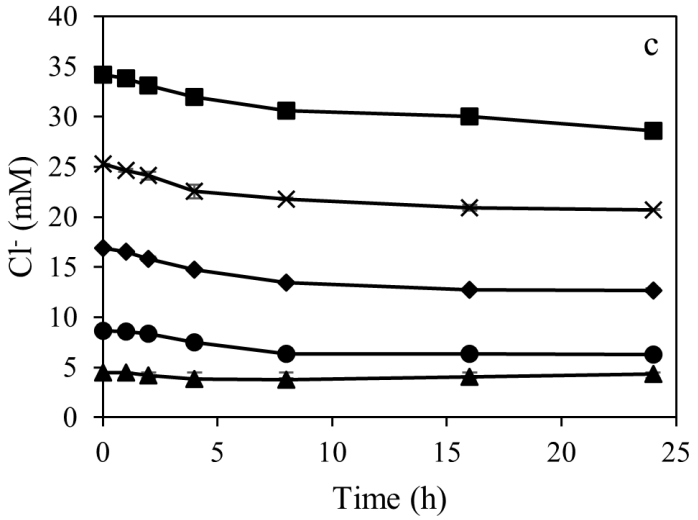

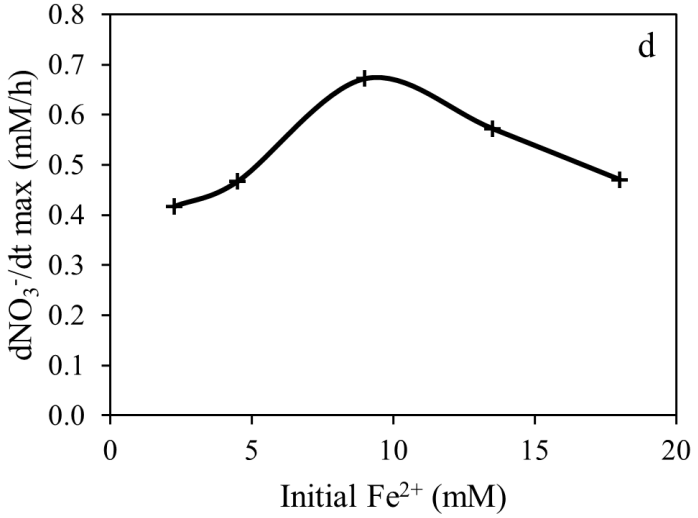

Figure 14 Continued

As shown in Figure 14a, over 90% and 99% of NO_3^- was removed at 8 h and 16 h, respectively, when initial Fe^{2+} was equal or greater than 4.5 mM. Figure 14c showed that all Cl^- concentrations declined monotonically except when initial Fe^{2+} was 2.25 (NO_3^-/Fe^{2+} = 1/0.75). Comparing Cl^- with Fe^{2+} results, it is obvious that, along with the removal of

NO_3^-, Cl^- concentrations decreased with excessive aqueous Fe^{2+}, where excessive means higher than required for magnetite formation in Eq. (1). This is consistent with the hypothesis drawn from the previous test, indicating a high Fe^{2+} to NO_3^- ratio (assumably close or higher than 1.5) favors GR formation (Figure 14b & c). After 24 h, for those with remaining Fe^{2+} were not zero, Fe^{2+} consumptions were 6.18 mM, 6.14 mM and 6.09 mM under NO_3^-/Fe^{2+} ratios of 1/3, 1/4.5 and 1/6, respectively (Figure 14b). This implies that in an aqueous Fe^{2+} enriched environment, the consumption of Fe^{2+} for same amount of NO_3^- reduction would be consistent. However, Cl^- decrease under ratios of 1/3, 1/4.5 and 1/6 were 4.19 mM, 4.58 mM and 5.53 mM, respectively, indicating higher excessive Fe^{2+} environment resulted in more GR remained after NO_3^- reduction (Figure 14c). In this test, Stage 1 and Stage 3 were not observed when initial Fe^{2+} concentration was 9 mM or above. It is probably because high Fe^{2+} greatly accelerated the activation of passive layer on ZVI surface, and excessive Fe^{2+} prolonged Stage 2 until NO_3^- was completely consumed.

As a layered double hydroxide, GR naturally has an ion exchange capacity due to the intercalation layer in its structure [53, 54]. Hansen and Koch [55] proposed a model for NO_3^- reduction by sulfate form of GR where GR initially can only exchange nitrate for sulphate on the exterior basal and edge sites. This model was also successfully applied on NO_3^- exchange with chloride form of GR by Hansen et al. in their subsequent research [34], where NO_3^- progressively exchange with Cl^- from edge and inwards. Comparing with sulfate form of GR, chloride form GR showed much higher reaction rates on NO_3^- removal, because monovalent anions have much lower affinity of the interlayer than higher-valent anions in analogues layered hydroxide [56]. For this reason, it is easy for

monovalent anions, like halogenides, at outer and even partial inner surface of GR to be exchanged out by NO_3^-. Therefore, when GR started forming on ZVI surface, NO_3^- would compete with Cl^- on those sites. Since $FeCl_2$ was used as Fe^{2+} source, when high Fe^{2+} dosage was introduced, it would consequently add twice as much of Cl^- in water, enhancing its competitiveness again NO_3^- on GR. Therefore, the reason why the maximum NO_3^- removal rate did not always increase with the increase of initial Fe^{2+}, but only peaked at 9 mM of initial Fe^{2+} (Figure 14d) is because high Cl^- concentration caused a hinder effect on NO_3^- contacting with GR.

X-ray Diffraction Analysis

The final precipitate formed from the condition of 10 g/L ZVI + 4.5 mM NO_3^- + 9 mM Fe^{2+} after 24 h was collected, sonicated and analyzed with XRD. The spectroscopy (Figure 15) indicates that the diffraction pattern of the final oxidation coating was identified as GR and magnetite. Also, it could be observed from the reactors, of which the initial Fe^{2+} was twice or higher than NO_3^-, that there were teal-green suspension and black media powder at the bottom by the end of reaction.

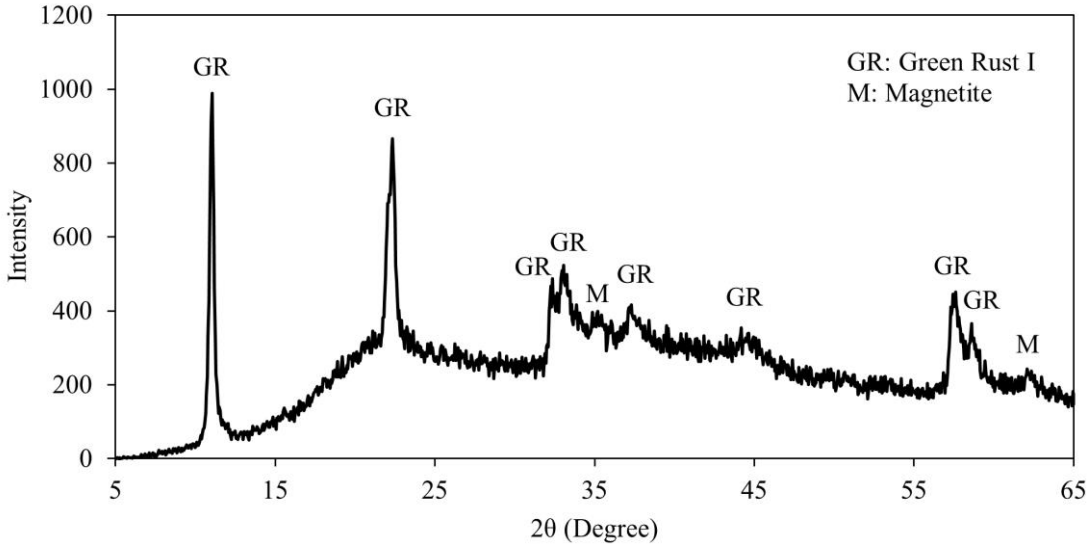

Figure 15 X-ray diffraction spectra analyses of oxide coating under condition of 50 g/L ZVI + 3 mM NO_3^- + 9 mM Fe^{2+}.

According to literatures, except for magnetite, most iron oxide corrosion on ZVI surface would generally passivate ZVI media, but active generation of green rust coating on ZVI was rarely discussed. Scherer et al. [48] presented three conceptual models describing the electron transfer mechanism from iron to exterior environment where oxide layers serves as (i) a physical barrier which isolates iron from oxidants, and electrons could only transfer via bare iron surface like pits in the oxide layer; (ii) a semiconductor where electros are transferred via conduction band of oxide layer; and (iii) a coordinating surface where electrons are from absorbed or lattice Fe^{II}. Additionally, Wander et al. [57] studied the feasibility of electron transfer within GR structure, suggesting that for any structurally Fe^{2+} site of GR that is oxidized to Fe^{3+} by an adsorbed oxidant, there is a facile tendency of electrons redistribution towards this particular site, and this tendency is much greater along the basal direction of iron oxide interlayer. Based on these efforts of previous

studies, a simplified conceptual model of GR as a combination of semiconductor and coordinating surface was established to demonstrate the mechanism of GR formation as portrayed in Figure 16. Initially, NO_3^- was reduced at Fe^0 surface and a layer of GR was formed with the help of considerable aqueous Fe^{2+} (progress not shown in Figure 16). It is assumed that most GR existed as chloride form, but there is still a possibility that nitrate form of GR also existed temporarily. Soon as GR forming on Fe^0, NO_3^- started exchanging with structural Cl^- in GR and thereafter being reduced to NH_4^+. At the edge-inward of GR where most redox reaction happened, aqueous Fe^{2+} was incorporated on the locally oxidized GR during NO_3^- reduction and became structural-Fe^{2+} to generated new GR structure. Meanwhile, electrons within GR inclined to diffuse to the oxidized sites rapidly, promoting the regeneration of lattice Fe^{2+} sites [57]. Such electron diffusion effect spread "inward" would eventually reach to Fe^0, where the electron transfer from underlying Fe^0 to GR is thermodynamically favorable [48]. Both Fe^0 and aqueous Fe^{2+} are essential for the reaction to proceed. Fe^0 as the main electron donor ensures the overall Fe^{2+} to Fe^{3+} ratio of the entire GR structure, maintaining the stability of electron diffusion, while aqueous Fe^{2+} prevents the local over-oxidation of GR edge, which would result in regional oxidative degradation of GR structure. Magnetite could also be found on XRD spectra. Since GR can solely reduce NO_3^- to NH_4^+ and transform to magnetite [34], magnetite in our system was regarded as the oxidation product of GR that was detached from ZVI.

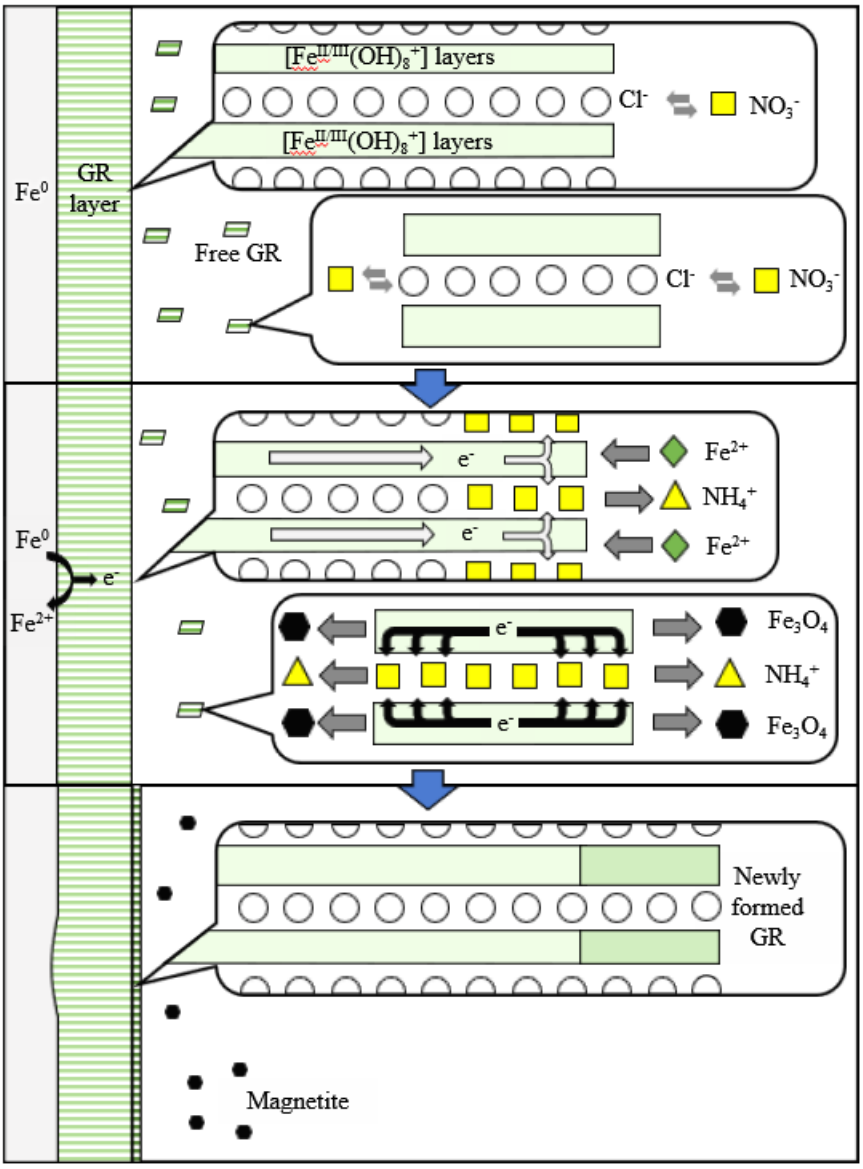

Figure 16 Schematic diagram of the green rust formation under excessive Fe^{2+}.

Quantitative Consumption of Fe^{2+} by NO_3^- Reduction

Batch tests were conducted to investigate the relationship between Fe^{2+} loss and NO_3^- reduction. The initial conditions were 50 g/L ZVI + 9 mM Fe^{2+} + 0 (as control), 1, 2, 3, 4, or 5 mM NO_3^-. As shown in Figure 17, results indicated that even without the

addition of NO_3^-, the passive iron oxide layer on pristine ZVI surface would consume Fe^{2+} and Cl^- (Figure 17b & c), presumably produce GR. No NO_3^- was left in solution after 16 h for any initial NO_3^- concentrations, and Fe^{2+} and Cl^- remained stable at 24 h. NH^+ was considered as the only reduction product of NO_3^-, and this was evidenced by the practically 100% nitrogen recovery at the end of each reaction showing on both Figure 17d and Figure 18.

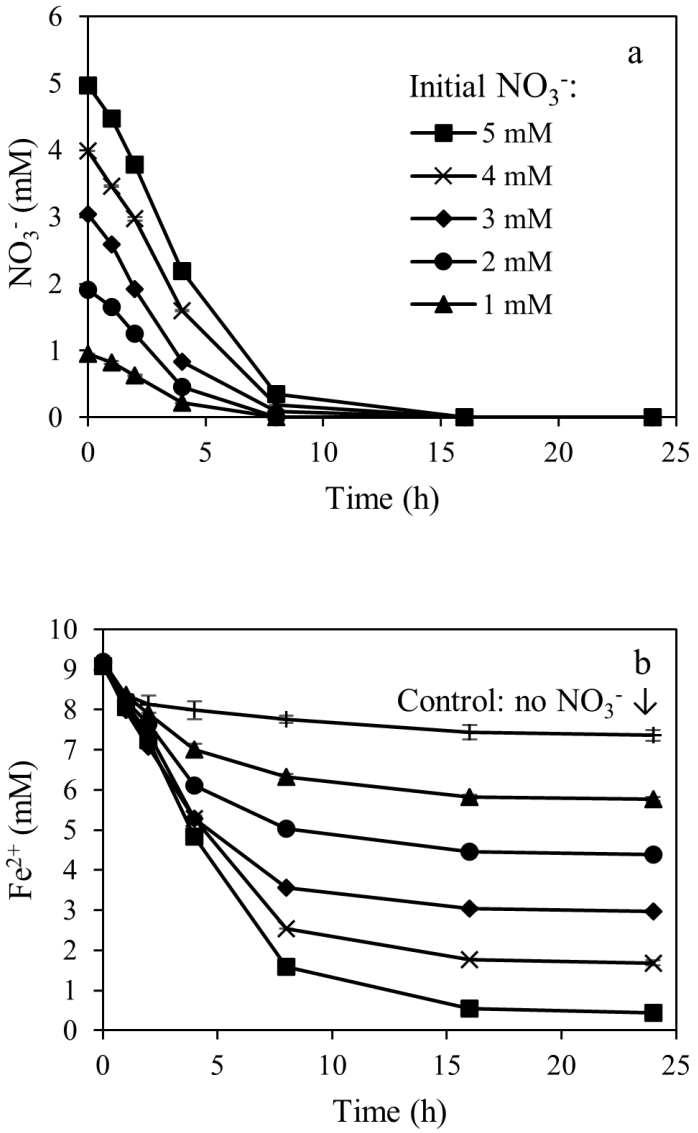

Figure 17 Time courses of (a) NO_3^-; (b) Fe^{2+}; (c) Cl^- and (d) NH_4^+ from nitrate removal by Fe^0 with excessive Fe^{2+} under various initial NO_3^- concentrations. The initial conditions of batch tests: 50 g/L Fe^0 + 9 mM Fe^{2+} + varying NO_3^- concentrations from 0 (as control) to 5 mM.

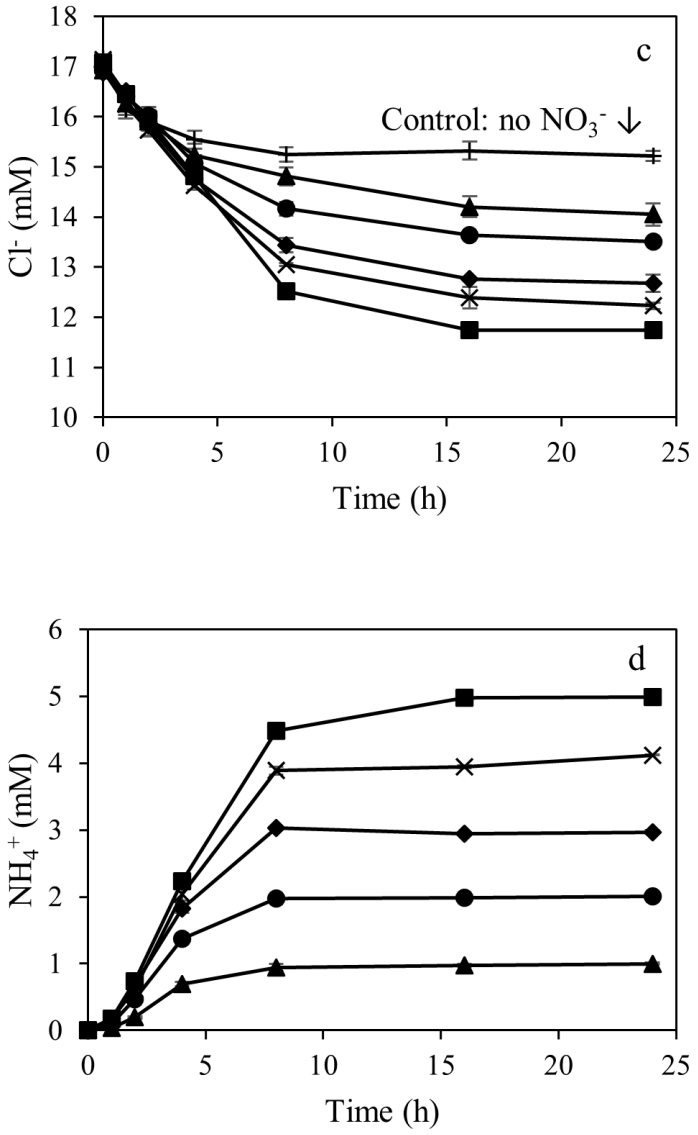

Figure 17 Continued

The total nitrogen (TN) consisting of NO_3^- and NH_4^+ in solution was shown in Figure 18. Between 0 to 8 h, there were apparent downward arcs throughout all sets of data trends. This TN missing from solution was believed caused by anion exchange effect between aqueous NO_3^- and interlayer Cl^- on GR. Hansen et al. [34, 55] did not observe a

nitrate-GR structure exiting during NO_3^- removal by GR_{Cl} and concluded rapid oxidization and dissolution of GR without temporary nitrate interlayer form formation. However, in our study, it was obvious that a significant amount of NO_3^- disappeared from solution and yet was not reduced to NH_4^+ simultaneously. Since no literature could be found reported NO_3^- reduced to NO_2^- under simple iron compound environment, and no gaseous nitrogenous substance would exist due to the complete nitrogen recovery overall in solution, the only explanation of the missing TN is that a portion of NO_3^- replaced Cl^- in the interlayer and existed in nitrate-form of GR temporarily. This phenomenon was consistent with the theory proposed in Figure 16.

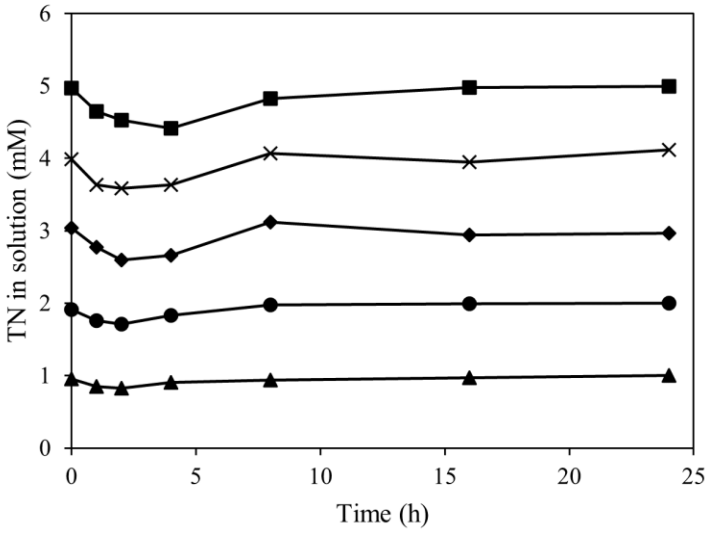

Figure 18 Time courses of total nitrogen (TN = NO_3^- + NH_4^+) in solution from nitrate removal by Fe^0 with excessive Fe^{2+} under various initial NO_3^- concentrations. The initial conditions of batch tests: 50 g/L Fe^0 + 9 mM Fe^{2+} + varying NO_3^- concentrations from 0 to 5 mM.

Figure 19 showed clear stoichiometry relationships of NO_3^- reduction and Fe^{2+} depletion (Figure 19a) along with Cl^- decline (Figure 19b) by ZVI under excessive

aqueous Fe^{2+}. Based on slope of the lines, 1.35 mM Fe^{2+} and 0.63 mM Cl^- corresponded to 1 mM NO_3^- removal. It needs to be noted that since 1.83 mM Fe^{2+} and 1.93 mM Cl^- would be reduced even without adding any NO_3^-, the amounts (1.83 & 1.93) must be deducted from those with adding NO_3^- as a correction. Therefore, the trend lines in Figure 19 were set to start at point (0, 1.83) and (0,1.93) for Fe^{2+} and Cl^-, respectively, instead of (0, 0). Based on these two stoichiometric coefficients and mass/charge balances, it is expected to initiate a reaction having Fe^0, NO_3^-, and Fe^{2+} as primary reactants, and GR and NH_4^+ as primary products. However, according to the calculation in Table 1, it is impossible to infer a single reaction equation that fits the stoichiometric relationships in Figure 19.

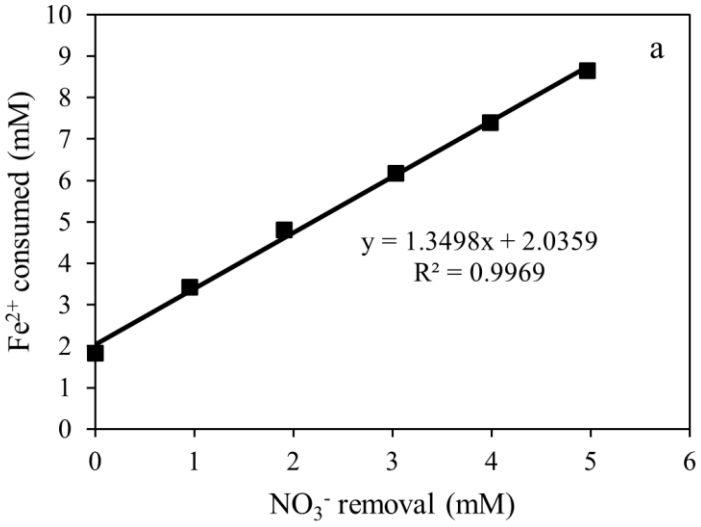

Figure 19 Nitrate removal by Fe^0 (50 g/L) with excessive Fe^{2+} (9 mM) under various initial NO_3^- concentrations (0–5 mM) show the stoichiometry between NO_3^- reduction and (a) Fe^{2+} consumption; (b) Cl^- missing.

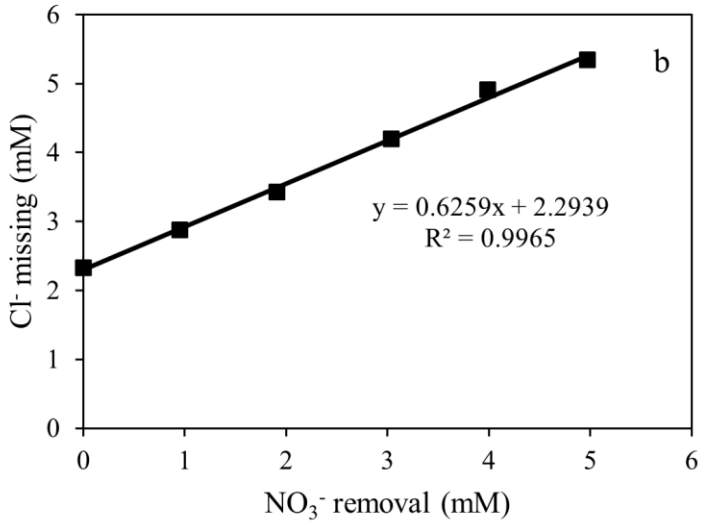

Figure 19 Continued.

Theoretically, to reduce 1 mol NO_3^- to NH_4^-, 8 moles of electrons are required. Only Fe^0 and Fe^{2+} are potential electron donors, and if the stoichiometric coefficient of Fe^{2+} (1.35) is secured, the equivalent Cl^- required (1.19) to complete the reaction is approximately twice as much as the observed stoichiometric coefficient (0.63) (Table 1). In a highly unlikely circumstance, where all 8 moles of electrons were hypothetically provided by Fe^0 to minimize the GR equivalent, the calculated required Cl^- was 8/2.25/4=0.89, which was still much higher than the observation. Since GR has a loose structure and could easily flake off from media during hydraulic mixing, NO_3^- could also be reduced by the structurally free GR, which transforms to magnetite and releases Cl^- back in solution. Therefore, assuming only two main processes were involved in the experiment (GR formation and GR consumption), the overall reaction that might reflect the experiment observations should be represented as a combination of two reactions.

Table 1 Calculation Steps of initiating a reaction equation based on mass/electron balances.

Mass balance (moles) *:					(Let **X** represent the ratio of Fe^0 to Fe^{2+})	
Primary Reactants**					**Primary Products**	
NO_3^-	Fe^{2+}	Fe^0	Cl^-	=>	$Fe^{III}_3Fe^{II}(OH)_8Cl$	NH_4^+
1	1.35	1.35**X**	¼*(1.35 + 1.35**X**)		¼*(1.35 + 1.35**X**)	1

Electron balance*:**

Half-cell reactions:					**Total electron transfer (moles)**
NO_3^-	→	NH_4^+	+	$8e^-$	8 * 1 = 8
Fe^{2+}	→	$Fe^{II}_3Fe^{III}(OH)_8Cl$	-	$0.25e^-$	-0.25 * 1.35 = -0.3375
Fe^0	→	$Fe^{II}_3Fe^{III}(OH)_8Cl$	-	$2.25e^-$	-2.25 * 1.35**X** = -3.0375**X**

Overall electron balance:

8 + (-0.3375) + (-3.0375**X**) = 7.6625 - 3.0375**X** = 0

X = 2.523

Check with Cl^- stoichiometric coefficient:

Cl^- = ¼*(1.35 + 1.35**X**)	Calculated required Cl^-:	1.19
	Observed required Cl^-:	0.63

*****Mass balances of hydrogen and oxygen are omitted due to their insignificant influences.

***** Calculation based on an assumption of reducing 1 mol NO_3^- under stoichiometric coefficient of NO_3^- to Fe^{2+} at 1 to 1.35.

***The average valence of Fe in $Fe^{II}_3Fe^{III}(OH)_8Cl$ is calculated as ((+2)*3+(+3))/4=+2.25.

The equivalent Fe^0 and Fe^{2+} for GR formation particularly are not known, neither is the ratio between GR formation and consumption. Complying with the two stoichiometric coefficients from Figure 19 and the mass/charge balances, the only fitting stoichiometry numbers could be calculated. As shown in Table 2, Eq (4) is the overall reaction, and it describes the stoichiometric relationships for both Fe^{2+} and Cl^-. Eq. (2a) and (3a) are derivatives of Eq. (2) and (3), where the stoichiometric number for NO_3^- are both 1. By multiplying the scale factors, Eq. (2a) and (3a) represent GR formation and

consumption, respectively. The scale factors add up to 1, which makes the overall NO_3^- coefficient 1 in Eq. (4).

Table 2 Calculated GR formation and consumption reaction equations.

Green rust formation:
$3.39Fe^0 + NO_3^- + 1.50Fe^{2+} + 1.22Cl^- + 7H_2O \rightarrow 1.22Fe_3^{II}Fe^{III}(OH)_8Cl + NH_4^+ + 0.23OH^-$ (2)
↓ **(×0.902)**
$3.06Fe^0 + 0.90NO_3^- + 1.35Fe^{2+} + 1.10Cl^- + 6.31H_2O \rightarrow 1.10Fe_3^{II}Fe^{III}(OH)_8Cl + 0.90NH_4^+ + 0.21OH^-$ (2a)
Green rust consumption:
$4.8Fe_3^{II}Fe^{III}(OH)_8Cl + NO_3^- \rightarrow 6.4Fe_3O_4 + NH_4^+ + 4.8Cl^- + 2.8H^+ + 15.8H_2O$ (3)
↓ **(×0.098)**
$0.47Fe_3^{II}Fe^{III}(OH)_8Cl + 0.10NO_3^- \rightarrow 0.63Fe_3O_4 + 0.10NH_4^+ + 0.47Cl^- + 0.27H^+ + 1.55H_2O$ (3a)
Overall reaction (combine the above two reactions after coefficient adjustment) *:
$3.06Fe^0 + NO_3^- + 1.35Fe^{2+} + 0.63Cl^- + 4.56H_2O \rightarrow 0.63Fe_3^{II}Fe^{III}(OH)_8Cl + 0.63Fe_3O_4 + NH_4^+ + 0.07H^+$ (4)

***** Calculation based on an assumption of reducing 1 mol NO_3^- to NH_4^+ under stoichiometric coefficient of NO_3^- to Fe^{2+} at 1 to 1.35, and NO_3^- to Cl^- at 1 to 0.63.

Based on the calculation, the stoichiometric relationships of Fe^0 and Fe^{2+} for GR formation were 3.39 and 1.50 in relation to 1 equivalent NO_3^- as shown in Eq. (2). In this test, about 90% of NO_3^- was consumed in GR formation and the remaining 10% would subsequently react with GR. One thing needs to be noted is that the ratio between GR formation and consumption is only applicable for interpreting this experiment, meaning it is not determined by these reactions intrinsically, but instead it is decided by GR which is structurally free of ZVI. The amount of free GR might be attributed to many factors, such as initial NO_3^- amount, the intensity of hydraulic stirring, size of the ZVI particle and the structural stability of GR.

CSTR Results

Because of the experimental characteristics of the CSTR tests, it is difficult to real-time monitor the ion changes in solution through time. In batch tests, the GR formation amount was measured by detecting the reduction of Cl^- from solution, which could not be easily achieved in CSTR tests. However, it is already known from Chapter II that the structural Cl^- in GR-Cl could be easily exchanged out by SO_4^{2-}. Therefore, assuming all the structural Cl^- were ion exchangeable and 50 mM SO_4^{2-} was high enough to force the Cl^- exhaustion within GR structure, the structural Cl^- could be determined by measuring its amount that was exchanged out by high concentration of SO_4^{2-}. The amount of solid taken from CSTR was 0.5 g and the exchanged Cl^- sample was taken from 10 ml solution containing that 0.5 g solid. Therefore, the actual EX_Cl based on 100 g/L media in CSTR was calculated and exhibited in Figure 20Figure 20 Continued. , where EX_Cl denotes the structural Cl^- that was exchanged out by SO_4^{2-}. The influent consisted of only 1 mM NO_3^- (as 14 ppm N), and less than 1 ppm of NO_3^--N could be detected in the effluent throughout all the tests. Reagent Fe^{2+} concentrations were kept at 0.75, 1.5, 2.25, 3, and 4.5 mM for different test, and the remained Fe^{2+} was shown in Figure 20b.

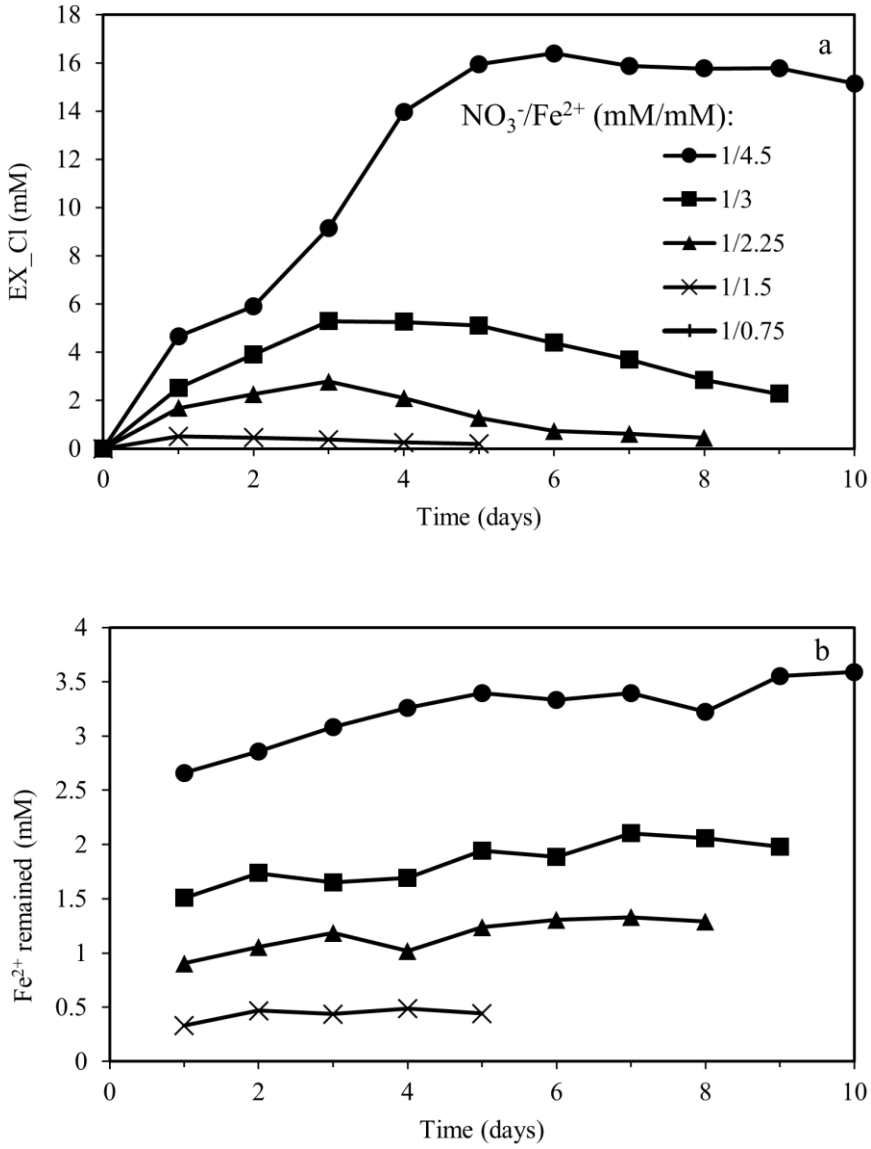

Figure 20 Time courses of (a) Exchanged out Cl^- from media under different Fe^{2+} concentration from 100 g/L media; (b) Remained Fe^{2+} in effluent; (c) Effluent pH from CSTR tests with conditions being controlled as: 100 g/L Fe^0 with different NO_3^-/Fe^{2+} concentrations.

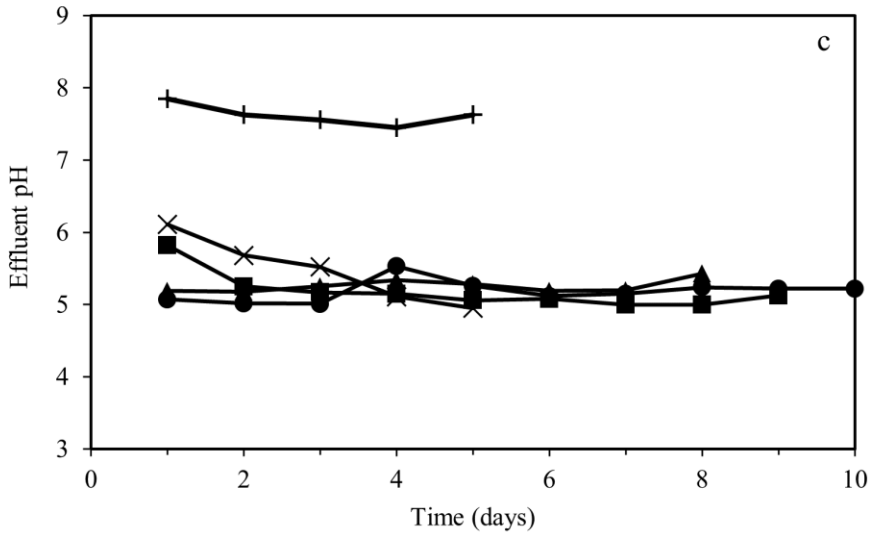

Figure 20 Continued.

Because the media was properly rinsed before mixed with SO_4^{2-}, it is safe to assume that all Cl^- detected in solution after mixing with 50 mM SO_4^{2-} came from GR structure which formed from NO_3^- reduction. No Cl^- was exchanged out in the 0.75 mM Fe^{2+} test, and no Fe^{2+} could be detected in the effluent, which agrees with the AIM preconditioning conditions (Equation 1). When Fe^{2+} reagent was greater than 0.75 mM, the exchangeable Cl^- began to exist in solution, and the amount of EX_Cl increased at first and then declined after reaching a peak, whose value positively correlates with the Fe^{2+} concentration. The 1.5mM Fe^{2+} test had its EX_Cl peak value only at 0.25 mM at day 1 and gradually diminished to 0.1 mM after day 5. Higher Fe^{2+} concentrations (e.g., 2.25, 3, & 4.5 mM) reached much greater peak value of EX_Cl and took longer time to reach the peak. Teal-green suspension could be observed in effluent and the green color got darker when EX_Cl was at higher level, indicating more suspended matter. It was also worth

noting that the higher concentration the Fe^{2+} reagent, the longer time EX_Cl stayed at the peak level. By the end of each test, the color of suspended solid in the effluent gradually turned black, and its turbidity also decreased. Except for test with 0.75 mM Fe^{2+}, the rest showed a slightly increasing tendency of the remained Fe^{2+} in the effluent. No pH adjustment for all tests and for most of the tests, the pH fell in the range of 5 to 6, except for the one with 0.75 mM Fe^{2+}, whose pH was over 7.5 after day 1 (Figure 20c).

Table 3 Green rust stability test.

CSTR test with 1 mM NO_3^- and 4.5 mM Fe^{2+}	Media after 10 days of reaction	Media idle for 10 days	Media idle for 40 days
EX_Cl from media extracted by SO_4^{2-} (mM)	15.14	14.38	13.32
Percentage	100%	95.0%	87.9%

Table 3 shows the results of the GR stability test. After 10 days of treatment of 1 mM NO_3^-, the media from 4.5 mM Fe^{2+} had an EX_Cl of 15.41 mM and a Fe^{2+} of 3.59 mM. After 10 and 40 days of inactivity, the EX_Cl only decreased by 5% and 12%, respectively, which may be caused by GR oxidation by DO from air, as the reactor was only partially covered by foam.

The accumulating effect and stability of GR following its production from NO_3^- reduction were investigated using CSTR tests. The results clearly exemplify that increased Fe^{2+} contributed to higher GR formation for the same amount of NO_3^- reduction, although this benefit did not last indefinitely. According to the proposed model in Figure 16, the more GR generated, the thicker the layer of GR on ZVI surface would be. Because

of the loose structure of GR, more micro-GR clusters would fall off the outer layer under the friction between media particles caused by hydraulic stirring, hence more iron-detached (free) GR in suspension. This explains the accumulation limitation of GR. Even though GR layer could serve as an electron bridge between inner iron core and NO_3^-, any structural breach within GR layer could cause regional breaking of the electron transmission chain, which leads to electron insufficiency and local oxidation of GR to magnetite. Therefore, as the reaction progressed, the transition of the outer side of GR layer, as well as free GR clusters, into magnetite began to take precedence, resulting in reduced GR generation. Green rust is also proven to be stable under anaerobic environment with the existence of Fe^0/Fe^{2+} in water. The findings of this study's CSTR test indicate that slowly feeding of NO_3^- into a Fe^{2+} enriched ZVI system will benefit in producing considerable amount of stable GR in a short period.

Conclusion

In this session, GR formation was observed during NO_3^- reduction to NH_4^+ by ZVI in Fe^{2+} abundant environment. A model is proposed where GR coated ZVI is oxidized by NO_3^- and regenerate from the particle surface. Excessive Fe^{2+} participated in NO_3^- reduction directly as partial electron donor and facilitated the transformation of the final products to GR instead of magnetite. Roles of GR coating were postulated as a combination of two models, semiconductor and coordinating surface: on one hand, GR concatenated ZVI with the outer surface and delivered electrons to where NO_3^- was reduced; on the other hand, GR as a reactive LDH provided substantial redox-active sites through its anion exchanging capacity. Under the experiment conditions, the results are

predominately GR with a tiny quantity of magnetite. Large amount of GR production can also be achieved with slow feeding of NO_3^- in the Fe^0/Fe^{2+} system. It is possible that under appropriate design, GR media could be used to treat a variety of anionic contaminants. Several aspects may help improve its efficiency in a real-life use. For example, in a similar situation, smaller ZVI particles (e.g.nZVI) could theoretically help enhance the GR production; sonication or violent hydraulic stirring could be used to accelerate the outer GR layer peeling off ZVI surface; sequencing batch reactors might be an appropriate design to achieve the continuous process of GR generation to GR application. Overall, this GR creation method based on ZVI media has a bright future and is worth further researching.

CHAPTER IV

STUDY OF SELENOCYANATE TRANSFORMATION AND IMMOBILIZATION BY AN ACTIVATED IRON SYSTEM

Introduction

As an essential element for both human and animals, selenium can be redistributed into different phases like aquatic, sedimentary, atmospheric and terrestrial compartments, and into different species. For human and animals, only a very little amount of selenium is adequate for nutrition, and excessive intake will cause adverse effects. The nutritional requirements of selenium are less than 0.5 Se mg/kg for potential receptors of concern waters [58]. When present at safe level, selenium protects main body from the toxicity of other heavy metal such as mercury, cadmium, arsenic, thallium, copper, zinc, silver, and many other harmful ingredients. However, excessive selenium exposure could cause reproductive impairment, embryo mortality and lower incubation survival [59].

Human activities are one of the major factors in the transportation of selenium including mining, fossil fuel combustion, oil refining and discharge of wastewater from irrigated agriculture [60]. The most common forms of selenium in stripped sour water (SSW) from refinery wastewater treatment plant are hydrogen selenide (H_2Se) and hydrogen selenocyanate (HSeCN), which predominate at acidic to neutral pH. However, depending on refinery layout and processing, other forms of selenium may predominate. Selenocyanate could be treated either by interacting with transition metals to form a variety of complexes and separating from water via precipitation or filtration, or by pretreatment oxidation, which would convert selenocyanate to selenite or selenate

followed by subsequent coprecipitation or adsorption [58, 61]. Manceau and Gallup [62] have reported that the treatment of 7 mg/L selenocyanate with copper(II) salts at elevated pH of 9-10 could result in approximately 95% removal. Some other heavy metals were found to be similarly potent at chemically precipitating $SeCN^-$, but most of the metals are regulated in the same way that selenium discharges are. In the case of $SeCN^-$ oxidative pretreatment, hydrogen peroxide (H_2O_2), chlorine dioxide (ClO_2), potassium permanganate ($KMnO_4$) and ozone (O_3) can be used as oxidant to turn $SeCN^-$ into selenite (Se^{IV}), which can be easily adsorbed by ferrihydrite iron coprecipitation. However, controlling the degree of oxidation to stop at selenite is challenging, according to Hill [58], and the oxidation reaction could proceed to selenate production, which is very poorly removed by chemical adsorption through iron co-precipitation.

ZVI based technology is a promising approach on remediating heavy metals on their oxidation states due to the great reduction ability of elemental iron and its low cost and toxicity. Even though selenium in $SeCN^-$ was in its reduced form, AIM technology combining with oxidation still has the potential to treat $SeCN^-$. Meng, Bang [63] reported that 10 g/L $SeCN^-$ as selenium can be removed by Fe^0 fillings in the presence of DO at pH around 6. The effect of DO, pH and co-precipitation with Fe^{II}/Fe^{III} on $SeCN^-$ removal were evaluated. However, from our research experience, aqueous Fe^{2+} added externally or hydrolyzed due to low pH could be playing an important role in $SeCN^-$ removal by ZVI based treatments. Additionally, previous pilot-scale tests have shown that AIM system could efficiently remove $SeCN^-$ and meet the EPA standards for selenium. However, post processing units indicated that there might be a second release of selenium which slightly

went over the criterion. The objective of this study was to determine selenocyanate removal by Fe^0 under oxygenated conditions, and the important role aqueous Fe^{2+} was playing. The possible mechanism of selenocyanate removal in AIM system will also be discussed.

Materials and Methods

Materials and Chemicals

Unless otherwise indicated, reagents used in this study were all at analytical reagent grade. Ferrous and selenocyanate solutions were prepared from $FeCl_2 \cdot 4H_2O$ (>99%, J.T. Baker, NJ) and KSeCN (>98.5% Alfa Aesar, MA), respectively. The -20 mesh iron powder (>99% Alfa Aesar, MA) was used as the ZVI powder. Deionized deoxygenated (DI) water was supplied by E-pure (Barnstead, USA) with resistivity around 18.2 M-cm. Any tests conducted anaerobically in this study were prepared in the anaerobic chamber (Coy Laboratory, MI), which was filled with approximate 95% N_2 and 5% H_2 and equipped with a palladium catalytic O_2 removal system and an O_2 sensor to ensure an anoxic environment.

Experimental Methods

Batch experiments were conducted using 1 L glass bottle (PYREX® Media Bottles, Graduated, Corning®, NY) as reactors. For each test, one bottle was prepared using the following procedures. (1) Chemicals were pre-weighted and dissolved in DDI water in anaerobic chamber. (2) Pre-weighted 25 g -20 mesh ZVI was transferred to the reactor containing prepared solution. (3) The reactor was immediately capped with a

rubber stopper, and since it was done in the anaerobic chamber, the headspace (125 ± 5 ml) was filled with a mixture of N_2 and H_2, which were assumed not participating in $SeCN^-$ removal. (4) The headspace of certain tests involving O_2 was flushed with oxygen gas for at least 3 min by inserting two needles through the stopper; for tests that required unlimited O_2 supply, a gas bag filled with O_2 was connected to the reactor by a silicon pipe with two syringe needles attached at both ends. (5) The reactors were placed in the tumbler (30 rpm) to provide complete mixing at room temperature while avoiding light; the ones with the gas bag were carefully arranged to avoid pressure on the bag. (6) At selected times, 5 ml of sample solution would be taken out using a syringe with needle through the rubber stopper; for completely sealed reactors (e.g., combinations without gas bag connected), the pressure inside the reactor was measured before sampling, and then balanced by temporarily connecting to a gas bag filled with N_2 after sampling. To avoid any probable gas leak, a small amount of petrolatum (Ward's Science, NY) was applied to cover the puncture holes caused by syringe needle piercing. (7) Sample solution taken from the reactor was filtrated via 0.45 μm membrane filters (VWR) for later analysis. Generally, each reactor would be sampled 6 times, making the overall sampled volume up to 30 ml, and because the total liquid volume in reactor was 1 L, the samples taken only accounted for 3% of the overall 1 L reactor volume. Therefore, the concentration differences caused by the sampling volume reduction was considered negligible. A schematic diagram of the unlimited O_2 batch test set up as an example is shown in Figure 21.

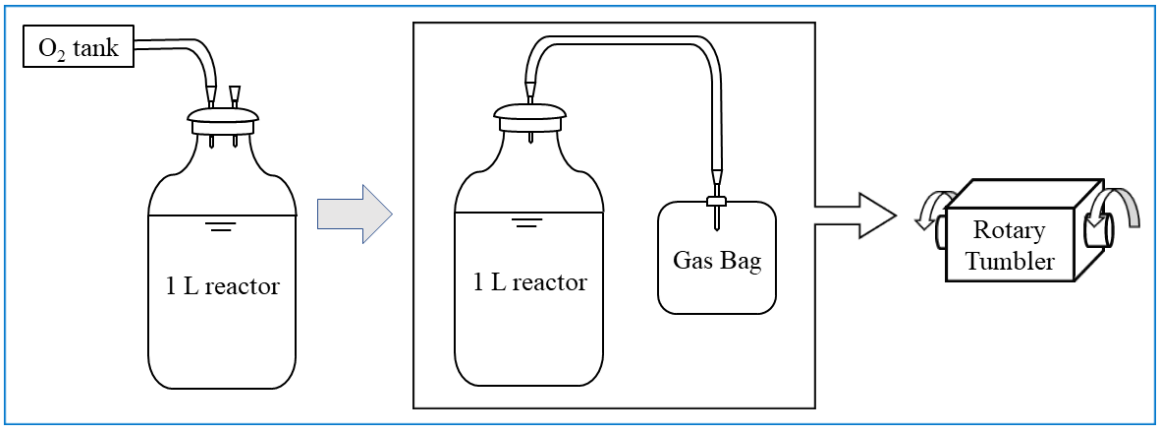

Figure 21 Batch test set up with gas bag for unlimited O_2 tests.

Sample Preparation and Analytical Methods

The filtrate was collected for IC (ion chromatography) analysis. A Dionex ICS-1100 system (Dionex Co., Synnyvale, CA) was used to analyze $SeCN^-$. Separation was achieved using a Dionex IonPac AS16 column with an AG16 guard column. The minimum detection limit of $SeCN^-$ were 2 mg/L. Dissolved Fe^{2+} was measured colorimetrically with the 1,10-phenanthroline method at the wavelength of 510 nm [32] on a UV-Vis spectrophotometer (M&A Instruments Inc, CA). In some experiments NH_4^+ was also determined. Filtrate solution with NH_4^+ was processed and tested on UV-Vis spectrophotometer at 640 nm following phenate methods [47]. A total organic carbon analyzer (TOC-LCPH with TNM-L Total Nitrogen Module, Shimadzu Scientific Instruments, Inc., MD) was used for total carbon (TC) and total nitrogen (TN) analysis of sample filtrate. Inductively coupled plasma mass spectrometry (7700x, Agilent, CA) was used for detecting total selenium in aqueous phases. The pH of filtrate was measured by pH Meters (Orion 2-Star Benchtop, Thermo Fisher Scientific Inc., MA). The pressure

changes in reactor were measured by a digital test pressure gauge (Ashcroft, CT) with a connected needle for puncture.

When necessary, certain experiments were repeated, and the reactors were transferred in the anaerobic chamber to prepare samples for X-ray powder diffraction (XRD) analysis. XRD was used to characterize the corrosion products on ZVI surface. The media in reactors was sonicated for 5 min before transferred in anaerobic chamber. Most suspended solid was withdrawn from the reactor using a syringe, and then forced through a 0.45 μm filter paper (Pall Laboratory, USA). Once the XRD samples were prepared, XRD analyses would be conducted within 1 hr. XRD patterns were recorded by Bruker-AXS D8 Advanced Bragg-Brentano X-ray Powder Diffractometer with Cu Kα radiation at a wavelength of 1.5406 Å.

The oxidation state of Se was determined by X-ray photoelectron spectroscopy (Omicron XPS/UPS system with Argus detector) using Mg Kα X-ray radiation at 1253.6 eV. Samples after preparation were dried anaerobically in a vacuum desiccator for two days. Constant Analyzer Energy (CAE) of 20 eV, a step size of 0.05 eV and dwell time of 0.5 s were used to obtain the high-resolution spectra. The binding energy of adventitious carbon (C (1s)) was set at 284.8 eV as the calibration reference peak to compensate the charging effect. The assignment of different Se speciation was based on NIST X-ray photoelectron spectroscopy database.

Results and Discussion

$SeCN^-$ Removal in Different Systems

Selenocyanate anion removal in different system is illustrated in Figure 22. As shown, $SeCN^-$ removal rate varied greatly among different systems. In the ZVI only system, $SeCN^-$ was removed only by ~6% after 24 h, demonstrating that Fe^0 alone has little effect on $SeCN^-$ breakdown or immobilization. The pH of 2mM $SeCN^-$ solution is about 8 due to the hydrolysis of $SeCN^-$ to HSeCN, and pH of ZVI only system was stable over 24 h (pH = 8 ~ 8.3) and the $SeCN^-$ removal might only be caused by the surface adsorption of ZVI media. Comparing with ZVI only system, the ZVI/Fe^{2+} combination has similar poor removal efficiency over 24 h, suggesting that neither Fe^{2+} alone nor weak acidic (pH = ~5) environment could effectively promote $SeCN^-$ removal by ZVI. In the Fe^{2+}/O_2 system (no ZVI), $SeCN^-$ removal rate was only ~2% and pink suspended solid was visible in the reactor after 1 h of mixing, which was believed to be elemental selenium. Aqueous Fe^{2+} were expected to be oxidized by O_2, but only limited Fe^{2+} reduction was observed after 24 h. It was reported by Golub and Skopenko [64] that hydrochloric acid could cause potassium selenocyanate to decompose at pH 5.5 – 4.9, and Fe^{3+} could bring the pH up to 6. However, from the observations in this study, this decomposition happens fairly slow and is not an effective way to remove $SeCN^-$. In the ZVI/O_2 combination, the solution became light yellow colloidal, and the turbidity increased over time, but only 9% $SeCN^-$ removal was detected over 24 h.

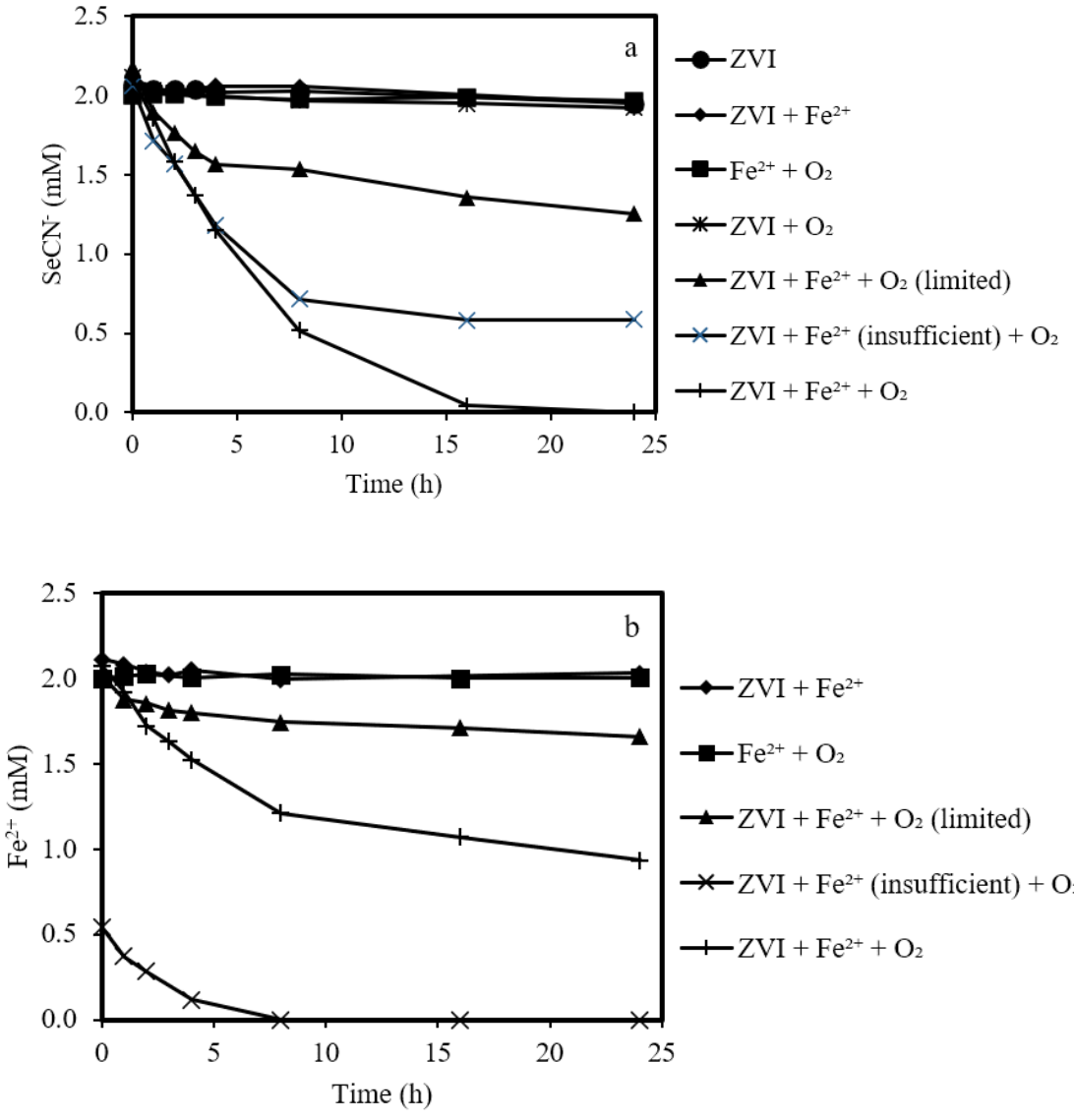

Figure 22 Time courses of (a) $SeCN^-$; (b) Fe^{2+} and (c) pH in the seven treatment systems with different combinations of 25 g/L ZVI, 2 mM Fe^{2+}, 2 mM $SeCN^-$ and O_2. Initial conditions of Fe^{2+} (insufficient) and O_2 (limited) was 0.5 mM Fe^{2+} and headspace O_2 only, respectively.

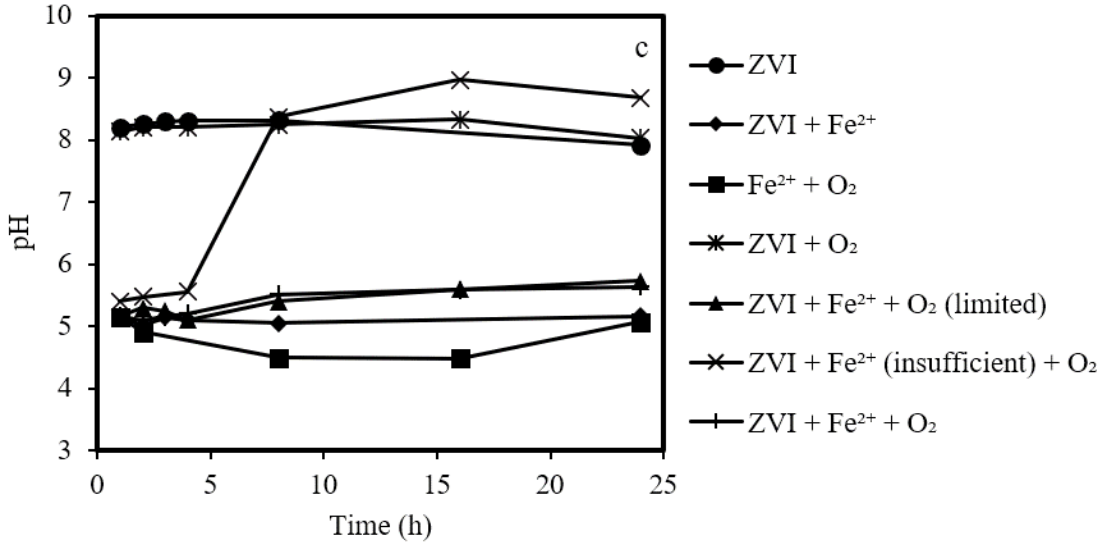

Figure 22 Continued.

The removal efficiencies of the combinations containing all three components (ZVI, Fe^{2+} and O_2) are significantly higher than that of combinations containing only one or two components. In the ZVI/Fe^{2+}/O_2(unlimited) set, the reactor headspace was first filled with O_2, and a gas bag filled with O_2 was connected to the reactor, therefore O_2 was considered excessive in the system. Added Fe^{2+} was considered excessive as well since half of the 2 mM was still in system as aqueous Fe^{2+} at 24 h. Its results exhibited the highest reactivity for $SeCN^-$ removal of all sets, reaching a 98% removal of ~2.112 mM $SeCN^-$ at 16 h and a completely removal at 24 h. A rapid decrease of dissolved Fe^{2+} was also observed during the $SeCN^-$ removal process, but the decreasing tendency slowed down after $SeCN^-$ was mostly removed (Figure 22b). This indicates that in an oxygenated environment, $SeCN^-$ removal would consume Fe^{2+} directly or indirectly. The pH increased slightly from 5 to 5.5 after 24 h, and since the system is unbuffered, the change in pH

regarding the amount of $SeCN^-$ removed may suggest that H^+ (or OH^-) was involved in the reactions (Figure 22c). In the ZVI/Fe^{2+}/O_2(limited) set, only the reactor headspace was filled with O_2 and no gas bag was connected to the reactor. The reaction rate was initially quick in this combination, but when the O_2 content fell, the $SeCN^-$ removal rate slowed. When O_2 in the reactor headspace was completely consumed after 4 h, a total of ~28% of $SeCN^-$ was removed. The overall removal percentage after 24 h, on the other hand, was only ~42%. Aqueous Fe^{2+} decreased concomitantly with $SeCN^-$ removal, and pH raised from 5.1 to 5.7 (Figure 22b & c). Similar to ZVI/Fe^{2+}/O_2(unlimited) set, the ZVI/Fe^{2+} (insufficient)/O_2 set had a rapid $SeCN^-$ removal rate at first, but it dropped drastically at 8 h when the aqueous Fe^{2+} was totally consumed. The pH eventually rose up to 8.5~9, which is even higher than the 2 mM $SeCN^-$ solution, further evidencing the involvement of OH^- in the $SeCN^-$ removal processes. These results confirmed that both O_2 and Fe^{2+} are essential for rapid $SeCN^-$ removal by ZVI.

It is also worth noting that for ZVI/Fe^{2+}/O_2(limited) set, after O_2 was totally consumed at 4 h, the remaining $SeCN^-$ was still getting removed from solution at a much slower rate (only 14.7% removal over 20 h). There appears to be a different removal mechanism here than the one requiring O_2, which will be discussed later.

Reaction Products Analysis

The oxidation state of Se in the corrosion coating from ZVI/Fe^{2+}/O_2 system was analyzed by X-ray photoelectron spectroscopy (XPS). Sample was obtained from media with the following conditions: 25 g/L ZVI + 2 mM Fe^{2+} + 2 mM $SeCN^-$ + unlimited O_2 at 16 h, when $SeCN^-$ was over 98% removed. Because of the substantial overlap between the

binding energy ranges of Se 3d and Fe 3p, the spectrum of Se 3p was collected. As illustrated in Figure 23, the doublet separation between Se $3p_{3/2}$ and $3p_{1/2}$ was set as 5.75 eV. Photoelectron lines of $3p_{3/2}$ were drawn with solid lines, and the ones of $3p_{1/2}$ were drawn with dashed lines. The area ratios of Se $3p_{3/2}$ to $3p_{1/2}$ peaks were constrained at 2:1. Any binding energies mentioned in this session for Se species identification were designated to the $3p_{3/2}$ spectral lines. According to NIST X-ray Photoelectron spectroscopy database, the binding energies of 158.6 eV, 161.2 eV and 164.9 eV were assigned to Se^{-II}, Se^0, and Se^{IV} or Se^{VI}, respectively. The percentages of Se^{-II}, Se^0, and Se^{IV} or Se^{VI} were calculated based on their $3p_{3/2}$ peak area as 4.7%, 87.7% and 7.6%.

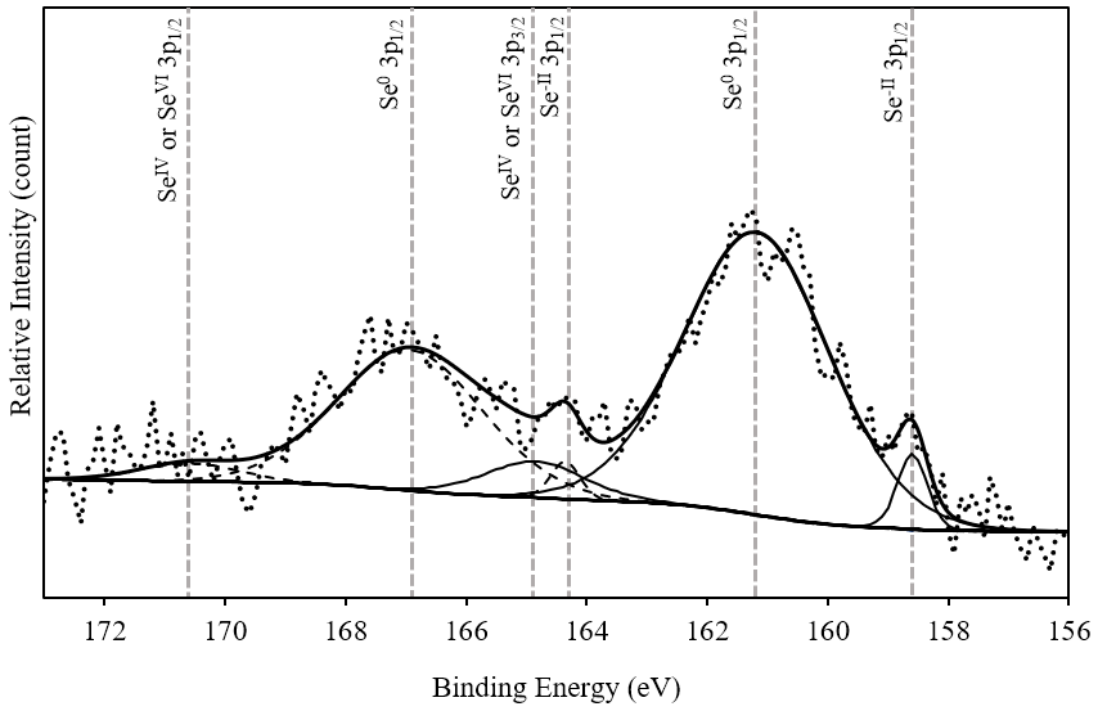

Figure 23 X-ray photoelectron spectroscopy (XPS) high resolution spectrum of Se 3p for corrosion coating from media: 25 g/L ZVI + 2 mM Fe^{2+} + 2 mM $SeCN^-$ + unlimited O_2 after 16 h reaction.

Chemical and XPS analysis of the pattern of Se distribution and evolution in the ZVI/Fe^{2+}/O_2 system revealed that the predominant process for $SeCN^-$ removal was by two steps: oxidation of Se^{-II} to Se^{IV} or Se^{VI}, then reduction to Se^0 or even back to Se^{-II}. Many previous studies have researched selenate (Se^{VI}) and selenite (Se^{IV}) removal by ZVI under different conditions, and Se^0 and/or FeSe were mostly observed as the final Se species [58, 65-67]. According to our observation, $SeCN^-$ could not easily react with ZVI, even with the help of Fe^{2+} or low pH, both of which are known to activate ZVI surface [17, 25, 68], and the addition of oxygen provided an oxygenated environment that oxidized $SeCN^-$ to higher oxidation states that are easier for ZVI to remove.

Table 4 Ratios of total carbon (TC), total nitrogen (TN) and total aqueous selenium to $SeCN^-$ in filtrate solutions at different reaction times under condition: 25 g/L ZVI + 2 mM Fe^{2+} + 2 mM $SeCN^-$ + unlimited O_2.

Time	$SeCN^-$	TN/$SeCN^-$	TC/$SeCN^-$	Se (aq)/$SeCN^-$
(h)	(mM)	(mM/mM)	(mM/mM)	(mM/mM)
1	1.855	1.069	1.046	0.966
2	1.581	1.024	1.033	0.980
4	1.147	1.021	1.004	0.970
8	0.517	1.000	0.998	0.954

X-ray diffraction was used for characterizing the corrosion products. XRD showed distinct peaks for magnetite structures, but no signs of other crystal structures (patterns not shown). NH_4^+ could not be detected in any filtrate pertaining the fate of nitrogen. Total carbon (TC) and total nitrogen (TN) were determined by TOC-TN, and total aqueous selenium was determined by ICP-MS. Table 4 illustrated the ratios of TC, TN and total aqueous selenium to $SeCN^-$ at different reaction times. All the ratios are close to 1 with less than 10% of differences, indicating a 1:1:1 relationship among the molar

concentrations of carbon, nitrogen, and selenium in solution throughout $SeCN^-$ removal process. As a result, $SeCN^-$ was most likely present in its entirety form prior to removal, and the removal procedure would separate both the [CN] group and selenium from water.

Quantitative Consumption of Fe^{2+} on $SeCN^-$ Removal by ZVI

Batch tests were conducted to investigate the relationship between Fe^{2+} loss and $SeCN^-$ removal. The initial conditions were 25 g/L ZVI + 2 mM Fe^{2+} + 0 (as control), 0.506, 1.037, 1.602, or 2.150 mM $SeCN^-$. As shown in Figure 24, results indicated that even without the addition of $SeCN^-$, 0.25 mM Fe^{2+} would be consumed at the start of the reaction and remained stable after its initial loss. This observation was in agreement with the results reported by Huang and Zhang [25]. Over 98% of $SeCN^-$ could be removed in solution after 16 h, and aqueous Fe^{2+} decreased together with $SeCN^-$ removal for all sets. The pH ranged from 5 to 5.5, and the slight increased pH may suggest OH^- production was involved in general (Figure 24c). A linear regression was used to describe the stoichiometric relationship between $SeCN^-$ and Fe^{2+} in an oxygenated environment. As illustrated in Figure 24d, Fe^{2+} was consumed with a $SeCN^-$ to Fe^{2+} stoichiometry of ~1:0.48. The starting point for this linear fitting was not the origin, because there was a small amount consumption of Fe^{2+} when dealing with oxygen only (control line in Figure 24b). It was observed that even after $SeCN^-$ was totally removed, the remaining Fe^{2+} in solution have different degrees of reduction in each set. Since oxygen alone does not consume Fe^{2+} in ZVI/Fe^{2+} system [25], aqueous Fe^{2+} reduction must be partially involved in the $SeCN^-$ removal mechanisms.

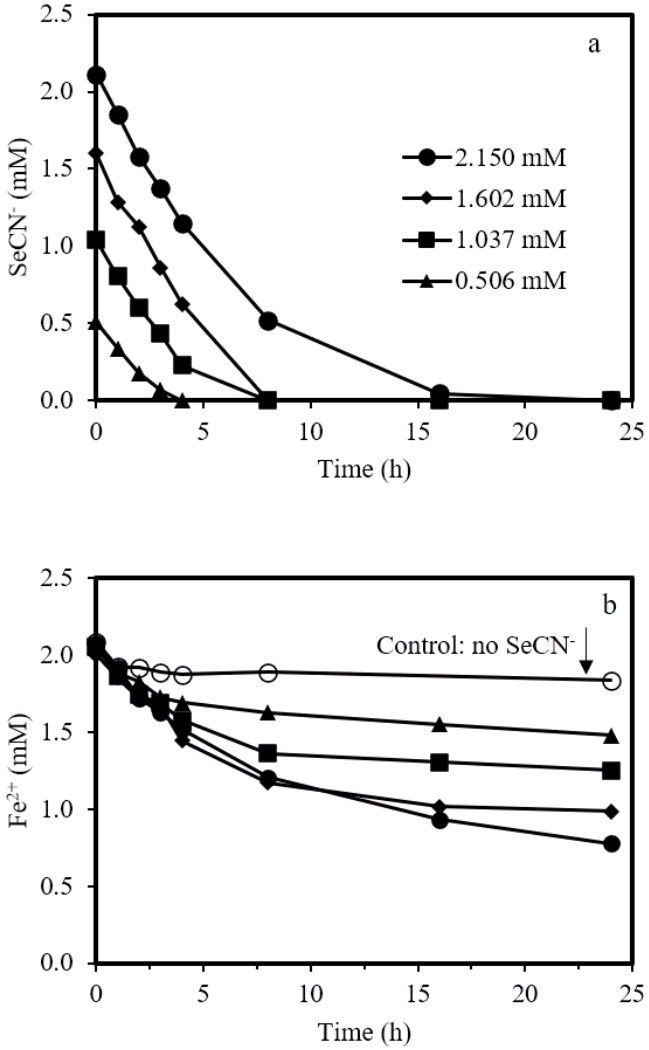

Figure 24 Time courses of (a) $SeCN^-$; (b) Fe^{2+}; (c) pH from different concentrations of $SeCN^-$ removal by Fe^0 with excessive Fe^{2+} under oxygenated conditions. The initial conditions of batch tests: 25 g/L Fe^0 + 2 mM Fe^{2+} + varying $SeCN^-$ concentrations from 0 (as control) to 2.15 mM + unlimited O_2; (d) The stoichiometry relationship between $SeCN^-$ removal and Fe^{2+} consumption.

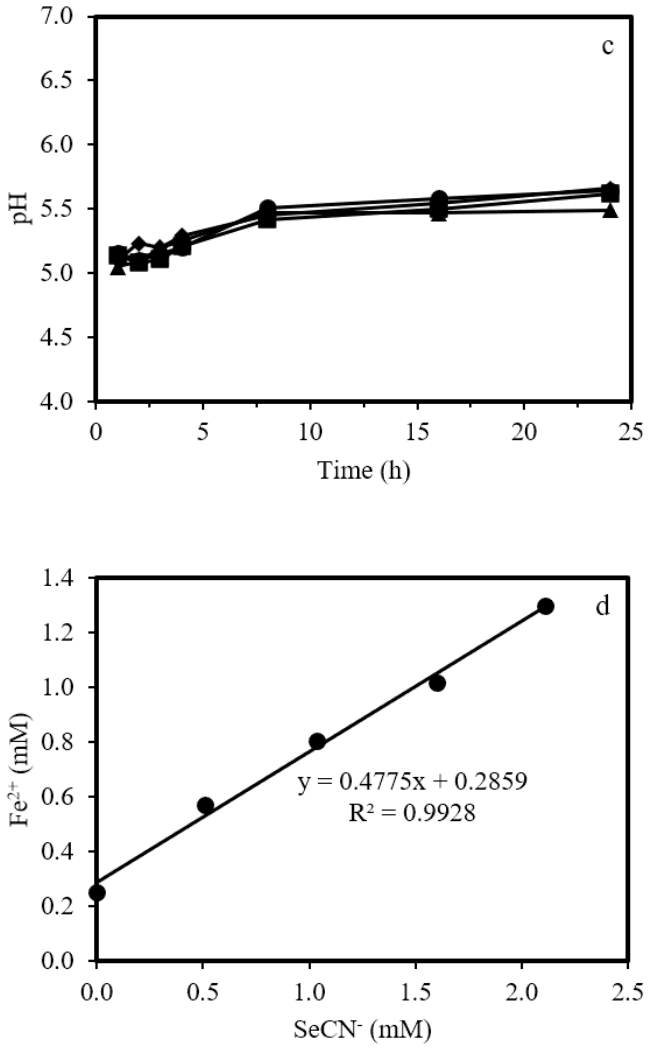

Figure 24 Continued.

Discussion

$SeCN^-$ removal by ZVI had been investigated by Meng, Bang [63], and their results accentuated the importance of slightly acidic pH and the present of dissolved oxygen (DO) in water. $SeCN^-$ removal mechanism was attributed to a simply deselenation reaction on ZVI surface as described in Eq. (5):

$$SeCN^- \xrightarrow{Fe^0} Se^0 + CN^- \qquad (5)$$

These findings, however, did not evidently explain the role of pH and oxygen in $SeCN^-$ removal, which will be the focus of this discussion.

The results of this study indicated that in an oxygenated Fe^0/Fe^{2+} aqueous systems, $SeCN^-$ could be removed rapidly at slight acidic pH (5-6), and the acidity was caused by addition of Fe^{2+}. Our findings from XPS analysis indicated a valance variation of selenium throughout $SeCN^-$ removal: the selenium in $SeCN^-$ was converted to Se^{IV} or Se^{VI}, from which a large percentage was reduced to Se^0 and a small fraction to Se^{-II} by ZVI. Since oxygen alone was unable to help ZVI in removing $SeCN^-$, it is assumed that oxidants created when ZVI was oxidized by oxygen, such as hydroxyl radical (OH·) or hydrogen peroxide (H_2O_2), are responsible for $SeCN^-$ oxidation.

It has been well demonstrated that ZVI or ferrous iron oxidation by DO favors the oxidative treatment of organic contaminants. For example, molinate, a selective, preemergence, thiocarbamate herbicide, could be effectively degraded by the strongly oxidizing radicals formed from the corrosion of ZVI by oxygen in water [69]. As(III) can be partially or completely oxidized in parallel with the oxidation of Fe^{2+} by oxygen and by H_2O_2 in aerated solution [70], while results from Katsoyiannis et al. [71] showed that As(III) oxidation and removal by ZVI from pH 3 to 11 in aerated water suggested that As(III) was oxidized primarily in solution by the Fenton reaction and removed by sorption on newly formed hydrous ferric oxides. Although some other oxidants, such as O_2^{2-}, O_2^{-}·

and $HO_2\cdot$, may also be generated during the ZVI oxidation, at a pH range from 5 to 6, the Eq. (6) to (9) have generally been used to represent the probable oxidants generation reactions that occur in a $Fe^0/H_2O/O_2$ system:

$$Fe^0 + O_2 + 2H^+ \rightarrow Fe^{2+} + H_2O_2 \qquad (6)$$

$$Fe^0 + H_2O_2 \rightarrow Fe^{2+} + 2OH^- \qquad (7)$$

$$Fe^{2+} + H_2O_2 \rightarrow Fe^{3+} + OH\cdot + OH^- \qquad (8)$$

$$Fe^{2+} + OH\cdot \rightarrow Fe^{3+} + OH^- \qquad (9)$$

$$SeCN^- + 6OH\cdot \rightarrow {SeO_4}^{2-} + CN^- + 2H_2O + 2H^+ \qquad (10)$$

Eq. (8) is the first step of Fenton reactions, which generates a reactive oxidant ($OH\cdot$) that may be the main source of radicals in this study. Even though Fe^{3+} could also react with H_2O_2 and produce free radicals, however, at pH higher than 5, any Fe^{3+} generated would either be reduced by ZVI to create surface-bound Fe^{2+} or hydrolyzed and precipitated as ferric hydroxide. Despite selenite or elemental selenium could still be the possible oxidation products, selenate is presumed the major product due to the great oxidizing ability of $OH\cdot$.

It is also known from the TOC-TN/ICP test results (Table 4) that [CN] group only existed as an entirety in $SeCN^-$ and was excluded from water along with $SeCN^-$ removal. The separated [CN] group is likely to act like a ligand and combine with the Fe^{2+} that works as a coordination center, forming ferrocyanide ($[Fe^{II}(CN)_6]^{4-}$) as described in Eq. (11). Although Fe^{3+} from Eq. (8) and (9) may combine with [CN] to form ferricyanide ($[Fe^{III}(CN)_6]^{3-}$), Fe^{3+} could not exist as ion at near neutral pH, and it would most likely precipitate on the ZVI surface as iron corrosion products.

$$Fe^{2+} + 6CN^- \rightarrow [Fe^{II}(CN)_6]^{4-} \qquad (11)$$

$$4[Fe^{II}(CN)_6]^{4-} + O_2 + 4H^+ \rightarrow 4[Fe^{III}(CN)_6]^{3-} + 2H_2O \qquad (12)$$

$$3Fe^{2+} + 2[Fe^{III}(CN)_6]^{3-} \rightarrow {Fe^{II}}_3[(Fe^{III}(CN)_6]_2\ (s) \qquad (13)$$

Since oxygen was provided and the reactor was constantly rotating, it was assumed that, except for regions on the ZVI surface, the bulk solution was saturated with DO. Eq. (14) to (16) are the standard reduction potentials for Fe^{3+}/Fe^{2+}, $[Fe^{III}(CN)_6]^{3-}/[Fe^{II}(CN)_6]^{4-}$ and O_2/H_2O [72], respectively. The reduction potential of Fe^{3+}/Fe^{2+} is higher than that of $[Fe^{III}(CN)_6]^{3-}/[Fe^{II}(CN)_6]^{4-}$, indicating that $[Fe^{II}(CN)_6]^{4-}$ is more likely than Fe^{2+} to be oxidized to $[Fe^{III}(CN)_6]^{3-}$ by DO (Eq. (12)). The oxidation production will further combine with excessive aqueous Fe^{2+} and precipitates as ${Fe^{II}}_3[Fe^{III}(CN)_6]_2$ (Turnbull blue) due to its insolubility in water (Eq. (13)).

$$Fe^{3+} + e^- \rightarrow Fe^{2+} \quad E^0 = +0.77\ V \qquad (14)$$

$$[Fe^{III}(CN)_6]^{3-} + e^- \rightarrow [Fe^{II}(CN)_6]^{4-} \quad E^0 = +0.37\ V \qquad (15)$$

$$O_2 + 4H^+ + 4e^- \rightarrow 2H_2O \quad E^0 = +1.229\ V \qquad (16)$$

However, the existence of Turnbull blue was not detected on the XRD test (data now shown), and only magnetite peaks was observable from the spectrum. This is probably because the amount of magnetite produced from oxygen reduction was way higher than the production of Turnbull blue. For example, in the ZVI/Fe^{2+}/O_2(limited) set (Figure 22), the total amount of O_2 was around 125 ml at 1 atm (25 ℃), which is equivalent to 5.12 mM DO in batch reactor (1 L volume). At 4 h of reaction, a 100% drop of pressure in the reactor indicated the complete consumption of oxygen, when only 0.61 mM $SeCN^-$ was removed. According to the DO removal mechanism by ZVI [25], consumption of 5.12 mM DO will produce 592.8 mg magnetite, whereas Turnbull blue generated from 0.61 mM $SeCN^-$ results in just 31.3 mg, accounting for barely 5% of total mass produced. When oxygen is continuously supplied, the amount of magnetite produced is substantially more than the estimation, resulting in much smaller percentage of Turnbull blue.

In studies conducted exploring oxygen-containing water on nano ZVI, lower pH promotes oxidant generation more than higher pH, and no oxidant production was seen at pH value greater than 8 [73]. Additionally, O_2 reduction on iron in buffered solution of pH 9.8 appeared to proceed without catalytic decomposition of peroxide as an intermediate [74]. These observations agree with our results from ZVI/O_2 system (Figure 22), in which only 9% of $SeCN^-$ was removed after 24 h, and pH was not adjusted and

stayed above 8. Because aqueous Fe^{2+} can act as an OH· scavenger, as shown in Eq. (9), Joo et al. [73] offered a proposal that radicals are generated on or adjacent to the ZVI surface, which may help explain such pH-related phenomenon. Since the ZVI media surface tends to be negatively charged towards high pH [75], anions (e.g., $SeCN^-$) have a lower affinity for the surface whilst cations (e.g., Fe^{2+}) have a higher affinity. As a result, if OH· is only present on or near the surface, $SeCN^-$ should be oxidized more slowly at higher pH. Furthermore, the presence of free Fe^{2+} is inhibited in alkaline solutions, which impedes the generation of OH· in Eq. (6) and (8).

After the oxidation of $SeCN^-$ to SeO_4^{2-}, the problem becomes the removal of selenate in a ZVI/Fe^{2+}/O_2 system. Many studies have shown that ZVI under low pH, or with the help of Fe^{2+}, is quite effective at removing selenate or selenite, even with the presence of oxygen [28, 65-67]. Tang et al. [28] reported that ZVI mixed with magnetite and Fe^{2+} boosts ZVI efficiency for selenate removal. It was also reported by Tang et al. [67] that Fe^{2+} was consumed with a Fe^{2+}:Se stoichiometry ratio of ~1:1, facilitating the transformation of the passive layer of iron coating to magnetite under anaerobic conditions. Sivan et al. [65] discussed the effects of low pH and limited aeration on selenate removal by ZVI, declaring that limited aeration increased the removal rates by 4 times due to the formation of reactive Fe^{II}-bearing intermediates on ZVI surface. In our study, no signs of aqueous SeO_4^{2-} or SeO_3^{2-} in solution was observed during $SeCN^-$ removal, hence it could be inferred that SeO_4^{2-}, as an intermediate, only existed briefly on the surface of ZVI, followed by rapidly reduction to Se^0 or even Se^{-II}. It was observed that in the ZVI/Fe^{2+}/O_2 system with unlimited O_2 and aqueous Fe^{2+}, the consumption of Fe^{2+}

did not stop immediately after the complete removal of $SeCN^-$, which could be due to the newly generated SeO_4^{2-} reduction by ZVI/Fe^{2+}.

Despite the fact that magnetite is beneficial for the SeO_4^{2-} reduction as proven by many studies, the effect of iron oxide coating (mainly magnetite) generated from DO reduction on $SeCN^-$ removal, especially during the initial oxidation process, was not thoroughly investigated in this study. DO reduction by ZVI generated a considerable amount of magnetite during $SeCN^-$ removal, however, the rate of removal did not appear to be influenced by the rapid growth of the magnetite layer. Surface adsorption on magnetite could also function as part of the $SeCN^-$ removal mechanism, since the growth of magnetite layer provided substantial surface area, which favored anion adsorption at acidic pH. For example, $SeCN^-$ was oxidized to SeO_4^{2-} in the ZVI/Fe^{2+}/O_2(limited) set at first, and following O_2 exhaustion, SeO_4^{2-} reduction by ZVI/Fe^{2+} also generated magnetite, although at a slower rate than O_2. This is most likely why $SeCN^-$ removal did not halt after O_2 exhaustion, but instead progressed at a reduced rate. However, this mechanism alone could not explain the valence variation of selenium and the needs for aqueous Fe^{2+} during $SeCN^-$ removal. Many studies have reported that dissolved oxygen and certain iron oxide could stimulate reactive oxygen species generation [76, 77]. For example, Ardo et al. [78] proposed a heterogeneous Fenton-like reactions for the removal of nalidixic acid (NAL), in which structural Fe^{2+} at magnetite surface was partially oxidized by dissolved oxygen, and OH· was proven to be involved in the NAL degradation. Therefore, it is possible that the magnetite coating might function similarly as ZVI in regard to OH· generation, and

the overoxidation to maghemite or lepidocrocite would likely to be neutralized by the synergetic reduction of ZVI core and aqueous Fe^{2+}.

Another unanswered question is the stoichiometry relationship between $SeCN^-$ removal and aqueous Fe^{2+}. DO removal by ZVI did not consume aqueous Fe^{2+} [25]. According to Eq. (10) to (13), to generated 1 mole of Turnbull blue needs approximate 12 moles [CN] from $SeCN^-$ and 5 moles $Fe^{2+/3+}$, in which Fe^{2+}:Se ratio is 5:12 (~0.42) if all $Fe^{2+/3+}$ come from aqueous Fe^{2+}. Moreover, SeO_4^{2-} removal by ZVI/Fe^{2+} system disclosed a near 1 to 1 relationship between Fe^{2+} consumption and Se reduction [67]. Therefore, combining the theoretical aqueous Fe^{2+} consumption from Turnbull blue and SeO_4^{2-} reduction (assuming all $SeCN^-$ was oxidized to SeO_4^{2-}), the required Fe^{2+} to removal 1 mole $SeCN^-$ is 1.42 mole. However, our results indicated that the actual needs of aqueous Fe^{2+} to removal 1 mole $SeCN^-$ was only 0.48 mole, which is close to the need of Turnbull blue precipitation (0.42). It was speculated that aqueous Fe^{2+} only facilitate in the formation of Turnbull blue, with solid iron media being primarily responsible for reducing the post-generated SeO_4^{2-} within structure.

Conclusion

The removal of $SeCN^-$ by ZVI under various conditions was investigated in this study to demonstrate that $SeCN^-$ could be effectively removed at a slightly acidic pH by ZVI/Fe^{2+}/O_2 synergetic system. The study emphasized and discussed the importance of both oxygen and aqueous Fe^{2+}. A 0.48 to 1 stoichiometry relationship was found between aqueous Fe^{2+} consumption and $SeCN^-$ removal. The possible removal mechanism involved was inferred as two parts: oxidation of $SeCN^-$ to SeO_4^{2-}, followed by reduction

of newly generated SeO_4^{2-} to Se^0 or Se^{-II}. Radicals excited by DO was considered responsible for initiating the oxidation processes. The [CN] group that broke away from $SeCN^-$ was discovered to exist in its entirety, with Turnbull blue being the most likely final form. Despite these findings, more studies are needed to investigate the mechanism for radical production regarding oxide coatings and Fe^{2+} consumption.

CHAPTER V

CONCLUSION

Summary of Experimental Results

This research began with the study of an intriguing feature of AIM, the rapid initial removal of anionic contaminant of freshly prepared AIM. Chapter II focused on the property of such initial capacity, including the generation conditions, media surface characterization, and the contaminant (SeO_4^{2-}) transformation process after ion exchange. The in-depth research of the development of GR as precursor/intermedia to the preparation of the activated iron media continued in Chapter III. Chapter IV was a relatively independent topic, targeting the selenocyanate transformation and immobilization by an AIM system. All these topics served to increase the understanding of the AIM technology and provide new insights from different perspectives.

In Chapter II, the production of chloride type GR as an intermediate and its interlayer anion exchange capacity was determined to be the nature of EX_{CAP}. Affinity order of anions was tested to be $SeO_4^{2-} > SO_4^{2-} > NO_3^- > Cl^-$ towards the green rust interlayer. Green rust production from AIM synthesis was proven to be impacted by AIM synthetic time, DO, and increased Cl^-. After interexchange into green rust structure, SeO_4^{2-} will be gradually reduced to Se^0 or Se^{-II}.

Chapter III further investigated the GR formation mechanism. Large-scale production of GR was observed during NO_3^- reduction to NH_4^+ by ZVI with excessive aqueous Fe^{2+}. A model is proposed in which excessive Fe^{2+} acts as partial electron donor, facilitating the transition of the end products to GR rather than magnetite. On one side,

GR connected ZVI with the outer surface and transported electrons to where NO_3^- was reduced; on the other hand, GR as a reactive LDH offered large redox-active sites through its anion exchanging layer. The possible reaction pathways for GR formation were also derived based on the experimental stoichiometry relationships.

Chapter IV explored the mechanism of $SeCN^-$ removal by ZVI/Fe^{2+}/O_2 system. A synergetic effect among ZVI, Fe^{2+} and O_2 was evidently confirmed essential for the removal effectiveness. The results indicated that $SeCN^-$ removal mechanism was proposed to be first oxidation to SeO_4^{2-}, followed by the reduction to Se^0 or Se^{-II}, and incorporated in the iron corrosion product. The oxidation process was postulated to be started by radicals that were generated by O_2. Turnbull blue was revealed to be the most likely final form of [CN].

Suggestions for Future Research

Regarding the GR application, under the right conditions, it could be utilized to treat a wide range of anionic pollutants. However, NO_3^- is not considered an ideal addition to any treatment system. Hence, more environment friendly oxidants are expected to be discovered. Moreover, with more GR accumulating on ZVI surface during the process, it was assumed that the generation would slow down due to the gap getting larger between ZVI and oxidant. Therefore, using smaller ZVI particle (e.g., nZVI) media or applying sequencing batch reactors with methods to peeling off GR layer may contribute to GR generation efficiency. For many of the unanswered question about $SeCN^-$ removal, the radicals involved in $SeCN^-$ oxidation was not experimentally observed in this study, and

it will be interesting to see how the system will behave with the addition of radical scavengers.

REFERENCES

1. Turekian, K.K. and K.H. Wedepohl, *Distribution of the Elements in Some Major Units of the Earth's Crust.* Geological Society of America Bulletin, 1961. **72**(2): p. 175-192.

2. Johnson, D.B. and K.B. Hallberg, *Acid mine drainage remediation options: a review.* Science of the Total Environment, 2005. **338**(1-2): p. 3-14.

3. Weber, K.A., L.A. Achenbach, and J.D. Coates, *Microorganisms pumping iron: anaerobic microbial iron oxidation and reduction.* Nature Reviews Microbiology, 2006. **4**(10): p. 752-764.

4. Millero, F.J., W.S. Yao, and J. Aicher, *The Speciation of Fe(II) and Fe(III) in Natural-Waters.* Marine Chemistry, 1995. **50**(1-4): p. 21-39.

5. Bowell, R.J., *Sorption of Arsenic by Iron-Oxides and Oxyhydroxides in Soils.* Applied Geochemistry, 1994. **9**(3): p. 279-286.

6. Cundy, A.B., L. Hopkinson, and R.L.D. Whitby, *Use of iron-based technologies in contaminated land and groundwater remediation: A review.* Science of the Total Environment, 2008. **400**(1-3): p. 42-51.

7. Guo, X.J., et al., *Adsorption of antimony onto iron oxyhydroxides: Adsorption behavior and surface structure.* Journal of Hazardous Materials, 2014. **276**: p. 339-345.

8. Peng, J.F., et al., *The remediation of heavy metals contaminated sediment.* Journal of Hazardous Materials, 2009. **161**(2-3): p. 633-640.

9. Tessier, A., et al., *Metal sorption to diagenetic iron and manganese oxyhydroxides and associated organic matter: Narrowing the gap between field and laboratory measurements.* Geochimica Et Cosmochimica Acta, 1996. **60**(3): p. 387-404.

10. Zachara, J.M., et al., *Chromate Adsorption on Amorphous Iron Oxyhydroxide in the Presence of Major Groundwater Ions.* Environmental Science & Technology, 1987. **21**(6): p. 589-594.

11. Newman, S.P. and W. Jones, *Comparative study of some layered hydroxide salts containing exchangeable interlayer anions.* Journal of Solid State Chemistry, 1999. **148**(1): p. 26-40.

12. Wilfert, P., et al., *The Relevance of Phosphorus and Iron Chemistry to the Recovery of Phosphorus from Wastewater: A Review.* Environmental Science & Technology, 2015. **49**(16): p. 9400-9414.

13. Rosales, E., M. Pazos, and M.A. Sanroman, *Advances in the Electro-Fenton Process for Remediation of Recalcitrant Organic Compounds.* Chemical Engineering & Technology, 2012. **35**(4): p. 609-617.

14. Guan, X.H., et al., *The limitations of applying zero-valent iron technology in contaminants sequestration and the corresponding countermeasures: The development in zero-valent iron technology in the last two decades (1994-2014).* Water Research, 2015. **75**: p. 224-248.

15. Zhou, H.M., et al., *Degradation pathway and kinetics of 1-alkyl-3-methylimidazolium bromides oxidation in an ultrasonic nanoscale zero-valent iron/hydrogen peroxide system.* Journal of Hazardous Materials, 2015. **284**: p. 241-252.

16. Wilkin, R.T. and M.S. McNeil, *Laboratory evaluation of zero-valent iron to treat water impacted by acid mine drainage.* Chemosphere, 2003. **53**(7): p. 715-725.

17. Huang, Y.H., et al., *Effects of oxide coating and selected cations on nitrate reduction by iron metal.* Journal of Environmental Quality, 2003. **32**(4): p. 1306-15.

18. Cahan, B.D. and C.T. Chen, *The Nature of the Passive Film on Iron .2. Ac Impedance Studies.* Journal of the Electrochemical Society, 1982. **129**(3): p. 474-480.

19. Sun, Y.P., et al., *Characterization of zero-valent iron nanoparticles.* Advances in Colloid and Interface Science, 2006. **120**(1-3): p. 47-56.

20. Crane, R.A. and T.B. Scott, *Nanoscale zero-valent iron: Future prospects for an emerging water treatment technology.* Journal of Hazardous Materials, 2012. **211**: p. 112-125.

21. Li, X.Q., D.W. Elliott, and W.X. Zhang, *Zero-valent iron nanoparticles for abatement of environmental pollutants: Materials and engineering aspects.* Critical Reviews in Solid State and Materials Sciences, 2006. **31**(4): p. 111-122.

22. Huang, Y.H., et al., *Hybrid zero-valent iron process for removing heavy metals and nitrate from flue-gas-desulfurization wastewater.* Separation and Purification Technology, 2013. **118**: p. 690-698.

23. Huang, Y.H. and T.C. Zhang, *Nitrite reduction and formation of corrosion coatings in zerovalent iron systems.* Chemosphere, 2006. **64**(6): p. 937-43.

24. Huang, Y.H., *Nitrate degradation by Fe^{0} : mechanisms, kinetics, and the role of iron oxide coatings*. 2002, University of Nebraska--Lincoln. p. xi, 246 leaves.

25. Huang, Y.H. and T.C. Zhang, *Effects of dissolved oxygen on formation of corrosion products and concomitant oxygen and nitrate reduction in zero-valent iron systems with or without aqueous Fe^{2+}*. Water Research, 2005. **39**(9): p. 1751-60.

26. Huang, Y.H., et al., *Pilot-scale demonstration of the hybrid zero-valent iron process for treating flue-gas-desulfurization wastewater: Part I.* Water Science and Technology, 2013. **67**(1): p. 16-23.

27. Huang, Y.H., et al., *Pilot-scale demonstration of the hybrid zero-valent iron process for treating flue-gas-desulfurization wastewater: Part II.* Water Science and Technology, 2013. **67**(2): p. 239-246.

28. Tang, C., et al., *Rapid removal of selenate in a zero-valent iron/Fe_3O_4/Fe^{2+} synergetic system.* Applied Catalysis B-Environmental, 2016. **184**: p. 320-327.

29. Huang, Y.H., et al., *Competitive Reduction of Nitrate, Nitrite, and Nitrobenzene in Fe0-Water Systems.* Journal of Environmental Engineering, 2014. **140**(8): p. 04014029.

30. Peak, D. and D.L. Sparks, *Mechanisms of Selenate Adsorption on Iron Oxides and Hydroxides.* Environmental Science & Technology, 2002. **36**(7): p. 1460-1466.

31. Kadirvelu, K. and J. Goel, *Ion Exchange and Inorganic Adsorption*, in *Water Encyclopedia*. p. 490-496.

32. American Public Health Association., et al., *Standard methods for the examination of water & wastewater*.

33. Hansen, H.C.B., *Composition, Stabilization, and Light-Absorption of Fe(II)Fe(III) Hydroxy-Carbonate (Green Rust).* Clay Minerals, 1989. **24**(4): p. 663-669.

34. Hansen, H.C.B., et al., *Kinetics of nitrate reduction by green rusts - effects of interlayer anion and Fe(II): Fe(III) ratio.* Applied Clay Science, 2001. **18**(1-2): p. 81-91.

35. Schwertmann, U. and H. Fechter, *The Formation of Green Rust and Its Transformation to Lepidocrocite.* Clay Minerals, 1994. **29**(1): p. 87-92.

36. Bernal, J.D., D.R. Dasgupta, and A.L. Mackay, *The oxides and hydroxides of iron and their structural inter-relationships.* Clay Minerals Bulletin, 1959. **4**(21): p. 15-30.

37. Refait, P., L. Simon, and J.M.R. Genin, *Reduction of SeO42- anions and anoxic formation of iron(II)-iron(III) hydroxy selenate green rust.* Environmental Science & Technology, 2000. **34**(5): p. 819-825.

38. Usman, M., et al., *Magnetite and Green Rust: Synthesis, Properties, and Environmental Applications of Mixed-Valent Iron Minerals.* Chemical Reviews, 2018. **118**(7): p. 3251-3304.

39. Hayashi, H., et al., *pH-dependence of selenate removal from liquid phase by reductive Fe(II)-Fe(III) hydroxysulfate compound, green rust.* Chemosphere, 2009. **76**(5): p. 638-643.

40. Myneni, S.C.B., T.K. Tokunaga, and G.E. Brown, *Abiotic selenium redox transformations in the presence of Fe(II,III) oxides.* Science, 1997. **278**(5340): p. 1106-1109.

41. Genin, J.M.R., et al., *Preparation and E-h-pH diagrams of Fe(II)-Fe(III) green rust compounds; hyperfine interaction characteristics and stoichiometry of hydroxy-chloride, -sulphate and -carbonate.* Hyperfine Interactions, 1998. **111**(1-4): p. 313-318.

42. Cornell, R.M. and U. Schwertmann, *The iron oxides: structure, properties, reactions, occurrences and uses*. 2003: John Wiley & Sons.

43. Gehin, A., et al., *Synthesis of Fe(II-III) hydroxysulphate green rust by coprecipitation.* Solid State Sciences, 2002. **4**(1): p. 61-66.

44. Williams, A.G.B. and M.M. Scherer, *Kinetics of Cr(VI) reduction by carbonate green rust.* Environmental Science & Technology, 2001. **35**(17): p. 3488-3494.

45. Hansen, H.C.B., O.K. Borggaard, and J. Sorensen, *Evaluation of the Free-Energy of Formation of Fe(II)-Fe(III) Hydroxide-Sulfate (Green Rust) and Its Reduction of Nitrite.* Geochimica Et Cosmochimica Acta, 1994. **58**(12): p. 2599-2608.

46. O'Loughlin, E.J., et al., *Reduction of Uranium(VI) by mixed iron(II/iron(III) hydroxide (green rust): Formation of UO_2 manoparticies.* Environmental Science & Technology, 2003. **37**(4): p. 721-727.

47. SOLÓRZANO, L., *DETERMINATION OF AMMONIA IN NATURAL WATERS BY THE PHENOLHYPOCHLORITE METHOD 1 1 This research was fully supported by U.S. Atomic Energy Commission Contract No. ATS (11-1) GEN 10, P.A. 20.* Limnology and Oceanography, 1969. **14**(5): p. 799-801.

48. Scherer, M.M., B.A. Balko, and P.G. Tratnyek, *The Role of Oxides in Reduction Reactions at the Metal-Water Interface*, in *Mineral-Water Interfacial Reactions*. 1999, American Chemical Society. p. 301-322.

49. Li, J. and D.J. Meier, *An AFM study of the properties of passive films on iron surfaces.* Journal of Electroanalytical Chemistry, 1998. **454**(1): p. 53-58.

50. Li, L., et al., *Synthesis, Properties, and Environmental Applications of Nanoscale Iron-Based Materials: A Review.* Critical Reviews in Environmental Science and Technology, 2006. **36**(5): p. 405-431.

51. Huang, Y.H. and T.C. Zhang, *Kinetics of Nitrate Reduction by Iron at Near Neutral pH.* Journal of Environmental Engineering, 2002. **128**(7): p. 604-611.

52. Hansen, H.C.B., et al., *Abiotic Nitrate Reduction to Ammonium: Key Role of Green Rust.* Environmental Science & Technology, 1996. **30**(6): p. 2053-2056.

53. Khan, A.I. and D. O'Hare, *Intercalation chemistry of layered double hydroxides: recent developments and applications.* Journal of Materials Chemistry, 2002. **12**(11): p. 3191-3198.

54. Fan, G., et al., *Catalytic applications of layered double hydroxides: recent advances and perspectives.* Chemical Society Reviews, 2014. **43**(20): p. 7040-7066.

55. Hansen, H.C.B. and C. Bender Koch, *Reduction of nitrate to ammonium by sulphate green rust: activation energy and reaction mechanism.* Clay Minerals, 1998. **33**(1): p. 87-101.

56. Miyata, S., *Anion-Exchange Properties of Hydrotalcite-Like Compounds.* Clays and Clay Minerals, 1983. **31**(4): p. 305-311.

57. Wander, M.C.F., K.M. Rosso, and M.A.A. Schoonen, *Structure and Charge Hopping Dynamics in Green Rust.* The Journal of Physical Chemistry C, 2007. **111**(30): p. 11414-11423.

58. Hill, C.M., *Review of available technologies for the removal of selenium from water.* Final Report, prepared for North American Metals Council (NAMC), 2010.

59. Eisler, R., *Handbook of chemical risk assessment*. 2000, Boca Raton, Fla.: Lewis Publishers. 1 online resource (3 volumes (1903 pages)).

60. Chapman, P.M., et al., *Ecological assessment of selenium in the aquatic environment*. 2010, Boca Raton: Taylor and Francis. 1 online resource (368 pages).

61. Twidwell, L., et al. *Technologies and potential technologies for removing selenium from process and mine wastewater*. in *Proceedings of the TMS Fall Extraction and Processing Conference*. 1999.

62. Manceau, A. and D.L. Gallup, *Removal of Selenocyanate in Water by Precipitation: Characterization of Copper−Selenium Precipitate by X-ray Diffraction, Infrared, and X-ray Absorption Spectroscopy.* Environmental Science & Technology, 1997. **31**(4): p. 968-976.

63. Meng, X., S. Bang, and G.P. Korfiatis, *Removal of selenocyanate from water using elemental iron.* Water Research, 2002. **36**(15): p. 3867-3873.

64. Golub, A.M. and V.V. Skopenko, *Metal Selenocyanates and Their Properties.* Russian Chemical Reviews, 1965. **34**: p. 901.

65. Klas, S. and D.W. Kirk, *Understanding the positive effects of low pH and limited aeration on selenate removal from water by elemental iron.* Separation and Purification Technology, 2013. **116**: p. 222-229.

66. Yoon, I.-H., et al., *Reduction and adsorption mechanisms of selenate by zero-valent iron and related iron corrosion.* Applied Catalysis B: Environmental, 2011. **104**(1): p. 185-192.

67. Tang, C., et al., *Reductive removal of selenate by zero-valent iron: The roles of aqueous Fe2+ and corrosion products, and selenate removal mechanisms.* Water Research, 2014. **67**: p. 166-174.

68. Huang, Y.H. and T.C. Zhang, *Effects of low pH on nitrate reduction by iron powder.* Water Research, 2004. **38**(11): p. 2631-42.

69. Joo, S.H., A.J. Feitz, and T.D. Waite, *Oxidative Degradation of the Carbothioate Herbicide, Molinate, Using Nanoscale Zero-Valent Iron.* Environmental Science & Technology, 2004. **38**(7): p. 2242-2247.

70. Hug, S.J. and O. Leupin, *Iron-Catalyzed Oxidation of Arsenic(III) by Oxygen and by Hydrogen Peroxide: pH-Dependent Formation of Oxidants in the Fenton Reaction.* Environmental Science & Technology, 2003. **37**(12): p. 2734-2742.

71. Katsoyiannis, I.A., T. Ruettimann, and S.J. Hug, *pH Dependence of Fenton Reagent Generation and As(III) Oxidation and Removal by Corrosion of Zero Valent Iron in Aerated Water*. Environmental Science & Technology, 2008. **42**(19): p. 7424-7430.

72. Rock, P.A., *The Standard Oxidation Potential of the Ferrocyanide-Ferricyanide Electrode at 25° and the Entropy of Ferrocyanide Ion.* The Journal of Physical Chemistry, 1966. **70**(2): p. 576-580.

73. Joo, S.H., et al., *Quantification of the Oxidizing Capacity of Nanoparticulate Zero-Valent Iron.* Environmental Science & Technology, 2005. **39**(5): p. 1263-1268.

74. Zečević, S., D.M. Dražić, and S. Gojković, *Oxygen reduction on iron: Part III. An analysis of the rotating disk-ring electrode measurements in near neutral solutions.* Journal of Electroanalytical Chemistry and Interfacial Electrochemistry, 1989. **265**(1): p. 179-193.

75. Hu, J., G. Chen, and I.M.C. Lo, *Selective Removal of Heavy Metals from Industrial Wastewater Using Maghemite Nanoparticle: Performance and Mechanisms.* Journal of Environmental Engineering, 2006. **132**(7): p. 709-715.

76. Fang, G.-D., D.-M. Zhou, and D.D. Dionysiou, *Superoxide mediated production of hydroxyl radicals by magnetite nanoparticles: Demonstration in the degradation of 2-chlorobiphenyl.* Journal of Hazardous Materials, 2013. **250-251**: p. 68-75.

77. Wu, H., et al., *Reactive oxygen species-related activities of nano-iron metal and nano-iron oxides.* Journal of Food and Drug Analysis, 2014. **22**(1): p. 86-94.

78. Ardo, S.G., et al., *Oxidative Degradation of Nalidixic Acid by Nano-magnetite via Fe2+/O2-Mediated Reactions.* Environmental Science & Technology, 2015. **49**(7): p. 4506-4514.